RESEARCH ON METALLURGICAL SYNTHESIS

by

B. A. Wilcox, G. T. Hahn, and R. I. Jaffee

BATTELLE MEMORIAL INSTITUTE
Columbus Laboratories

December, 1972

FOREWORD

This Interim Technical Report covers work performed by Battelle, Columbus Laboratories staff members under USAF Contract No. F33615-71-C-1679, Research on Metallurgical Synthesis. The project was initiated under Project 7351, "Metallic Materials", Task No. 735103. The program was administered under the direction of the Air Force Materials Laboratory, Air Force Systems Command, USAF, with Dr. Harold H. Gegel, LLS, as Project Engineer.

This report covers the period from 15 June 1971 through 30 June 1972. The manuscript was released by the authors on 4 August 1972 for publication as an AFML Technical Report.

This technical report has been reviewed and is approved.

C. M. Pierce

C. M. PIERCE
Metal and Ceramic Synthesis Branch
Metals and Ceramics Division
Air Force Materials Laboratory

ABSTRACT

This research program consists of various tasks on metallurgical synthesis, which are aimed at developing improved microstructures in metals and ceramics of interest to the Air Force. The tasks are considered "next step" research, in that prior critical experiments have demonstrated the feasibility of a concept. The research is aimed at developing the potential usefulness of the basic concept, and to determine the circumstances under which it might be expected to operate. The tasks discussed in this report deal chiefly with research on aluminum and titanium alloys.

TABLE OF CONTENTS

TABLE OF CONTENTS
(Continued)

TABLE OF CONTENTS
(Continued)

LIST OF TABLES

LIST OF TABLES
(Continued)

LIST OF FIGURES

LIST OF FIGURES
(Continued)

LIST OF FIGURES
(Continued)

LIST OF FIGURES
(Continued)

RESEARCH ON METALLURGICAL SYNTHESIS

by

B. A. Wilcox, G. T. Hahn, and R. I. Jaffee

INTRODUCTION

The main purposes of this program are to exploit work emerging from in-house research efforts of the Air Force Materials Laboratory and to reduce the time in research and development between conception and application. The overall objective of this program on Metallurgical Synthesis is to provide better structural materials for defense applications in less time for a lower cost.

Each task is considered to be a "next step" research effort; i.e., the critical experiment has already been accomplished. These tasks are intended to develop the potential usefulness of the basic concept and to determine the circumstances under which it might be expected to operate. At the end of each task it is intended that recommendations be made as to whether or not the concept is fully viable and should be further developed by a separate larger scale effort.

A total of approximately twelve tasks are being undertaken over the two-year period June 15, 1971-June 15, 1973, and each task is approximately 6 to 9 months in duration. It is contemplated that at least eight of the tasks will be initiated from the AFML based on in-house research by AFML scientists, and approximately four tasks will be initiated from Battelle, Columbus Laboratories (BCL). A task is initiated when sufficient preliminary evidence suggests that "next-step" experiments are warranted. A

steering committee comprised of cognizant AFML and BCL personnel meets quarterly to discuss task initiation, evaluate performance, and makes recommendations at the conclusion of a task.

Table 1 lists the tasks contemplated, the cognizant AFML scientist, the BCL principal investigator(s), and the task starting date. Tasks A, I, III, and VI have been completed. In this report the respective sections describing these tasks constitute a final report on the tasks. Tasks B and II are in progress, Tasks C, D, and V will be initiated in the near future, and Tasks IV, VII, and VIII will be initiated at a later date.

TABLE 1. TASKS ON THE METALLURGICAL SYNTHESIS PROGRAM[a]

Task No.	Title	BCL Principal Investigator	Cognizant AFML Scientist	Task Start Date	Task Completion Date
A	Microstructural Synthesis in Combined Precipitation Hardened-Dispersion Strengthened (PH-DS) Aluminum Alloys	B. A. Wilcox	H.L. Gegel	June 15, 1971	March 15, 1972
B	Synthesis of Dispersion Strengthened Titanium Alloys by Attritor Milling	I. G. Wright/ B. A. Wilcox	S.R. Lyon	March 15, 1972	In progress
C	Microstructural and Mechanical Property Evaluation of Ti-Y_2O_3 Base Alloys	I. G. Wright/ B. A. Wilcox	S.R. Lyon	September, 1972 (Anticipated)	
D	Microstructural Factors Influencing Fracture Toughness of Ceramics	G. T. Hahn/ A.R.Rosenfield	R. Ruh	October, 1972 (Anticipated)	
I	Evaluation of New High Temperature Titanium Alloys	A. H. Clauer	H. L. Gegel	June 15, 1971	March 15, 1972
II	Vapor Deposition of Metals on Aluminum and Boron	W. R. Stowell/ D. Hauser	G. Metzger	March 1, 1972	In progress
III	Evaluate Refractory Oxide Crucible Materials by Induction Melting of Titanium and Titanium Alloys	D. E. Niesz/ C.A. Alexander/ N.M.Griesenauer	S. R. Lyon	October 1, 1971	May 13, 1972
IV	Control of Deformed Beta Grain Structure in Titanium Alloys by Alloying Additions	R. A. Wood/ D. N. Williams	A. M. Adair		
V[b]	Multiple Component Alloying to Achieve Superior Solid Solution Strengthening	E. W. Collings	H. L. Gegel	August 1, 1972 (Anticipated)	
VI	Low Temperature Mechanical Treatments to Enhance Formability of Alpha Titanium Alloys	J. D. Boyd	S. Fujishiro	January 1, 1972	June 15, 1972
VII	Fracture Toughness-Strength Relationships in High Purity Maraging Alloys Heat Treated to 220-240 ksi Tensile Strength	C. W. Marschall/ A. R. Rosenfield	T.M.F. Ronald		
VIII	(To be determined)				

(a) Tasks A-D are BCL initiated and Tasks I-VIII are AFML initiated.

(b) This Task replaces the original Task V, "New High Temperature Columbium Alloys". The AFML scientist who was to have cognizance of this Task was F. Ostermann, who has since left the Air Force.

TASK A

MICROSTRUCTURAL SYNTHESIS IN COMBINED PRECIPITATION HARDENED-DISPERSION STRENGTHENED (PH-DS) ALUMINUM ALLOYS

by

B. A. Wilcox

INTRODUCTION

Work on Ni-base superalloys by Benjamin[1] has shown that it is possible to combine precipitation hardening by γ' and dispersion strengthening by Y_2O_3 and ThO_2. This research resulted in the development of IN 853 which has the following nominal composition: Ni-20 w/o Cr-1.5 w/o Al-2.5 w/o Ti-2.5 v/o Y_2O_3. The γ' precipitates result in low temperature strengthening (to ~ 800°C) and the dispersoids promote a stable elongated grain structure (high grain aspect ratio[2]) which results in high temperature (~ 800 - 1100°C) strength equivalent to TD Nickel.

One objective of this task was to apply this concept to synthesize 7075 and 2024 precipitation hardening aluminum alloys with a high volume fraction of dispersoid (> 10 vol.% Al_2O_3). A powder metallurgy approach was employed, where ribbon of melt spun[3] 7075 and 2024 alloys were ball milled to fine flake, compacted and extruded. Hereafter, these alloys are designated as PH-DS 7075 and PH-DS 2024.

It was reported previously[3] that 7075 aluminum compacted directly from melt spun ribbon (without ball milling) had a very fine equiaxed grain size of 1 to 10 μm which resulted in high temperature superplastic tendencies. This alloy had a low dispersoid content, about 1 vol.% Al_2O_3. A secondary objective of this task was to further examine the superplastic

behavior in 7075 and 2024 alloys produced in this fashion. Hereafter these alloys are designated MS 7075 and MS 2024.

EXPERIMENTAL

The melt spun ribbon was produced by a method described previously[3] and Figure A-1 illustrates the morphology of such ribbon. In Figure A-1(b) it is seen that the ribbon surface was non-uniform with a high degree of porosity and numerous surface asperities.

The PH-DS alloys were fabricated in the following way. The melt spun ribbon of 7075 and 2024 was ball milled to fine flake (~ 0.25 μm thick) by Alcan Metal Products of Elizabeth, New Jersey.* The processing to extruded rod was as follows:

(1) The powder was outgassed under argon for 3 hours at 450°C, followed by vacuum outgassing for 3 hours at 450°C.

(2) Cylindrical pellets were hot pressed at 450°C and 7000 psi for 2 hours. This yielded pellets which were 75-80% of theoretical density.

(3) The pellets were canned in $3\frac{1}{8}$-inch diameter 6061 aluminum billets and extruded 36:1 at 350°C.

The MS alloys were consolidated by essentially the same route, with the exception of an initial cold pressing of the ribbon to pellets of about 50% of theoretical density. For comparison purposes, billets of commercial 7075 and 2024 were extruded under the same conditions.

---

* It was originally intended to similarly ball mill melt spun ribbon of a highly alloyed 7000-series alloy (Al-10Zn-3Mg-2Cu-1.5Mn-0.2Cr), but the charge was inadvertently destroyed during milling.

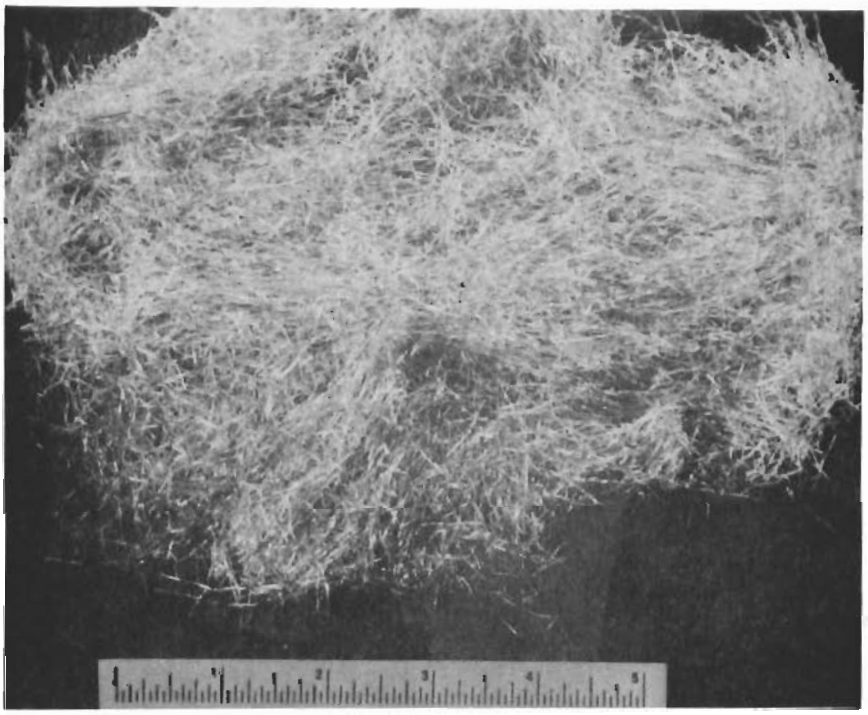

(a)

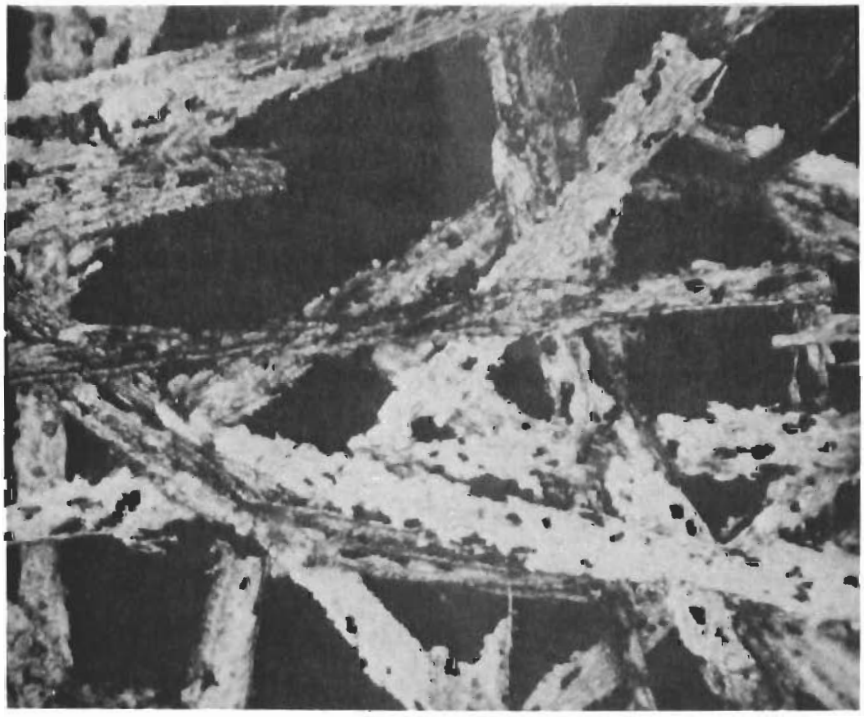

(b)

FIGURE A-1. Examples of melt-spun 7075 aluminum ribbon (a) showing macroscopic features, (b) higher magnification showing porosity and surface asperities, 25X.

RESULTS AND DISCUSSION

Combined Precipitation Hardening and Dispersion Strengthening

The optical microstructures of as-extruded 2024 and the same alloy heat treated to the T6 condition are shown in Figure A-2. The elongated heavily worked extruded structure is typical of SAP type alloys. The 500°C anneal used in solution treating to the T6 condition did not recrystallize this alloy, as seen in Figure A-2(b). The transmission electron micrograph in Figure A-3 shows the high density of second phase particles (presumably mostly Al_2O_3), which resemble those in some SAP-type alloys.[6] If it is assumed that an Al_2O_3 film, about 0.015 μm thick[7], formed on each surface of the 0.25 μm thick flake there would be 12 volume percent alumina present. The extrusion process fragments this Al_2O_3 skin producing the dispersed particles. The microstructures of PH-DS 7075 were essentially the same as those for PH-DS 2024.

The PH-DS alloys were chemically analyzed for major alloying constituents and the results are compared in Table A-1 with typical values

TABLE A-1. CHEMICAL ANALYSES (WEIGHT PERCENT) OF PH-DS ALLOYS COMPARED WITH TYPICAL VALUES FOR CORRESPONDING COMMERCIAL ALLOYS

Alloy	Element			
	Mg	Cu	Zn	Cr
PH-DS 7075	2.2	1.5	5.5	0.1
Commercial 7075	2.5	1.5	5.5	0.2
PH-DS 2024	1.3	4.0	-	-
Commercial 2024	1.5	4.5	-	-

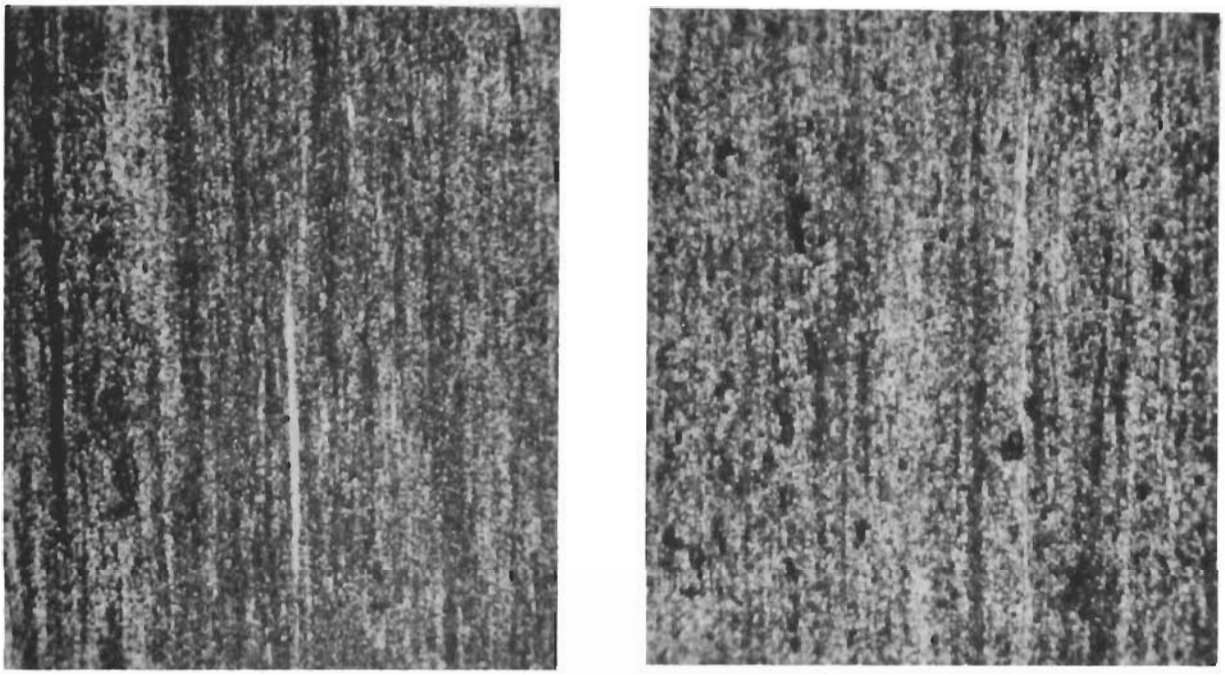

(a) As-extruded. 500X (b) Heat treated to T6 condition, 500X

FIGURE A-2. Optical microstructures of PH-DS 2024.

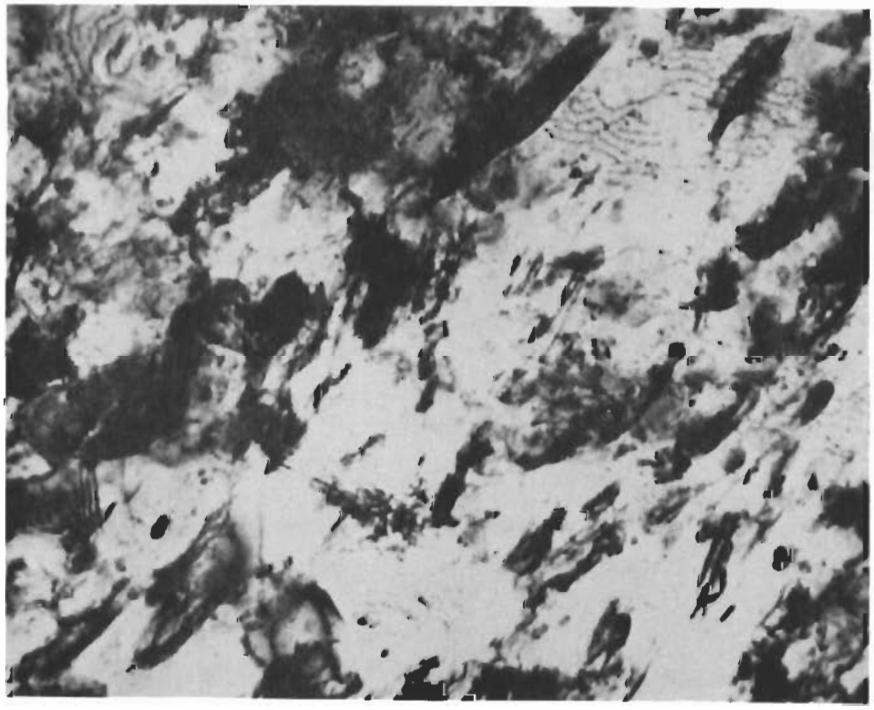

FIGURE A-3. Transmission electron micrograph of as-extruded PH-DS 2024 showing a high density of dispersed Al_2O_3 particles, 40,000X.

for commercial alloys. The comparative analyses are in reasonable accord, suggesting that no substantial depletion of the major alloying constituents occurred during synthesis of the PH-DS alloys.

Tension tests on the as-extruded PH-DS alloys were conducted from 25°C to 450°C at a strain rate of 0.01 min^{-1} and the results are given in Table A-2. As is typical with SAP type alloys, the ductilities were low

TABLE A-2. TENSILE PROPERTIES OF PH-DS 7075 AND PH-DS 2024 AS A FUNCTION OF TEMPERATURE

Condition	Test Temperature, °C	0.2 % Y.S., psi	UTS, psi	Total Elongation, %
		PH-DS 7075		
As-extruded	25	54,300	59,100	0.9
As-extruded	100	48,300	50,700	0.9
As-extruded	200	32,900	34,400	4.5
As-extruded	300	25,800	26,500	1.3
As-extruded	400	18,500	18,600	0.5
As-extruded	450	16,000	16,100	0.4
T6 Condition[(a)]	25	53,800	57,200	0.9
		PH-DS 2024		
As-extruded	25	55,600	61,100	1.1
As-extruded	100	48,900	55,000	1.5
As-extruded	200	37,200	39,400	2.6
As-extruded	300	28,700	29,300	1.0
As-extruded	400	20,100	20,200	0.4
As-extruded	450	13,000	13,300	0.3
T6 Condition[(b)]	25	50,200	56,400	1.3

(a) T6 Condition for 7075 was: SHT 1 hr 500°C, W.Q., age 24 hrs 120°C.

(b) T6 Condition for 2024 was: SHT 1 hr 500°C, W.Q., age 13 hrs 190°C.

(~ 0.5 - 4.5% elongation). Also shown in Table A-2 are room temperature tensile properties of PH-DS 7075 and PH-DS 2024 heat treated to the T6 condition. The yield strengths of both alloys are slightly lower than

corresponding values in the as-extruded condition indicating that the anticipated additional hardening by precipitation was not realized. It is unlikely that this lack of heat treatment response is associated with matrix composition changes (see Table A-1). To examine the possibility that resolution of precipitates during heat treating was retarded by the PH-DS microstructure, specimens were solution annealed 5 hours at 500°C (customary annealing is 1 hour), water quenched and aged. The resulting room temperature yield strengthes were 46,700 psi and 48,200 psi for PH-DS 7075 and PH-DS 2024, respectively. These values are lower than those obtained for the conventional T6 treatment and suggest that the additional solution annealing time at 500°C served merely to remove more of the dislocation substructure. The lack of precipitation hardening is not understood. It may be that the kinetics of precipitation are drastically altered by PH-DS microstructures, that precipitates nucleate preferentially on the Al_2O_3 particles, or that the normal precipitates do not form.

The yield strength of as-extruded PH-DS 7075 as a function of temperature is compared in Figure A-4 with values from the literature for 7075-T6 and a SAP alloy containing 14 volume percent Al_2O_3. A similar comparison for 2024 alloy is made in Figure A-5. At room temperature the PH-DS alloys are about 17,000 psi stronger than SAP 865, and the PH-DS 2024 strength is equivalent to commercial 2024-T6 (Y.S. = 55,000 psi). Thus in this case, although not heat-treatable, the PH-DS 2024 microstructure results in a yield strength equivalent to 2024 containing the relatively coarse S' precipitates arising from the T6 heat treatment. The PH-DS alloy strengths are lower than those of commercial alloys heat treated to optimum strength (7075-T6 and 2024-T81) up to about 250°C, where the precipitates in commercial alloys severely overage.

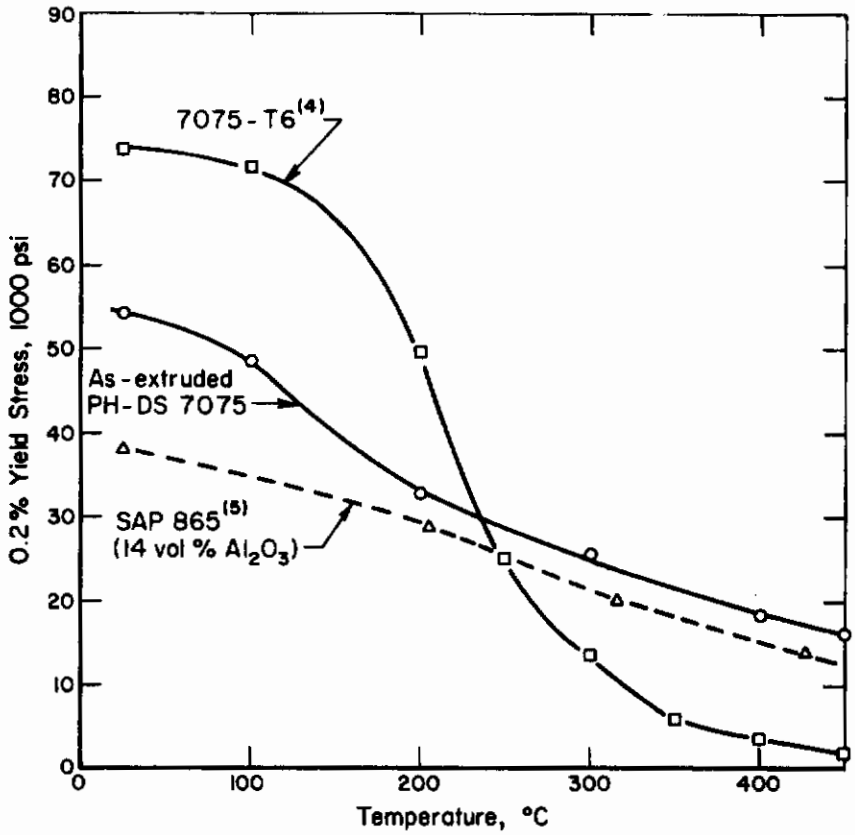

FIGURE A-4. Yield strength of as-extruded PH-DS 7075 as a function of temperature, compared with data from the literature on commercial 7075-T6 and a SAP alloy.

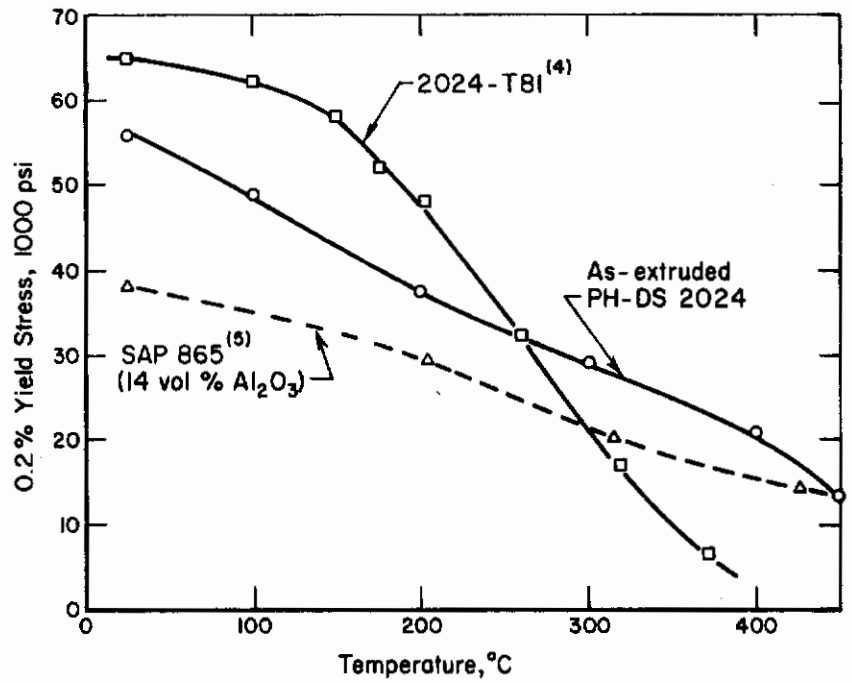

FIGURE A-5. Yield strength of as-extruded PH-DS 2024 as a function of temperature, compared with data from the literature on commercial 2024-T81 and a SAP alloy.

An interesting observation is that the yield strength of the PH-DS alloys is greater than SAP-865 from 25-400°C. Thus an increment in strength is realized, possibly due to some solid solution strengthening combined with a small strengthening increment from the usual insoluble dispersoids (Cr-rich in 7075, and Mn-rich in 2024).

Preliminary studies indicated that substantial creep strengthening was derived from the PH-DS microstructures, in accord with previous results for SAP-type alloys.[5,8] This is illustrated in Figure A-6 which compares the creep curves for commercial 7075-T6 and as-extruded PH-DS 7075 at 450°C and 1500 psi. The curves are plotted semi-logarithmically to facilitate comparison. The PH-DS 7075 test was stopped after 650 hours and a total creep strain of 0.45 percent. The commercial alloy reached this creep strain in 1.7 hours and ruptured after 6.6 hours. The nonuniform creep deformation ("bumpy" creep curve) of the PH-DS 7075 specimen is typical of SAP-type alloys[8], although the origin of this inhomogeneous creep is not known.

Superplastic Tendencies in MS Alloys

Superplastic deformation of alloys has received considerable attention in recent years, as is reflected by a number of review articles on this subject.[9-12] Previous work[3] which has shown that MS 7075 can be deformed ~ 200% at 400°C provided the initiative to undertake the present study.

The microstructures of MS 7075, MS 2024 and their commercial counterparts are shown in Figures A-7 and A-8 after having been annealed for 1 hour at 500°C and furnace cooled. This is the solution annealing temperature for the T6 heat treatment. Since all deformation studies were at elevated temperatures, the quench plus ageing treatments were omitted because precipitates would rapidly overage and essentially not affect the flow properties.

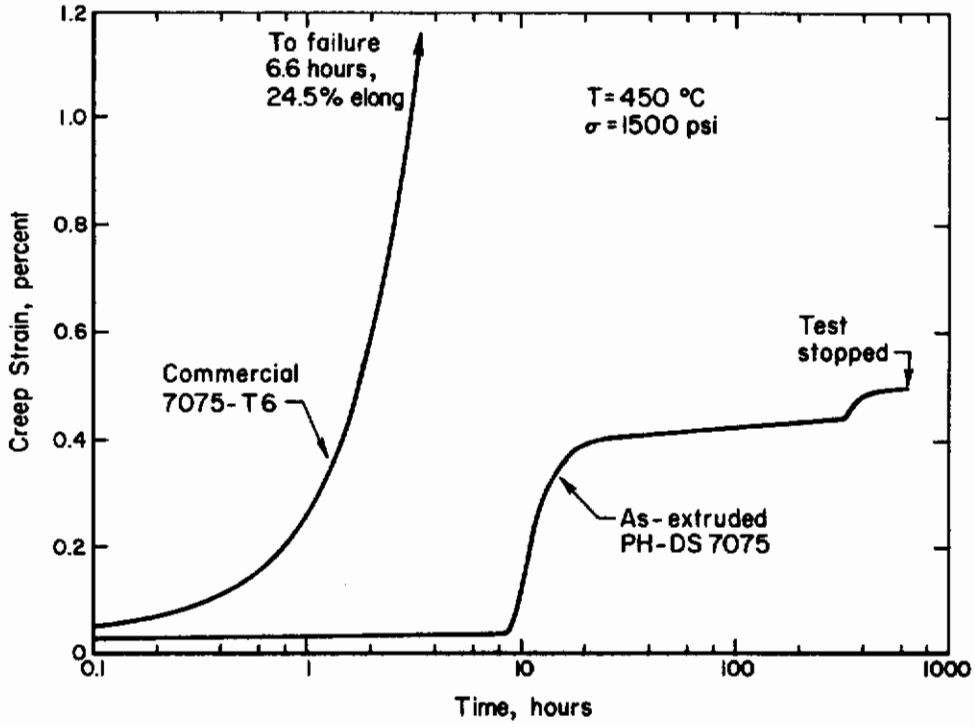

FIGURE A-6. Comparison of creep behavior at 450°C between PH-DS and commercial 7075.

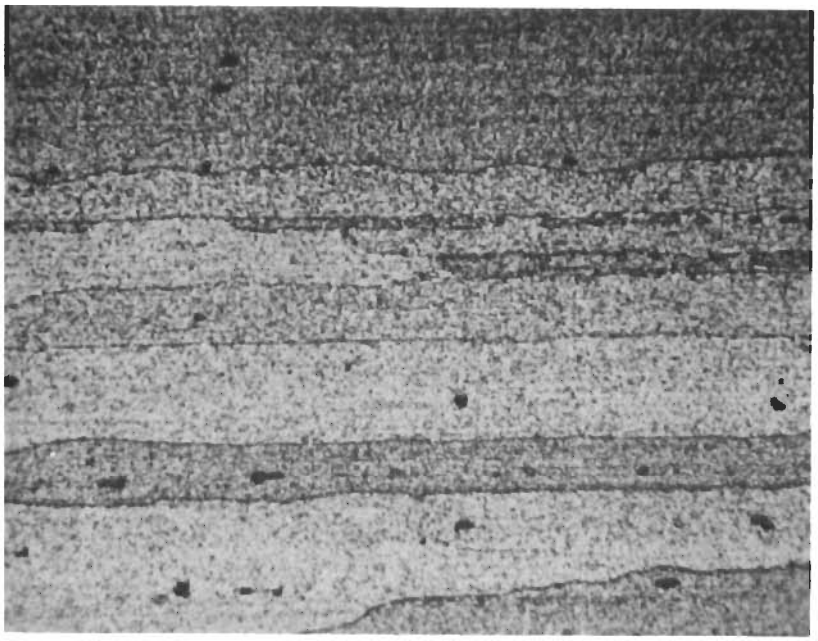

(a) Commercial 7075. 500X

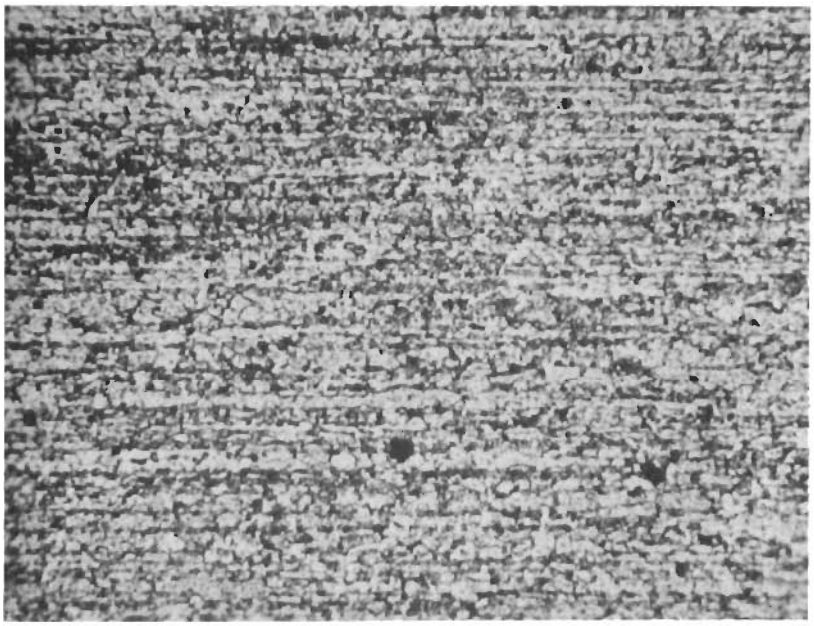

(b) MS 7075. 500X

FIGURE A-7. Commercial and melt spun 7075, extruded and annealed 1 hour at 500°C.

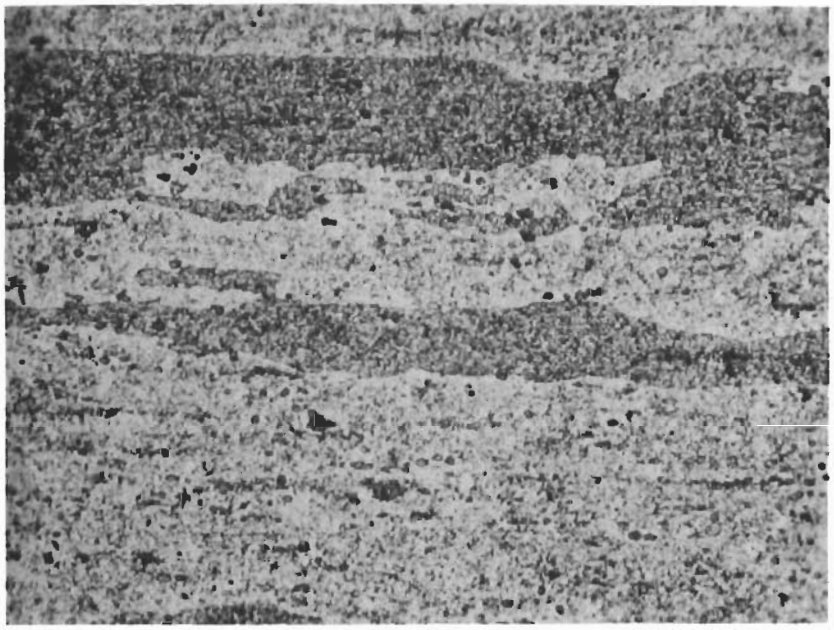

(a) Commercial 2024. 500X

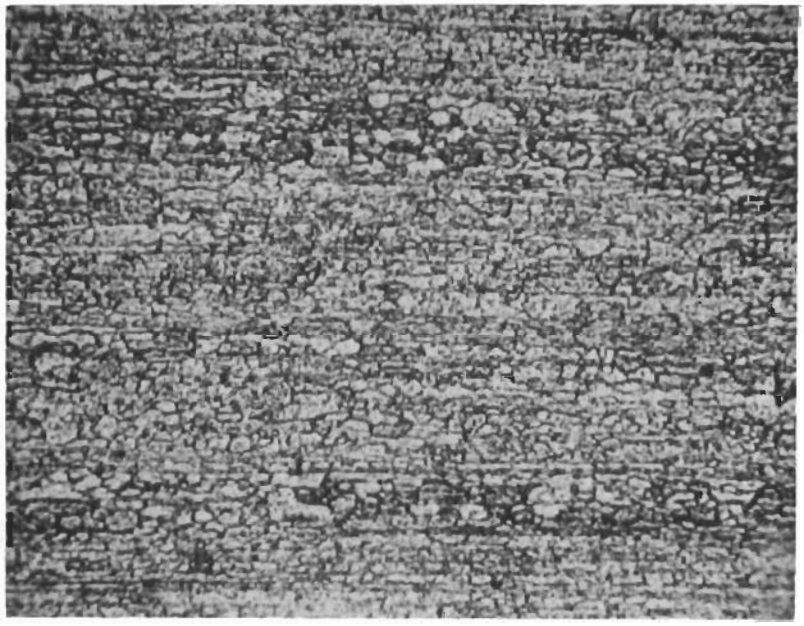

(b) MS 2024. 500X

FIGURE A-8. Commercial and melt spun 2024, extruded and annealed 1 hour at 500°C.

It is seen that the commercial alloys have coarse elongated recrystallized grains, whereas the MS alloys have a fine equiaxed grain structure with grains 1 to 10 μm in diameter.

The MS alloys were deformed in tension in an Instron over the temperature range 350-490°C at various cross-head speeds ranging from 0.002 to 20 in./min.* For selected comparisons, the commercial alloys were deformed at 0.02 in./min over the temperature range 350-490°C. The results of the deformation studies are given in Table A-3, and Figures A-9 through A-12 compare the behavior of commercial and MS alloys and illustrate the influence of strain rate on ductility and flow stress of the MS alloys.

Figure A-9 plots the total elongation of all four alloys as a function of temperature for a cross-head speed of 0.02 in./min. It is seen in all cases that the MS alloys are more ductile than the corresponding commercial alloys. There is very little temperature dependence of the total elongation, with the exception of MS 2024 which has a sharp maximum in ductility (160% elongation) at 450°C. The ductility of the MS 7075 alloy would undoubtedly decrease at lower temperatures.

As anticipated from previous studies on superplasticity, the flow stresses of the fine-grained MS alloys were substantially lower (2000-4000 psi) than the corresponding commercial alloys. This is illustrated in Figure A-10.

The influence of crosshead speed on ductility of the MS alloys at 450°C is shown in Figure A-11. Here it is evident that there is a sharp maximum for both alloys, at 0.2 in./min for MS 7075 and at 0.02 to 0.2 in./min for MS 2024. The strain rate sensitivity, m, was determined at 450°C, where m is defined by

---

* The gauge lengths of all specimens were 1 inch.

TABLE A-3. TENSILE DEFORMATION OF MS 7075 AND MS 2024 AS A FUNCTION OF STRAIN RATE AND TEMPERATURE

Material	Temp., °C	Crosshead speed, in./min	Initial Flow Stress, psi	UTS, psi	% Total Elongation
M.S. 7075	450	0.002	1080	1230	50
M.S. 7075	450	0.02	1530	1760	110
M.S. 7075	450	0.2	2660	2900	185
M.S. 7075	450	2.0	5380	5380	130
M.S. 7075	450	20.0	-	3400	25
M.S. 7075	475	0.02	1130	1270	125
M.S. 7075	400	0.02	2730	3090	125
M.S. 7075	350	0.02	4750	5570	125
Commercial 7075	350	0.02	6700	7350	38
Commercial 7075	400	0.02	3600	4070	39
Commercial 7075	450	0.02	3400	3650	45
Commercial 7075	475	0.02	3070	3300	46
M.S. 2024	450	0.002	1700	2060	35
M.S. 2024	450	0.02	2020	2310	160
M.S. 2024	450	0.2	3630	3910	160
M.S. 2024	450	2.0	6180	6270	130
M.S. 2024	450	20.0	-	4450	30
M.S. 2024	490	0.02	1070	1170	85
M.S. 2024	400	0.02	4660	4870	85
M.S. 2024	350	0.02	7760	8300	25
Commercial 2024	350	0.02	12,400	13,900	20
Commercial 2024	400	0.02	6360	7000	25
Commercial 2024	450	0.02	3780	4150	30
Commercial 2024	490	0.02	2750	3060	30

$$m = \frac{d \log \sigma}{d \log \dot{\epsilon}} \quad , \qquad (1)$$

where σ = initial flow stress and $\dot{\epsilon}$ = strain rate. Figure A-12 shows a linear relation for MS 2024, whereas for MS 7075 there is a slight increase in the log σ versus log $\dot{\epsilon}$ plot at high strain rates. The m values calculated were

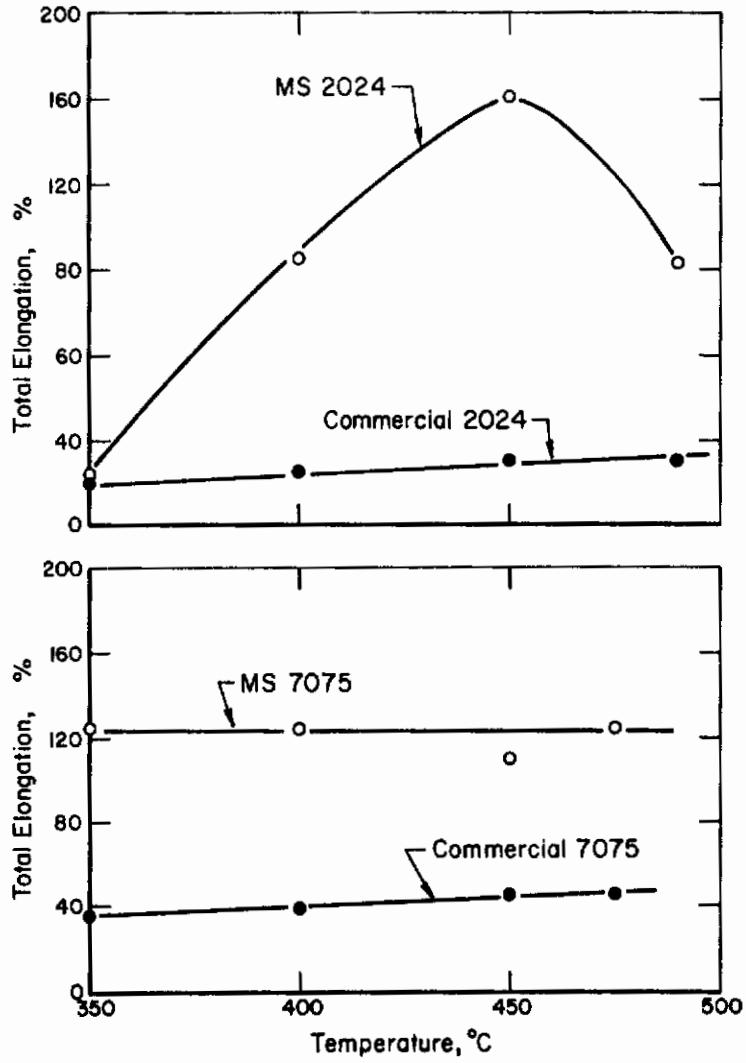

FIGURE A-9. Effect of test temperature on total elongation of MS 7075, MS 2024, commercial 7075 and commercial 2024 tested at a crosshead speed of 0.02 in./min.

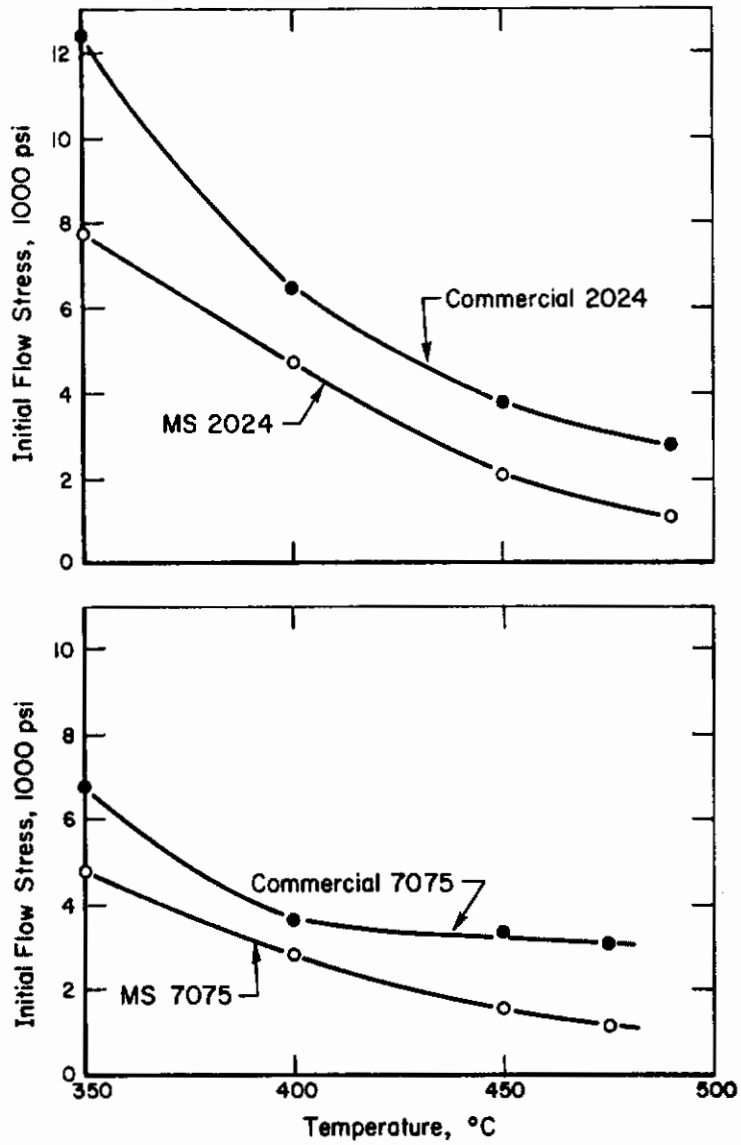

FIGURE A-10. Effect of test temperature on initial flow stress of MS 7075, MS 2024, commercial 7075 and commercial 2024, tested at a crosshead speed of 0.02 min^{-1}, i.e., $\dot{\epsilon}$ = 0.02 min^{-1}.

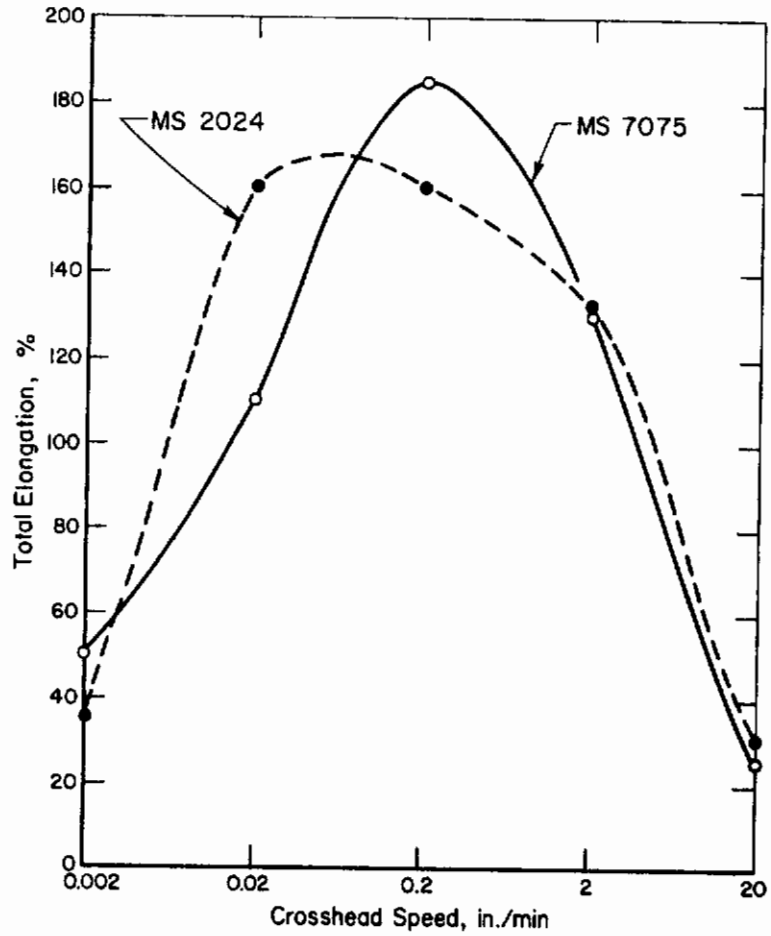

FIGURE A-11. Effect of crosshead speed on total elongation of MS 7075 and MS 2024 tested at 450°C.

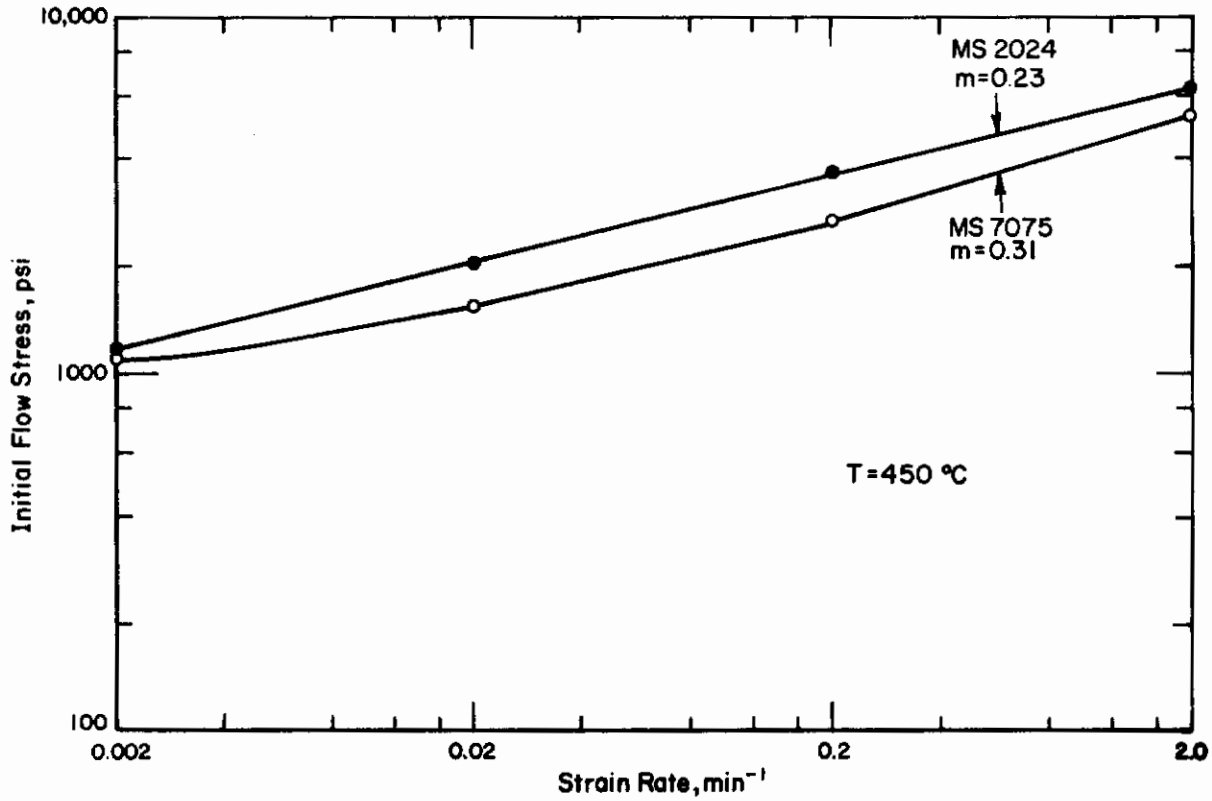

FIGURE A-12. Influence of strain rate on the initial flow stress of MS 2024 and MS 7075 at 450°C.

0.23 for MS 2024 and 0.31 (maximum) for MS 7075. These values are compared in Table A-4 with previous work on materials which exhibit very large degrees of superplasticity. The m values here are typically 0.5 to 0.6.

TABLE A-4. COMPARISON OF STRAIN RATE SENSITIVITY OF MS 2024 AND MS 7075 WITH PREVIOUS WORK ON SUPERPLASTIC ALLOYS

Alloy*	Deformation Temperature, °C	Maximum m	$\dot{\epsilon}$ at max. m, sec^{-1}	Reference
Eutectoid 71 Zn-29 Al	250	0.50	10^{-4} to 10^{-5}	13
Hydrided Mg-6 Zn-0.5 Zr	450	0.58	1.3×10^{-4}	14
Eutectic 67Al-33 Cu	520	0.68	7.0×10^{-3}	15
Eutectic 30 Pb-70 Sn	26	0.51	1.7×10^{-3}	16
MS 2024	450	0.23	3.3×10^{-5} - 3.3×10^{-2}	This Work
MS 7075	450	0.31	3.3×10^{-3} - 3.3×10^{-2}	This Work

* Compositions in weight percent.

In the previous work the slopes of log σ versus log $\dot{\epsilon}$ plots usually decreased at high strain rates, giving maximum values of m. This did not happen in the present work (Figure A-12), although possibly the slope would decrease at strain rates greater than those examined.

The low strain rate sensitivities in the present work and the relatively low total elongations (maximum elongation of 185% compared with superplastic eutectic alloys which have elongations of ~ 1000%) suggest that the MS alloys exhibit only marginal superplasticity. The fact that the elevated temperature flow stresses are measurably lower than those of the commercial alloys (Figure A-10) could, however, be useful in certain metal-forming operations, e.g., press forging.

It is generally accepted that grain boundary sliding is a major mode of deformation in superplastic flow, although there must be accommodation by diffusional processes or dislocation motion to preserve compatibility at grain boundaries. Examination of fractured specimens of the MS alloys suggests that here, too, substantial grain boundary sliding occurred. Figure A-13(a) shows that numerous voids have formed near the fracture, and examination at higher magnifications showed that many of these were on grain boundaries. The scanning electron fractograph in Figure A-13 (b) shows individual grains and groups of grains on the fracture surface. Examination of fractured specimens by transmission microscopy revealed that some of the accommodation deformation must have occurred by dislocation motion. Figure A-14(b) shows a relatively high dislocation density within grains after deformation at 450°C, compared with the nearly dislocation-free structure prior to deformation (Figure A-14(a)).

CONCLUSIONS

Various microstructures have been synthesized in 7075 and 2024 aluminum alloys produced by direct extrusion of melt spun ribbon (MS alloys) or extrusion of compacted powder made by ball milling melt spun ribbon (PH-DS alloys). The PH-DS alloys had a high Al_2O_3 content ($\sim$ 12 volume percent) and did not recrystallize on annealing at 500°C. The MS alloys had about 1 volume percent Al_2O_3 dispersoid and recrystallized to fine equiaxed grains, 1 to 10 μm in diameter, during annealing at 500°C.

The as-extruded PH-DS 2024 and PH-DS 7075 had yield strengths superior to the strongest SAP alloy over the temperature range 25 to 400°C. At temperatures greater than 250°C the PH-DS alloys had higher strength than

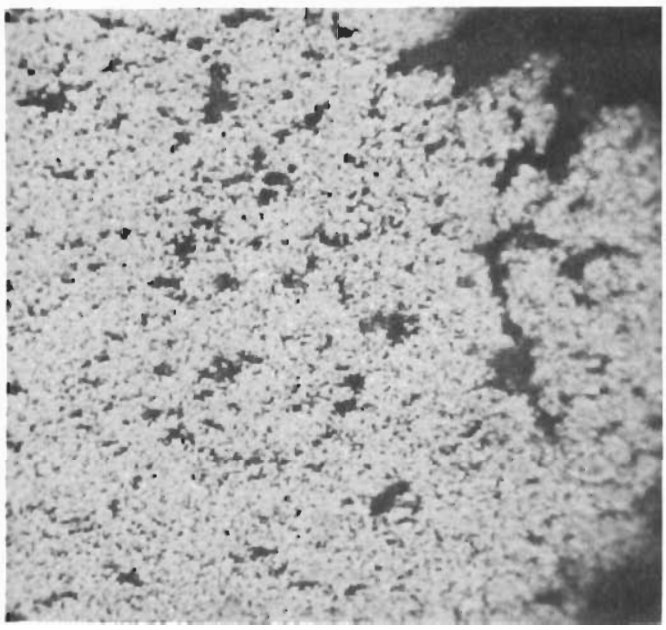

(a) Optical micrograph near fracture. 500X

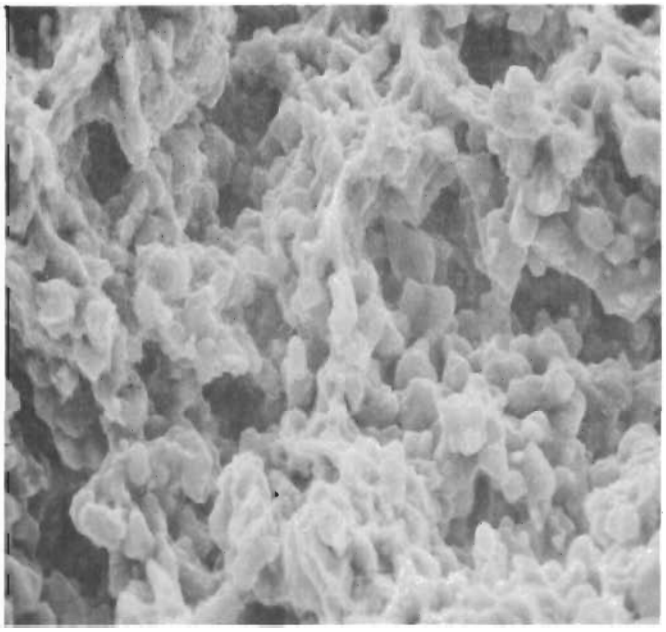

(b) Scanning electron fractograph, secondary electron mode. 1000X.

FIGURE A-13. Fracture of MS 2024 at 450°C and a crosshead speed of 0.2 min^{-1}. This specimen has 160% elongation.

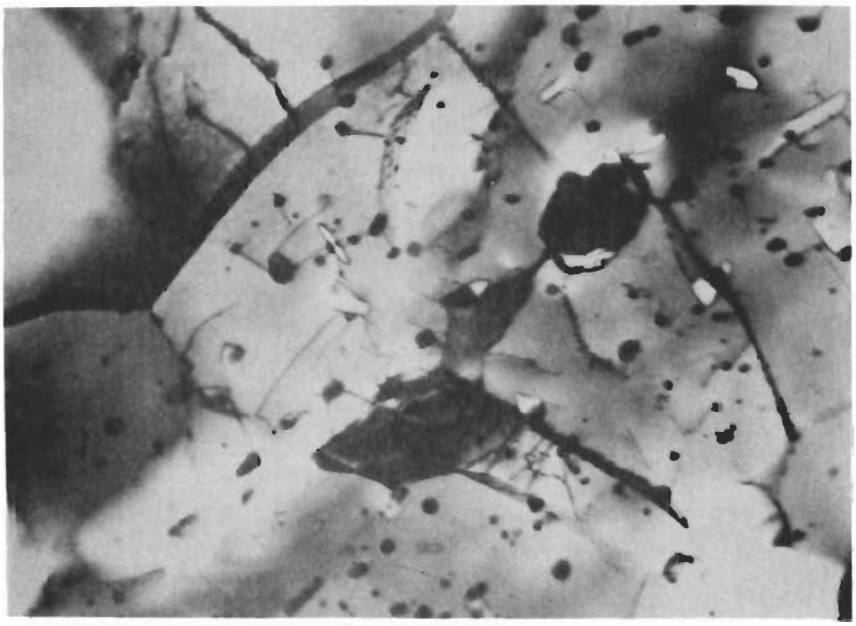

(a) MS 7075, undeformed. 28,000X

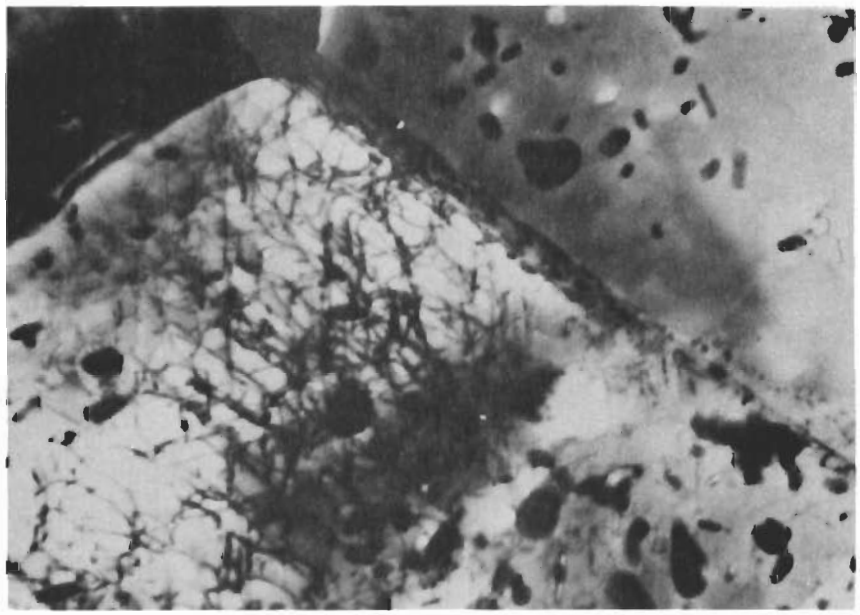

(b) MS 7075 deformed 185% in tension at 450°C and a crosshead speed of 0.2 in./min. 28,000X

FIGURE A-14. Transmission electron micrographs of MS 7075 before and after high temperature tensile deformation.

their commercial counterparts heat treated to optimum strength (7075-T6 and 2024-T81). The room temperature yield strength of as-extruded PH-DS 2024 (55,000 psi) was equivalent to commercial 2024 in the T6 condition. The ductility of PH-DS alloys was low (~ 0.5 to 4% elongation), which is typical of most SAP-type alloys. An attempt was made to heat treat the extruded PH-DS 7075 and PH-DS 2024 to the T6 condition. This was unsuccessful, and the lack of heat treatment response is not understood. The high temperature creep strength of the PH-DS alloys was far superior to commercial alloys.

The fine equiaxed grains in extruded and annealed MS alloys resulted in superplastic tendencies. Elongations as high as 185% were observed, and the total elongation at 450°C was a function of strain rate, the maximum ductilities occurring at crosshead speeds of 0.2 in./min (MS 7075) and 0.02 to 0.2 in./min. (MS 2024). The flow stress of MS alloys was 2000 to 4000 psi lower than commercial 2024 and 7075 over the temperature range 350-475°C. The strain rate sensitivity parameter, m, was 0.23 for MS-2024 and 0.31 for MS-7075. These values are considerably lower than truly superplastics alloys; i.e., those with total elongations of ~ 1000%, where m = 0.5 to 0.6. It is concluded that the MS 2024 and MS 7075 alloys exhibit only marginal superplasticity.

RECOMMENDATIONS

The PH-DS 2024 and PH-DS 7075 alloys are the strongest SAP-type alloys ever produced even though they do not respond to heat-treatment. Future developmental research to exploit the excellent high temperature strength properties would be warranted if definite applications could be

found. It is recommended that no further exploratory research be conducted at this time.

Research on MS alloys has provided guidelines for synthesizing aluminum alloys with superplastic tendencies. The fine equiaxed grains in MS 2024 and MS 7075 result in marginal high temperature superplasticity. The relatively low flow stresses could be beneficial in some metalworking operations, such as press forging. When applications develop which need superplastic forming capabilities for aluminum alloys, further developmental research on MS alloys should be undertaken. However, it is recommended that, at present, no further exploratory research be undertaken.

REFERENCES

(1) J. S. Benjamin, Met. Trans., 1, 2943 (1970).

(2) B. A. Wilcox and A. H. Clauer, Acta Met., 20, 743 (1972).

(3) C. E. Mobley, A. H. Clauer, and B. A. Wilcox, J. Inst. Met., 100, 142 (1972).

(4) J. A. Nock, Jr., "Properties of Commercial Wrought Alloys", Aluminum, Properties, Physical Metallurgy, and Phase Diagrams, Vol. 1, K. R. Van Horn, Ed., American Society for Metals, Metals Park, Ohio, 1967, p. 303.

(5) J. P. Lyle, Jr., "Properties of Powders and Powder Metallurgy Products", ibid., p. 337.

(6) R. S. Goodrich, Jr., and G. S. Ansell, Trans. AIME, 230, 1373 (1964).

(7) F. V. Lenell, A. B. Backensto, and M. V. Rose, Trans. AIME, 209, 124 (1957).

(8) G. S. Ansell and J. Weertman, Trans. AIME, 215, 838 (1959).

(9) E. E. Underwood, J. Met., 14, 914 (1962).

(10) R. H. Johnson, Met. Rev., 15, 115 (1970).

(11) G. J. Davies, J. W. Edington, C. P. Cutler, and K. A. Padmanabhan, J. Mat. Sci., 5, 1091 (1970).

(12) T.Y.M. Al-Naib and J. L. Duncan, Int. J.Mech. Sci., 12, 463 (1970).

(13) A. Bael and M. M. Hutchinson, Met. Sci. J., 3, 1 (1969).

(14) A. Karim and W. A. Backofen, Met. Trans., 3, 709 (1972).

(15) D. L. Holt and W. A. Backofen, Trans. ASM, 59, 755 (1966).

(16) S. W. Zehr and W. A. Backofen, Trans.ASM, 61, 300 (1968).

TASK B

SYNTHESIS OF DISPERSION STRENGTHENED TITANIUM ALLOYS BY ATTRITOR MILLING

by

I. G.Wright and B. A. Wilcox

INTRODUCTION

The aim of this task is to impart improved high-temperature tensile and creep strength (and low-temperature ductility) to α-titanium alloys by means of a dispersion of inert second phase particles. The approach being used is to introduce particles into experimental and conventional alloys using an attritor milling technique[1], and then to compare the structures and mechanical properties of as-extruded alloys with equivalent dispersion-free alloys which have been fabricated by the same route. Major emphasis is being placed on minimizing oxygen and nitrogen contamination during attritor milling.

RESEARCH PROGRESS

Materials

Preliminary studies were undertaken using Ti-6Al-4V powder obtained from the AFML. Powders of commercial purity titanium, Ti-3.5w/oAl, and Ti-7.5w/oAl, prepared by the hydride-dehydride process, have been obtained from Titanium Metals Corp. of America, Henderson, Nevada. The unalloyed Ti represents the base for comparison, the 3.5w/oAl alloy is an alpha solid solution alloy well below the $\alpha + \alpha_2$ field, and the 7.5w/oAl alloy is within the $\alpha + \alpha_2$ field but can be quenched to produce all α. Thus, the alloy selection permits a comparison of dispersed particles on α and on $\alpha + \alpha_2$. It is expected

that the dispersed particles may promote ductilizing in the $\alpha + \alpha_2$ alloy, as in the Cr-ThO_2 system.[2]

Yttria was chosen as the dispersoid because it is thermodynamically very stable in titanium and is commercially available as fine particles. Yttria particles were obtained from Research Chemicals of Phoenix, Arizona. These are mostly in the size range 300 to 1500 Å diameter, with a few larger particles of about 1 μm diameter.

Experimental Progress

Attritor milling produces very fine powders with consequently very large areas of fresh surface. Because of the pyrophoric nature of titanium powder and the desire to minimize oxygen and nitrogen contamination, all of the powder handling is being done in an inert atmosphere. A Szegvari 1-SB attritor has been modified to operate under vacuum or under slowly flowing purified helium, the loading and unloading operations being accomplished in a helium atmosphere by first evacuating the relevant vessels and connector tubing and then backfilling with helium. After attriting, the alloy powder is transferred in a helium-filled sealed glass bottle to an argon-filled glove box, where it is screened, weighed, sampled, and then tamped into mild steel extrusion cans. The extrusion cans are electron beam welded shut and vacuum outgassed at 300°C through a nose tube, and then extruded at a slow speed, at a temperature of 915°C.

The first step in the preparation of these alloys was to precoat the internal surfaces of the attritor and the charge of 0.25 inch diameter carbon-steel balls with the Ti-alloy to be attrited. A charge of 966 grams of Ti-6 w/o Al-4 w/o V alloy powder and 34 grams of Y_2O_3 powder was weighed in air (this titanium alloy powder was relatively old stock and not considered a fire risk), placed in the loading arm of the attritor, and the whole

apparatus evacuated to 10^{-2} torr for 4 hours and then purged with flowing helium for 18 hours. The attriting was started by pouring the powder onto the moving ball charge, and was continued for 50 hours at 210 rpm after which 280 grams of alloy powder were recovered. The coated attritor was thereafter kept under a helium atmosphere.

The next step was to determine the extent of oxygen pickup with attriting time. A further charge of 1000 grams of Ti-6 w/o Al-4 w/o V-3 v/o Y_2O_3 powder was attrited at 180 rpm and samples removed for chemical analysis after 25, 50, 75, and 100 hours. Some resulting analyses performed by National Spectrographic Labs., Inc., Cleveland, are given below.

TABLE B-1. PRELIMINARY CHEMICAL ANALYSES ON Ti-6Al-4V POWDER AND THE SAME ALLOY CONTAINING Y_2O_3 AFTER ATTRITING. ALL VALUES IN WEIGHT PERCENT.

	Ti-6 w/o Al-4 w/o V		Ti-6 w/o Al-4 w/o V-3 v/o Y_2O_3		
	Vendor's Analysis	Battelle Analysis	After 50 hr Precoating (run T1)	After 25 hr at 180 rpm (run T2)	After 50 hr at 180 rpm (run T2)
Iron	0.1199	0.10	0.20	0.14	0.15
Carbon	0.0230	0.026	0.28	0.25	0.33
Oxygen	0.1860	0.15	0.23	0.15	0.15
Nitrogen	0.0148				
Hydrogen	0.0056				

Because of a discrepancy in the sample size submitted to National Spectrographic, the accuracy of the analyses is ± 10% of the quoted values for oxygen. Since the method used to determine the oxygen content involves melting the sample, together with its platinum and iron containers, at approximately 2500°C, it is expected that the oxygen content of the Y_2O_3 would also be

measured so that the expected minimum oxygen content would be 0.15 w/o + 0.751 w/o (from 3 v/o Y_2O_3). Clearly the reported results do not include a contribution from the Y_2O_3, so that it seems possible that the yttria particles, which melt at 2410°C, floated out of the molten sample (melting point of platinum is 1769°C) without melting. These preliminary results seem to indicate that little change in oxygen content occurs during the attriting process, although there is some pickup of carbon and iron.

A duplicate analysis of the same material was made at the AFML with the results shown in Table B-2. From the analyzed yttrium contents in Table B-2, the oxygen levels expected from the Y_2O_3 in the run T2 samples are 0.708, 0.601, 0.717, 0.708, and 0.718 w/o, respectively. Again, it can be seen that the oxygen analyses are inadequate.

Two further batches of Ti-6Al-4V-3v/o Y_2O_3 powder (runs T4 and T5) were attrited for 48 hours at 180 rpm, and canned in mild steel extrusion containers as described above. Then an yttria-free Ti-6Al-4V alloy (run T7) was prepared by the same procedure, the attritor chamber and impeller first being cleaned by pickling for 4 hours in 50/50 HNO_3/HCl, and a new set of balls being precoated with the Y_2O_3-free alloy for 48 hours at 180 rpm (run T6).

Because of the progressive increase in carbon content with attriting time during run T2, which was apparently not related to the iron contamination from the attritor materials, a sulfuric acid trap was included in the helium supply line for runs T5, T6, and T7, and an acetone/solid CO_2 cold trap was placed in the vacuum line for runs T6 and T7 to prevent hydrocarbon contamination from the vacuum system.

The alloy powders from runs T4, T5, and T7 were sampled, canned as described above, and extruded at the AFML at 915°C at 1.5 inches per second and

TABLE B-2. AFML ANALYSES OF ATTRITED POWDERS. ALL VALUES IN WEIGHT PERCENT.

Element	Ti-6 w/o Al-4 w/o V Starting Analysis	Ti-6 w/o Al-4 w/o V-3 Y_2O_3 After 50 h Precoating (run T1)	After 25 h at 180 rpm (run T2)	After 50 h at 180 rpm (run T2)	After 75 h at 180 rpm (run T2)	After 100 h at 180 rpm (run T2)
Fe	0.180	0.192	0.126	0.137	0.140	0.161
C	0.025	0.363	0.258	0.410	0.448	0.733
O	0.154	0.540	0.570	0.810	0.760	0.800
Y	-	2.62	2.53	2.66	2.62	2.66

a reduction ratio of approximately 15:1. Full details of the extrusions are given in AFML Extrusion Data Sheets 4700 and 4701. The analytical results for the powders produced during runs T4 and T5 from National Spectrographic are shown in Table B-3. Doubt still exists about the suitability of this method for analyzing oxygen in Y_2O_3-containing alloys; some reduction in carbon pick-up with the sulfuric acid-trapped helium is apparent.

TABLE B-3. ANALYSIS OF POWDERS PRODUCED BY ATTRITOR RUNS T4 AND T5, WEIGHT PERCENT

Element	Ti-6 w/o Al-4 w/o V-3 v/o Y_2O_3 After 48 hours at 180 rpm (run T4)	(run T5)
Fe	0.12	0.11
C	0.20	0.12
O	> 0.77	> 0.74

An analysis at Battelle was also made of the Y_2O_3-free extruded alloy T7, after the mild steel can had been removed by pickling in 50/50 HNO_3/H_2O and the results are shown in Table B-4. Compared to the Vendor's analysis for this material, the following increases have occurred: iron has increased by 0.07 w/o, carbon by 0.027 w/o, nitrogen by 0.105 w/o, hydrogen by 0.011 w/o (possibly from pickling), and oxygen by 0.112 w/o.

TABLE B-4. ANALYSIS OF EXTRUDED Ti-6Al-4V (attritor run No. T7)

Element	Composition, w/o	Procedure
Fe	0.19	wet chemical analysis
C	0.050	wet chemical analysis
N	0.12	micro-Kjeldahl analysis
H	0.0165	vacuum fusion analysis
O	0.2979	vacuum fusion analysis

Metallographic examination of the as-extruded alloys from runs T4, T5, and T7 reveals the expected elongated structures (Figures B-1 to B-3) parallel to the direction of extrusion. The alloy structure appears to be untransformed alpha with the notable exception of the apparently dispersion-free zones in alloys T4 and T5 (Figures B-1 and B2). The alloys also contain large dark-appearing spherical inclusions which are equally as numerous in the Y_2O_3-containing and Y_2O_3-free alloys, but which are smaller in the dispersion-free alloy.

FUTURE WORK

These alloys will be examined by electron probe microanalysis, after which the size and distribution of the Y_2O_3-dispersion will be determined by transmision and direct replica electron microscopy. Tensile test specimens are being prepared from the as-extruded and extruded plus annealed alloys. The annealing treatment to be used is 950°C for 4 hours in vacuum. Work is under way to prepare c.p. titanium and then Ti-3.5 w/o Al and Ti-7.5 w/o Al alloys by this route, which will be compared to their equivalent dispersion-containing compositions.

REFERENCES

(1) J. S. Benjamin, Met. Trans., 1, 2943 (1970).

(2) B. A. Wilcox, N D. Veigel, and A. H. Clauer, Met. Trans., 3, 273 (1972).

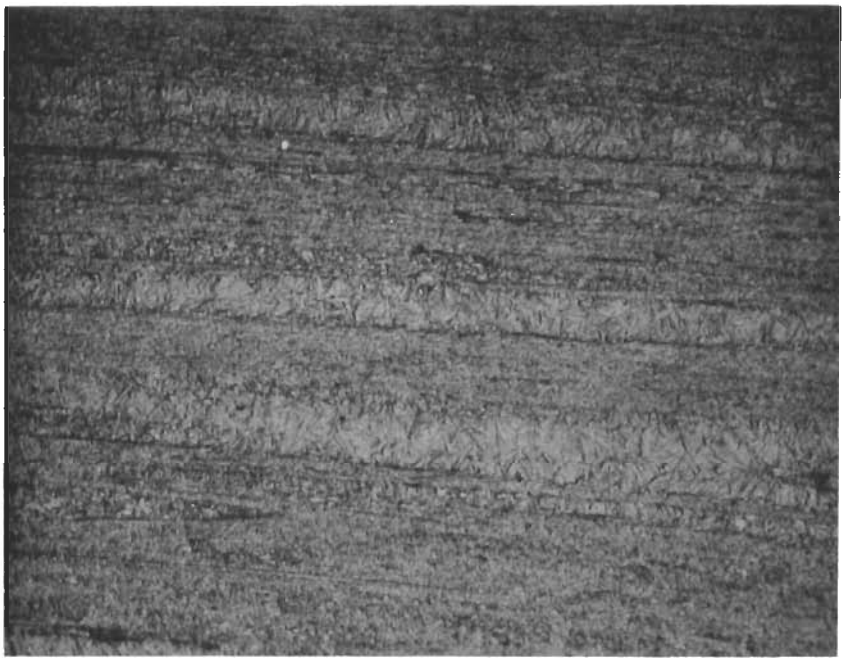

250X

FIGURE B-1. Ti-6 w/o Al-4 w/o V-3 v/o Y_2O_3 (run T4) as extruded, longitudinal section.

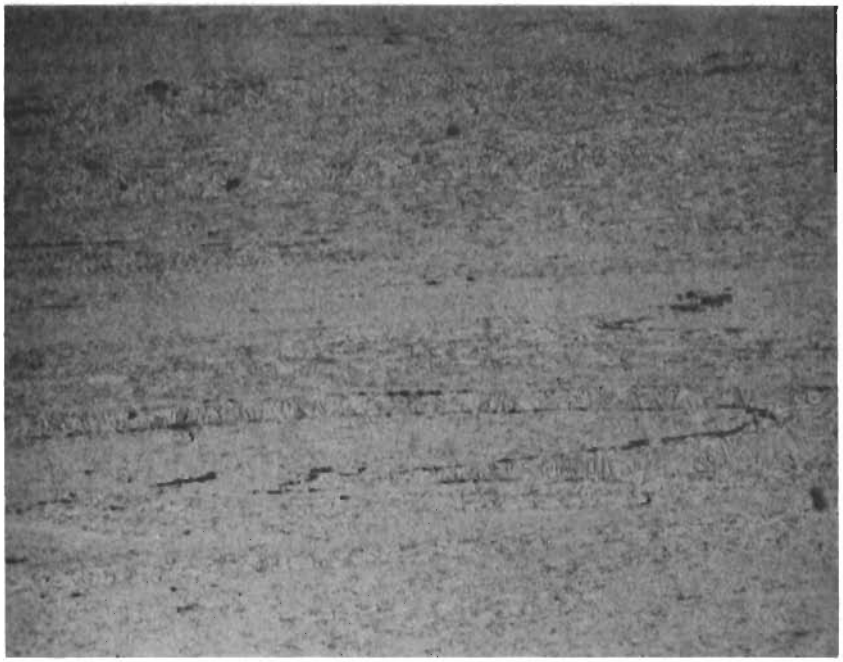

250X

FIGURE B-2. Ti-6 w/o Al-4 w/o V-3 v/o Y_2O_3 (run T5) as extruded, longitudinal section.

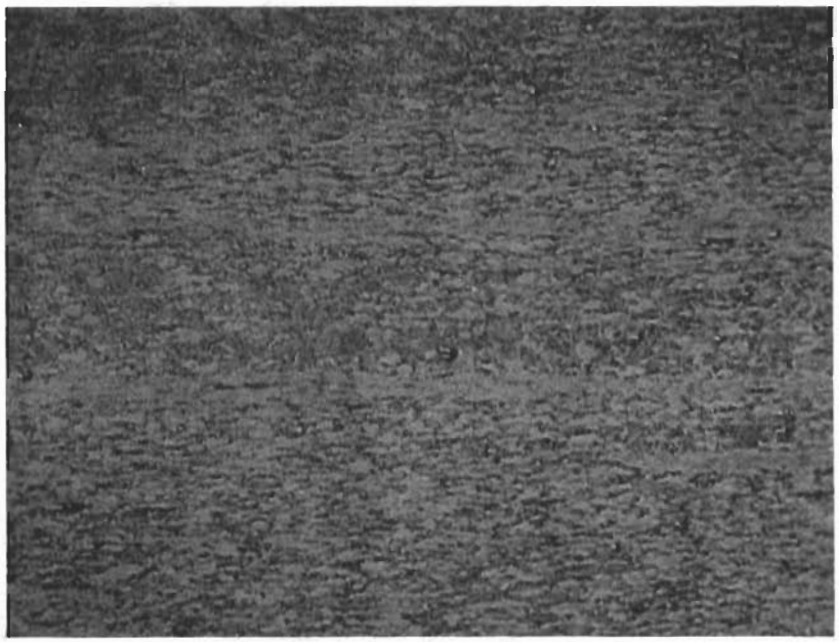

250X

FIGURE B-3. Ti-6 w/o Al-4 w/o V (run T7) as extruded, longitudinal section.

TASK I

EVALUATION OF NEW HIGH TEMPERATURE TITANIUM ALLOYS

by

A. H. Clauer, G. W. Waters, and B. A. Wilcox

INTRODUCTION

In recent years a number of investigators have studied Ti-Al-Ga-base alloys, including research on creep behavior[1,2], ordered phases[3,5], tensile deformation behavior[4,5] and physical and thermodynamic properties[6-8]. The desirability for high temperature titanium alloys with improved creep resistance, coupled with the promising mechanical properties and reasonably low air contamination rates[9] of Ti-Al-Ga-base alloys provided the stimulus for undertaking this task. The objective was to synthesize Ti-Al-Ga-base alloys with different microstructures (e.g., α-annealed and β-annealed) and compare tensile and creep strength, ductility and stability (measured by post-creep ductility) with present alloys.

ALLOYS AND MICROSTRUCTURES

Five alloys were prepared by quadruple arc melting finger ingots, hot rolling at 950°C and hot swaging at 900°C to approximately 1/4-inch diameter rod. The compositions are given in Table I-1. It is well known that addition of dilute amounts of silicon produces silicides which lead to improved high temperature creep resistance. The direct influence of silicides on tensile and creep strength was studied by comparing Alloy 1 (Ti-3.4Al-8.7Ga-0.5Si) with Alloy 5 (Ti-3.4Al-8.7Ga). Alloys 2, 3, and 4 each contain silicon in addition to beta-stabilizing elements, which is a common alloying practice.

TABLE I-1. NOMINAL COMPOSITIONS AND CHEMICAL ANALYSES OF ALLOYS 1-5

Alloy No.		Element (a) Al	Ga	Si	Mo	Cb	Zr	O	H
1	Nominal Composition	3.4	8.7	0.5	-	-	-	-	-
	Analysis	3.39	8.70	0.48	-	-	-	470	90
2	Nominal Composition	3.4	8.7	0.5	1.0	1.0	5.0	-	-
	Analysis	3.39	8.80	0.51	1.00	0.98	5.07	400	60
3	Nominal Composition	3.4	8.7	0.5	1.0	-	-	-	-
	Analysis	3.41	8.80	0.56	1.03	-	-	400	105
4	Nominal Composition	2.3	11.8	0.5	1.0	-	-	-	-
	Analysis	2.34	11.8	0.49	0.97	-	-	360	65
5	Nominal Composition	3.4	8.7	-	-	-	-	-	-
	Analysis	3.46	8.7	-	-	-	-	-	-

(a) In weight percent except O and H in p.p.m.

Various heat treatments were used to determine the α-transus and β-transus, which were found to be $\sim$ 940°C and $\sim$ 975°C, respectively. Two heat-treatments, hereafter designated α-anneal and β-anneal, were employed to produce different microstructures, which are shown in Figures I-1 (α-anneal) and I-2 (β-anneal).* The annealing treatments, in an inert atmosphere, were:

α-anneal: 800°C, 24 hrs, furnace cooled to 550°C, held at 550°C for 25 hrs, furnace cooled to room temperature.

β-anneal: 1060°C, 24 hrs, furnace cooled to 550°C, held at 550°C for 25 hrs, furnace cooled to room temperature.

* Alloy 5 was not examined in the β-annealed condition.

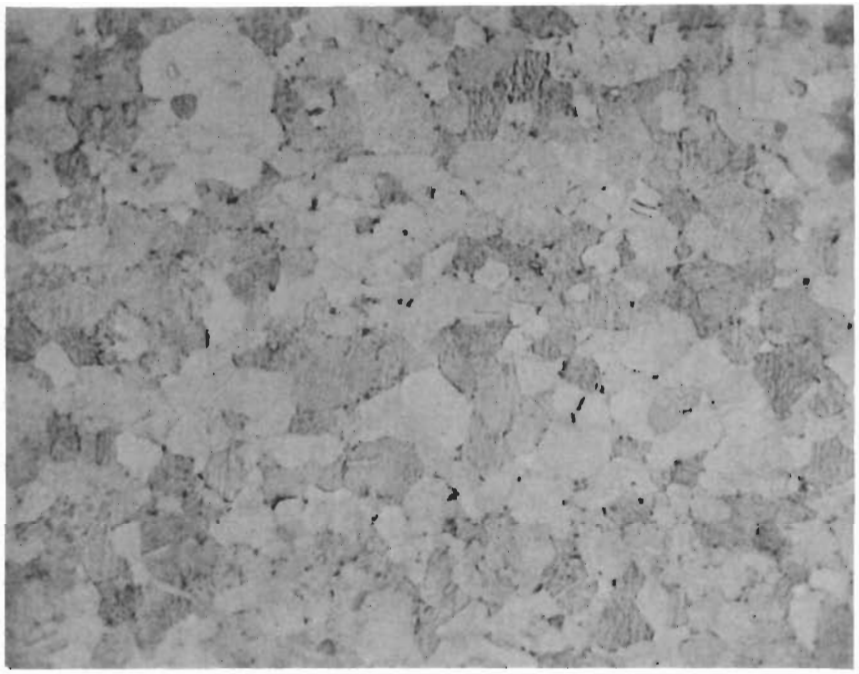

(a) Alloy 1. Ti-3.4Al-8.7Ga-0.5Si, 250X

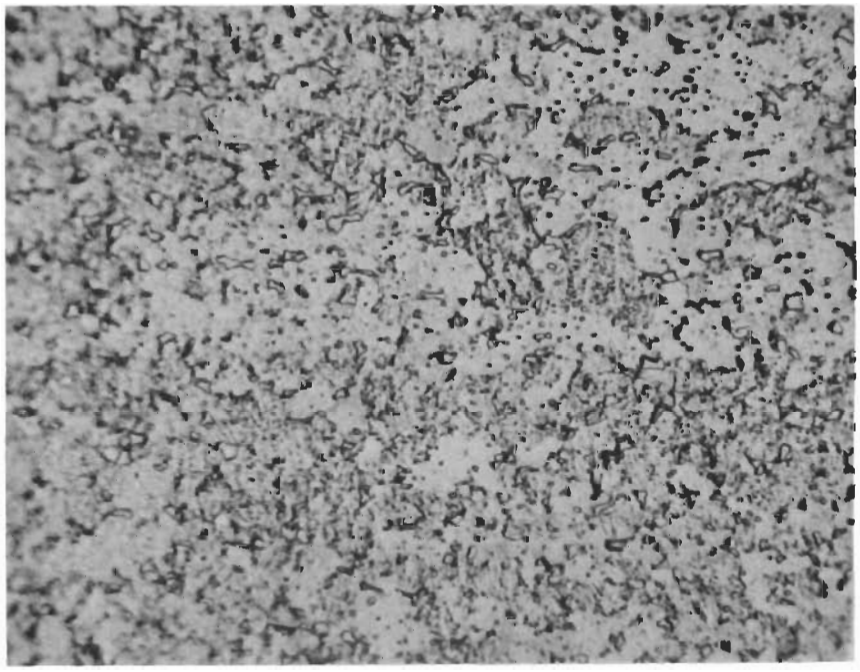

(b) Alloy 2. Ti-3.4Al-8.7Ga-1Mo-1Cb-5Zr-0.5Si, 1000X

FIGURE I-1. Microstructure of Alloys 1 through 5 after α-annealing.

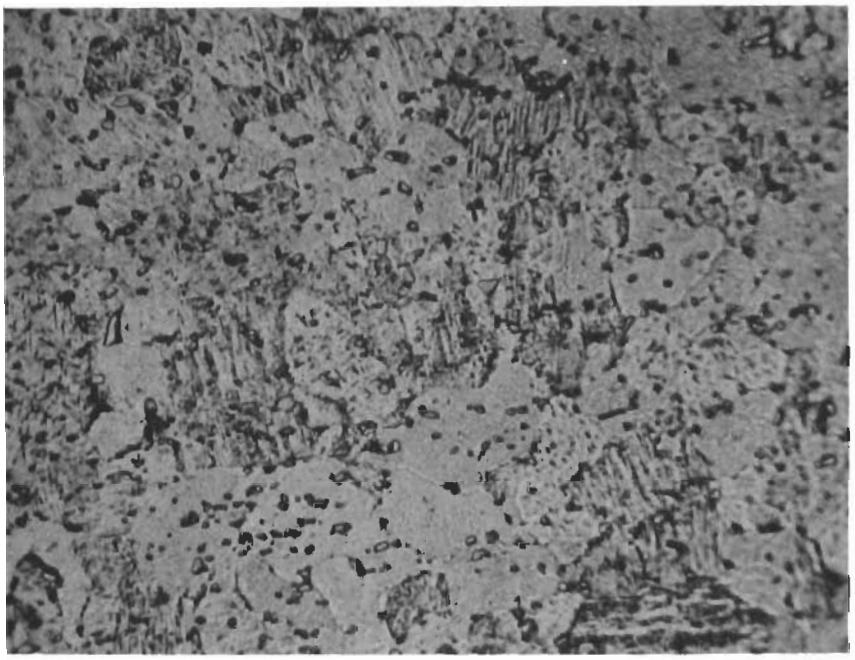

(c) Alloy 3. Ti-3.4Al-8.7Ga-1Mo-0.5Si, 1000X

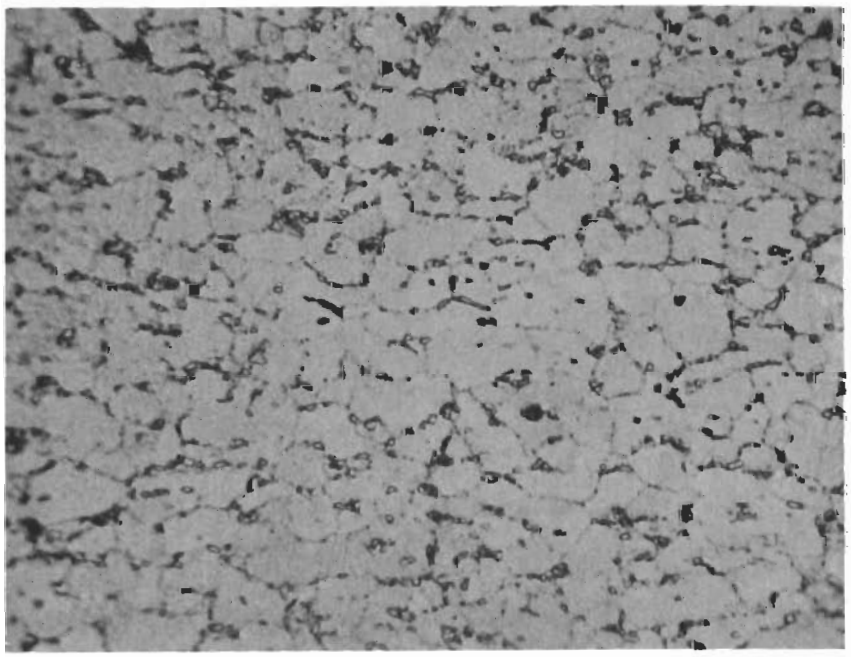

(d) Alloy 4. Ti-2.3Al-11.8Ga-1Mo-0.5Si, 1000X

FIGURE I-1. (Continued).

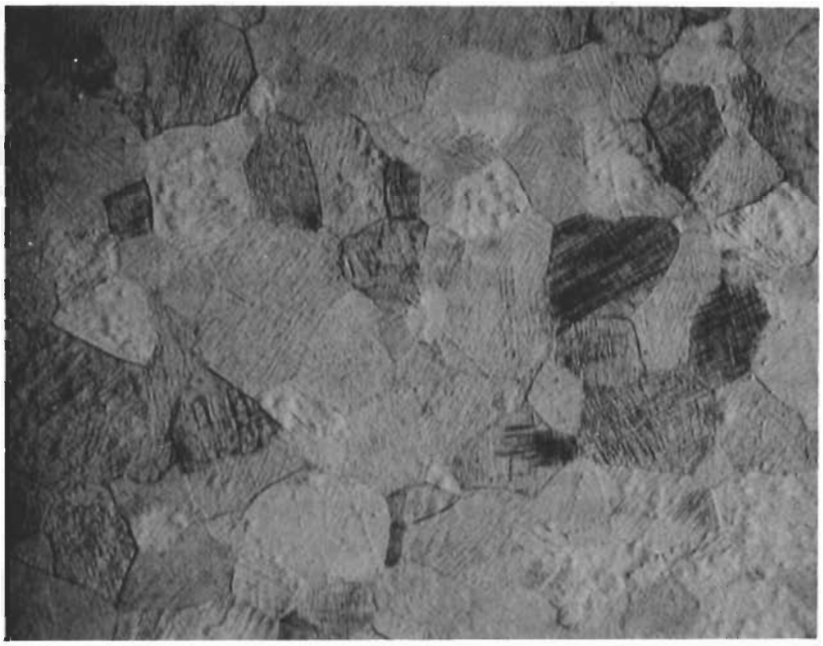

(e) Alloy 5. Ti-3.4Al-8.7Ga, 250X

FIGURE I-1. (Continued).

(a) Alloy 1. Ti-3.4Al-8.7Ga-0.5Si, 100X

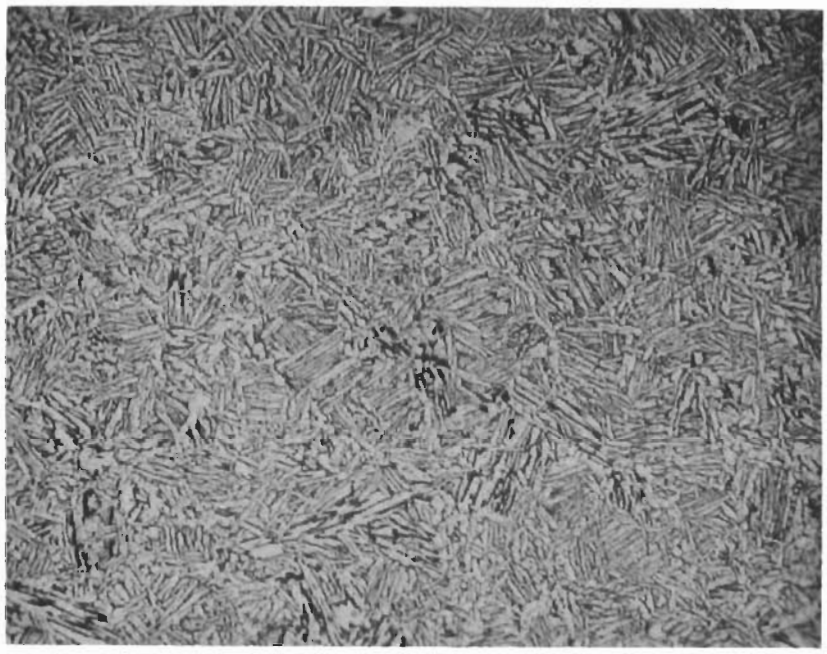

(b) Alloy 2. Ti-3.4Al-8.7Ga-1Mo-1Cb-5Zr-0.5Si, 100X

FIGURE I-2. Microstructure of Alloys 1 through 4 after β-annealing.

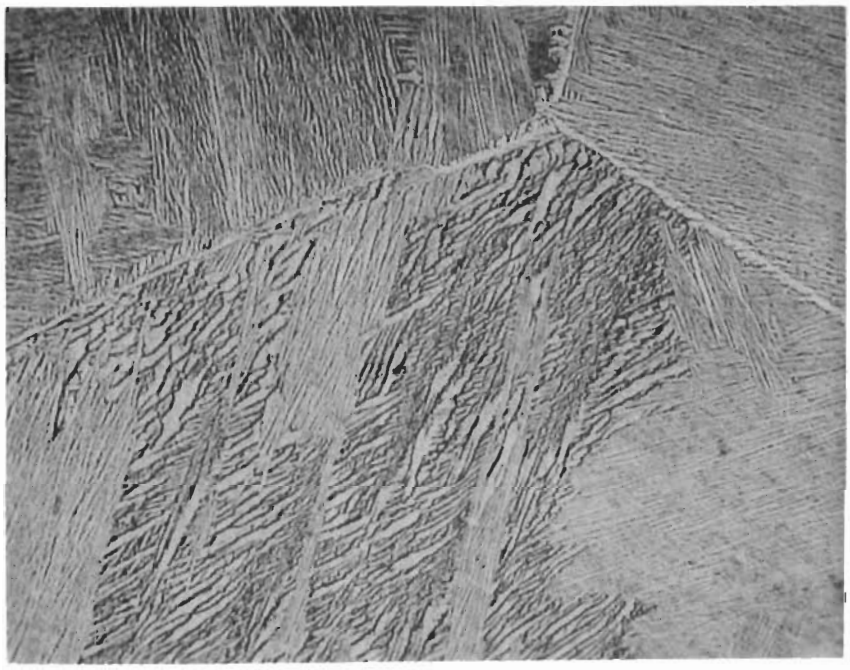

(c) Alloy 3. Ti-3.4Al-8.7Ga-1Mo-0.5Si, 100X

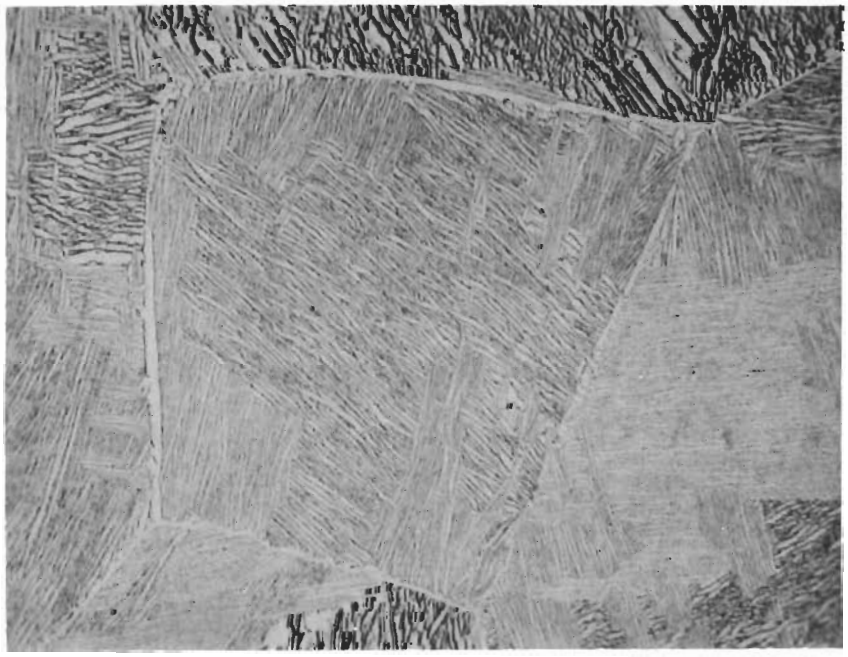

(d) Alloy 4. Ti-2.3Al-11.8Ga-1Mo-0.5Si, 100X

FIGURE I-2. (Continued)

The α-annealed alloys had a relatively fine grain size, ~ 30 μm for Alloy 1, ~ 10 μm for alloys 2,3, and 4 and ~ 60 μm for Alloy 5. The grain sizes resulting from β-annealing were very coarse transformed β, ~ 1000 μm. Each of the α-annealed alloys 1-4 contained dispersed second phase particles, but these were not observed by optical metallography in the β-annealed condition. An attempt was made to identify the particles by electron microprobe analysis on alloys 2 and 4. Specimens were annealed just below the α-transus for a long time (930°C, 72 hrs) to coarsen the particles. The microstructures are shown in Figure I-3 and microprobe X-ray scans for Alloys 2 and 4 are illustrated in Figures I-4 and I-5, respectively. The X-ray scan over particles in Alloy 2 showed peaks for silicon and zirconium, but none for the other alloy additions. It is thus probable that the particles are Ti-Zr silicides such as $(TiZr)_5Si_3$[10], Ti_2ZrTi[11] or $(Zr_3Ti_2)Si_3$[12]. Figure I-5 shows strong peaks for silicon and the possibility of corresponding oxygen peaks (Figure I-5(c)). Again scans across the particles were unable to detect any of the other alloying elements. The particles may be Ti_5Si_3[10] or if indeed oxygen is present possibly a Ti-Si-O compound.

RESULTS AND DISCUSSION

All tensile testing was done in an Instron at a strain rate of 0.01 min^{-1}. Tests at room temperature and 500°C were conducted in air and tests at 700°C were done in vacuum. Creep tests were run at one temperature, 550°C, under constant stress conditions, and the creep strain was measured by LVDT's and recorded continuously as a function of time. The atmosphere was a dynamic vacuum of about 10^{-5} torr, with the exception of several air tests to assess the effect of possible reduction in post creep ductility by contamination.

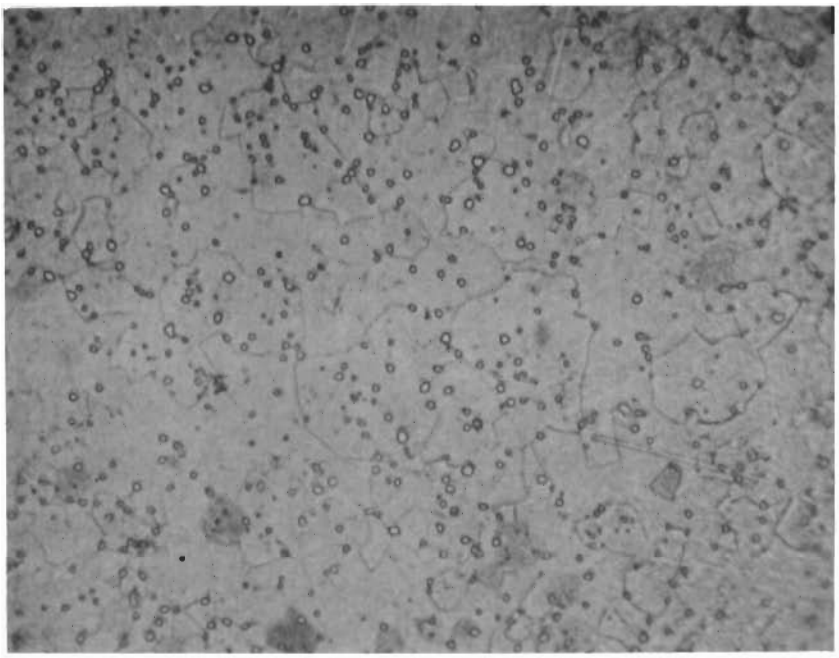

(a) Alloy 2. Ti-3.4Al-8.7Ga-1Mo-1Cb-5Zr-0.5Si, 1000X

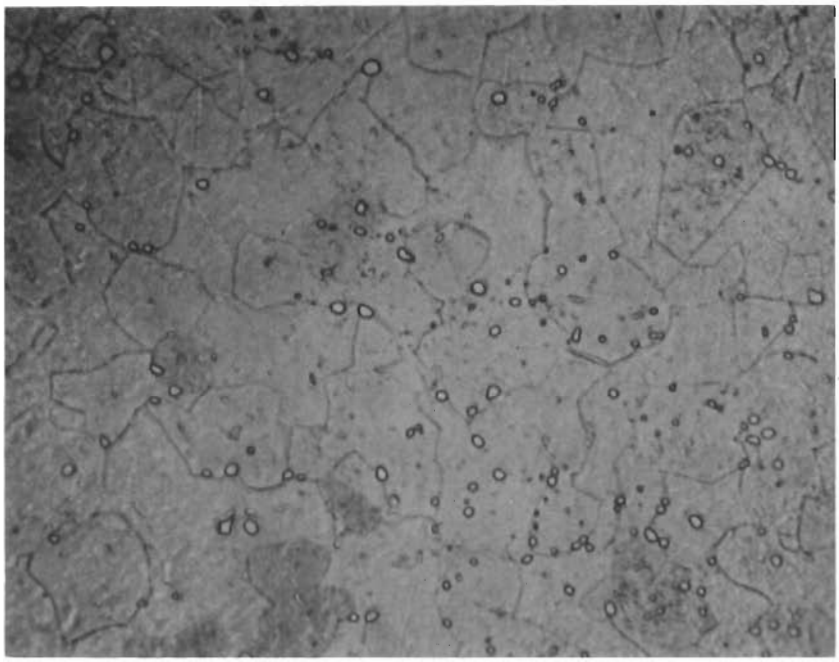

(b) Alloy 4. Ti-2.3Al-11.8Ga-1.0Mo-0.5Si, 1000X

FIGURE I-3. Alloys 2 and 4 after solution-treating for 72 hours at 930°C and water quenching.

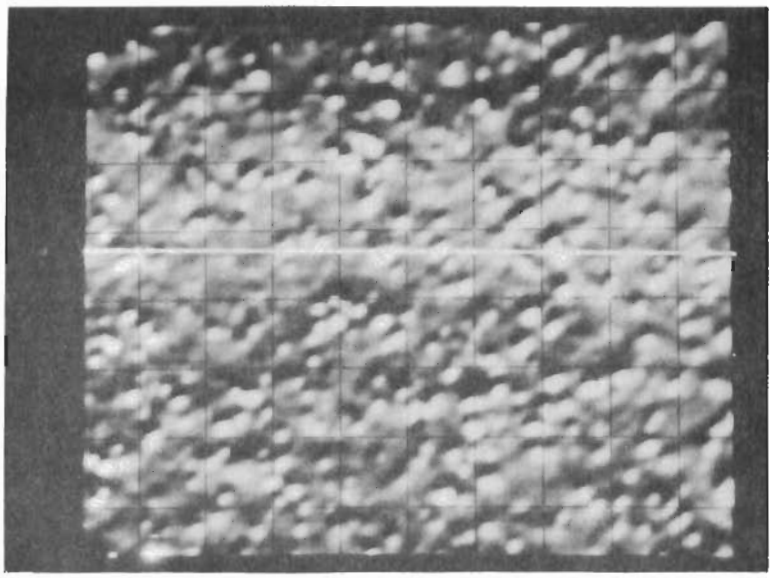

(a) Back-scattered electron photomicrograph, 1000X.

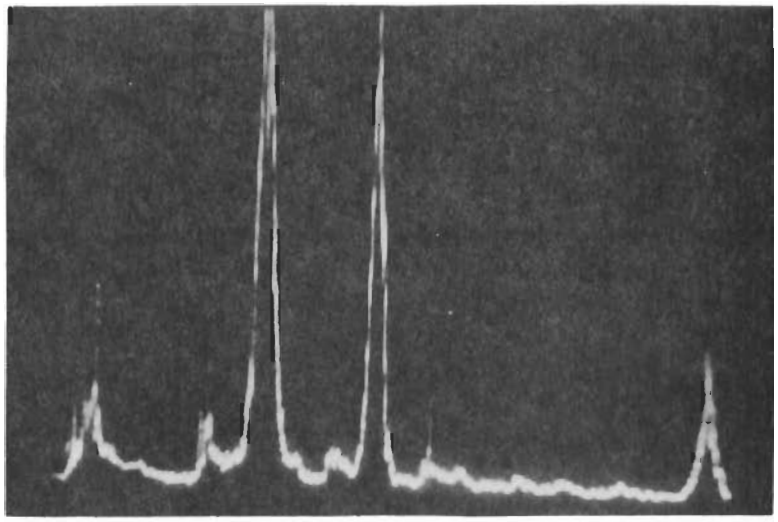

(b) X-ray scan for Si, 1000X.

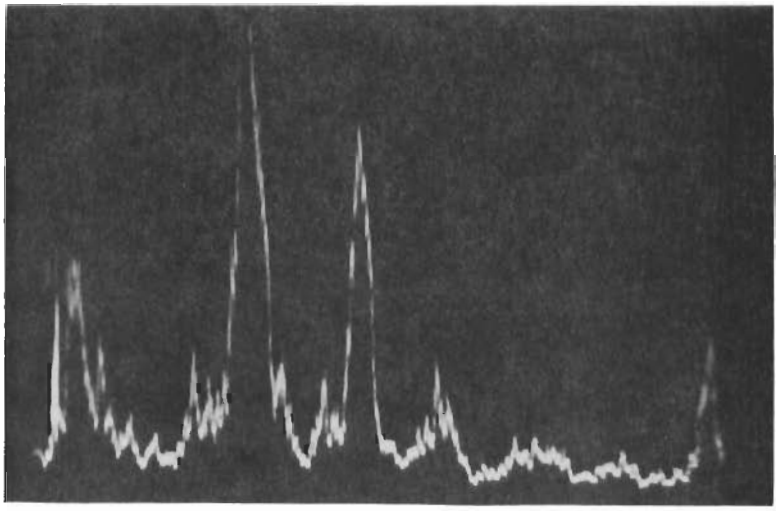

(c) X-ray scan for Zr, 1000X.

FIGURE I-4. Microprobe analysis on particles in Alloy 2. See optical microstructure in Figure I-3(a).

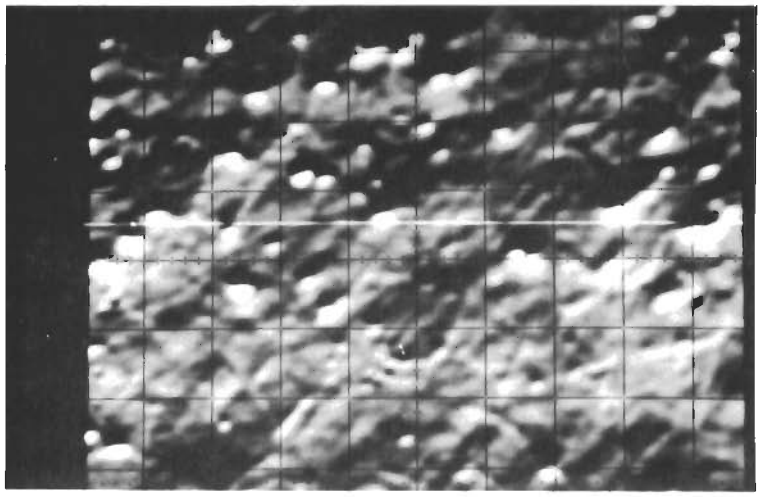

(a) Back-scattered electron photomicrograph, 1000X.

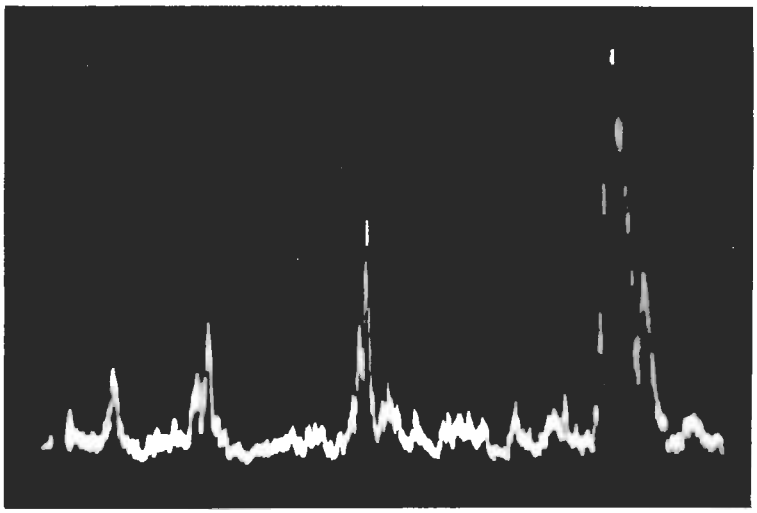

(b) X-ray scan for Si, 1000X.

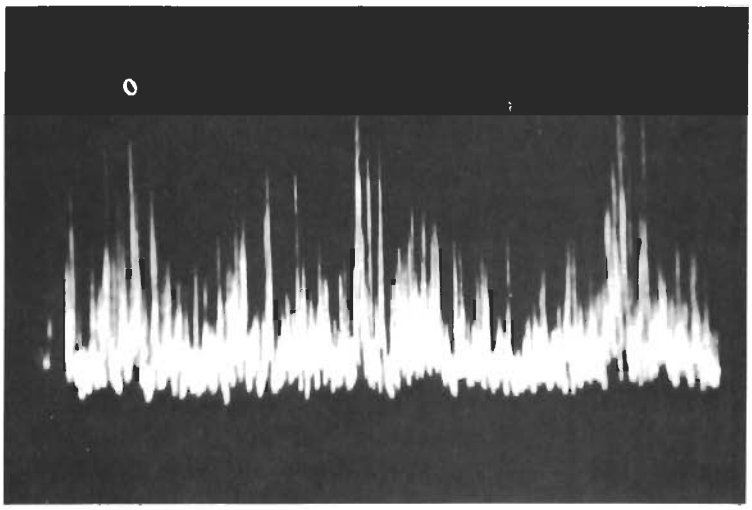

(c) X-ray scan for O_2, 1000X.

FIGURE I-5. Microprobe analysis on particles in Alloy 4. See optical microstructure in Figure I-3(b).

Most of the creep results (i.e., steady state creep rates) were obtained by stress cycling individual specimens with the tests being terminated after about 10-15 percent strain for the α-annealed alloys and about 2 to 3 percent strain for the more brittle β-annealed alloys. Selected tests on the α-annealed alloys were run at constant stress (no stress cycling) to facilitate comparison with results from the literature on other titanium alloys.

Tensile Deformation

The tensile results are recorded in Table I-2, and Figures I-6 and I-7 plot ductility and strength, respectively, as a function of test temperature. At room temperature the β-annealed alloys are very brittle ($\sim$ 1% total elongation) whereas the α-annealed alloys have 10-12% elongation. The superior ductility of α-annealed alloys at 500°C and 700°C is also evident in Figure I-6. The yield and ultimate strengths of α-annealed specimens are, in general, greater than those of β-annealed specimens at room temperature and 500°C, but are somewhat lower at 700°C (Figure I-7). The temperature dependence of the yield strength of several commercial alloys is included in Figure I-7, and it is seen that α-annealed Alloy 2 (Ti-3.4Al-8.7Ga-1Mo-1Cb-5Zr-0.5Si) has strength comparable to Ti-6Al-2Sn-4Zr-6Mo up to $\sim$ 500°C. This alloy was chosen for comparison since, as will be seen later, the creep properties of the α-annealed alloys are very similar to this commercial alloy.

Creep Studies

Steady state creep rates as a function of stress are listed in Table I-3 for α-annealed alloys and Table I-4 for β-annealed alloys. These results are plotted for individual alloys in Figures I-8, I-9, I-10, and I-11

TABLE I-2. TENSILE RESULTS OF α- AND β-ANNEALED ALLOYS AS A FUNCTION OF TEST TEMPERATURE

Alloy	Test Temperature °C	Anneal	0.2% Y.S., 10^3 psi	UTS 10^3 psi	Uniform Elong., %	Total Elong., %	Reduction in area %
1	25	α	142.6	156.2	9.5	10.4	29.4
1	25	β	118.4	130.9	0.9	0.9	3.3
2	25	α	172.0	180.5	8.0	11.6	41.0
3	25	α	150.0	161.0	10.3	12.3	36.0
3	25	β	156.6	158.6	0.9	1.1	5.7
4	25	α	167.5	179.5	6.1	9.2	34.7
4	25	β	-(b)	143.1	~ 0.2	~ 0.2	~ 0.2
5	25	α	121.7	130.1	17.4	23.0	33.4
1	500	α	86.5	107.2	14.2	16.2	13.9
1	500	β	69.2	74.4	3.7	5.5	48.5
2	500	α	110.0	131.0	13.6	18.9	12.1
3	500	α	93.8	112.5	13.7	17.8	28.1
3	500	β	90.0	95.3	2.2	3.2	24.2
4	500	α	101.5	125.5	12.7	17.6	28.1
4	500	β	105.5	115.7	3.0	3.7	11.7
5	500	α	68.7	86.5	21.6	25.2	43.9
1	700	α	57.1	59.9	0.7	40.6	66.6
1	700	β	56.8	63.8	2.5	14.9	36.5
2	700	α	40.3	44.1	1.2	> 87.8(a)	> 55.9(a)
2	700	β	62.5	70.5	2.3	26.7	38.6
3	700	α	44.0	47.4	1.0	62.7	93.4
3	700	β	70.1	72.5	1.1	1.3	1.8
4	700	α	38.2	44.0	4.0	59.8	87.6
4	700	β	70.2	75.2	1.7	2.5	7.4

(a) Test terminated before fracture.

(b) Test broke shortly before 0.2% elongation.

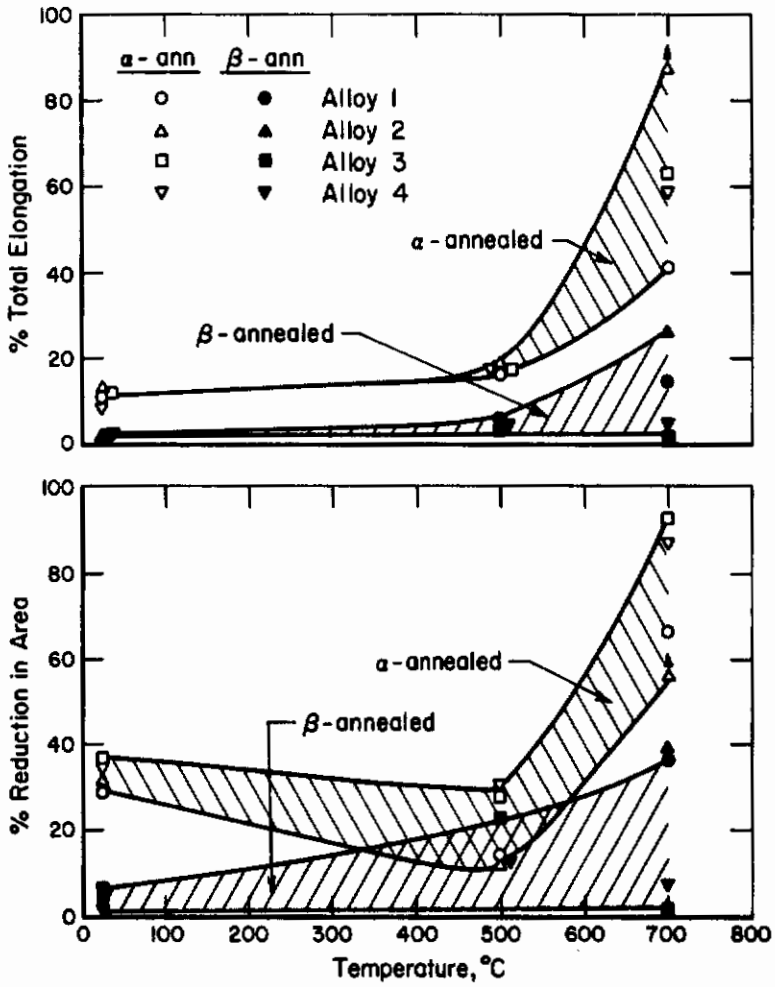

FIGURE I-6. Tensile ductility versus temperature for α-annealed and β-annealed alloys 1, 2, 3, and 4.

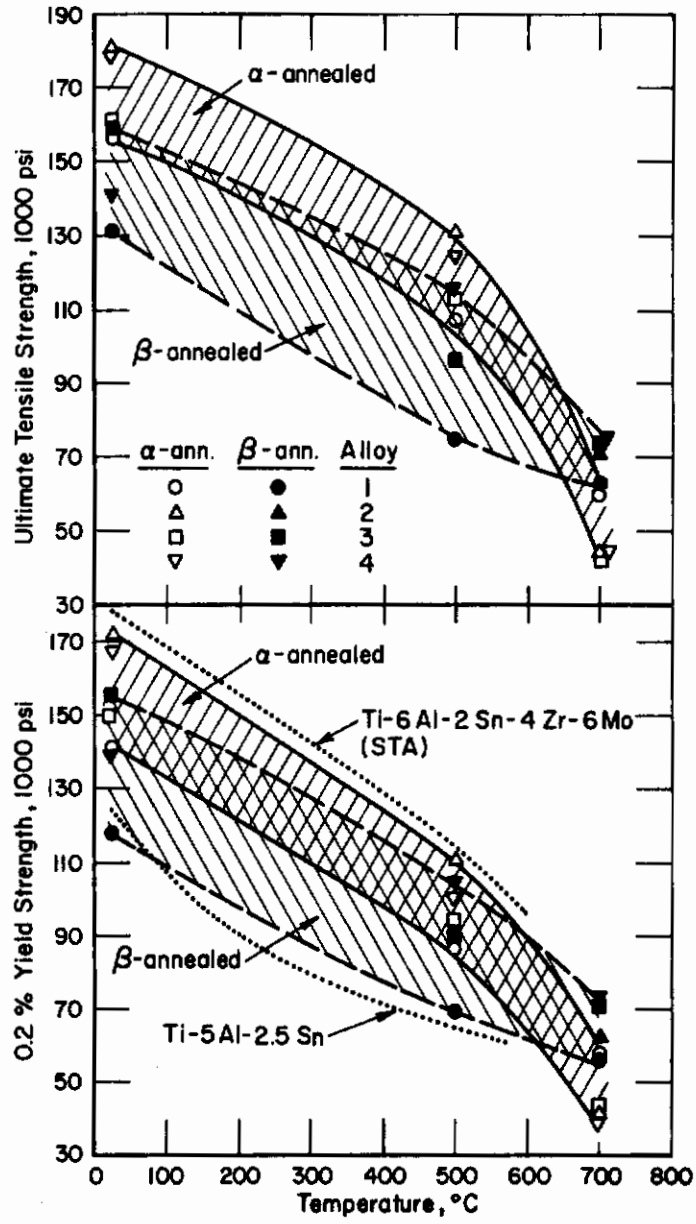

FIGURE I-7. Yield and ultimate strength versus temperature for α-annealed and β-annealed alloys 1, 2, 3, 4.

TABLE I-3. STEADY STATE CREEP RATE OF α-ANNEALED ALLOYS AS A FUNCTION OF STRESS AT 550°C

Alloy	Stress, psi	Steady State Creep Rate, hr^{-1}	Alloy	Stress, psi	Steady State Creep Rate, hr^{-1}
1	40,000	5.74×10^{-6}	4	30,000	1.80×10^{-5}
1	40,000(a)	7.50×10^{-6}	4	40,000(a)	3.20×10^{-5}
1	60,000	5.88×10^{-5}	4	45,000	5.65×10^{-5}
1	60,000	4.00×10^{-5}	4	60,000	8.00×10^{-5}
1	75,000	1.35×10^{-4}	4	60,000	1.00×10^{-4}
1	84,100	3.95×10^{-4}	4	60,000	2.15×10^{-4}
1	90,000	3.36×10^{-4}	4	75,000	3.20×10^{-4}
1	90,000	5.56×10^{-4}	4	105,000	1.90×10^{-3}
1	118,000	1.32×10^{-2}	4	120,000	6.80×10^{-3}
2	35,000	2.70×10^{-5}	4	120,000	3.40×10^{-3}
2	40,000(a)	3.41×10^{-5}	4	150,000	1.11×10^{-1}
2	45,000	4.85×10^{-5}	5	30,000	5.72×10^{-5}
2	60,000	8.40×10^{-5}	5	30,000	3.93×10^{-5}
2	60,000	7.35×10^{-5}	5	35,000	1.27×10^{-4}
2	75,000	1.59×10^{-4}	5	35,000	8.70×10^{-5}
2	75,000	1.28×10^{-4}	5	40,000	4.30×10^{-4}
2	90,000	4.02×10^{-4}	5	45,000	1.17×10^{-3}
2	105,000	1.42×10^{-3}	5	45,000	5.00×10^{-4}
2	120,000	1.16×10^{-3}	5	55,000	2.58×10^{-3}
2	120,000	3.95×10^{-3}	5	60,000	4.40×10^{-3}
3	40,000(a)	7.61×10^{-5}			
3	45,000	9.10×10^{-5}			
3	45,000	1.20×10^{-4}			
3	60,000	3.15×10^{-4}			
3	60,000	2.27×10^{-4}			
3	75,000	6.35×10^{-4}			
3	90,000	8.00×10^{-3}			
3	90,000	4.90×10^{-3}			
3	105,000	7.80×10^{-2}			
3	120,000	4.60×10^{-1}			

(a) Single test, not stress cycled.

TABLE I-4. STEADY STATE CREEP RATE OF β-ANNEALED ALLOYS AS A FUNCTION OF STRESS AT 550°C

Alloy	Stress, psi	Steady State Creep rate, hr^{-1}
1	30,000	8.00×10^{-6}
1	45,000	4.50×10^{-5}
1	50,000	1.20×10^{-4}
1	60,000	1.70×10^{-4}
1	60,000	2.85×10^{-4}
1	65,000	9.00×10^{-4}
2	30,000	4.50×10^{-6}
2	45,000	1.10×10^{-3}
2	60,000	2.25×10^{-5}
3	30,000	8.10×10^{-6}
3	45,000	2.10×10^{-5}
3	60,000	3.55×10^{-5}
3	75,000	5.52×10^{-5}
3	80,000	7.00×10^{-5}
4	45,000	1.05×10^{-5}
4	60,000	1.50×10^{-5}
4	60,000	1.90×10^{-5}
4	65,000	2.70×10^{-5}

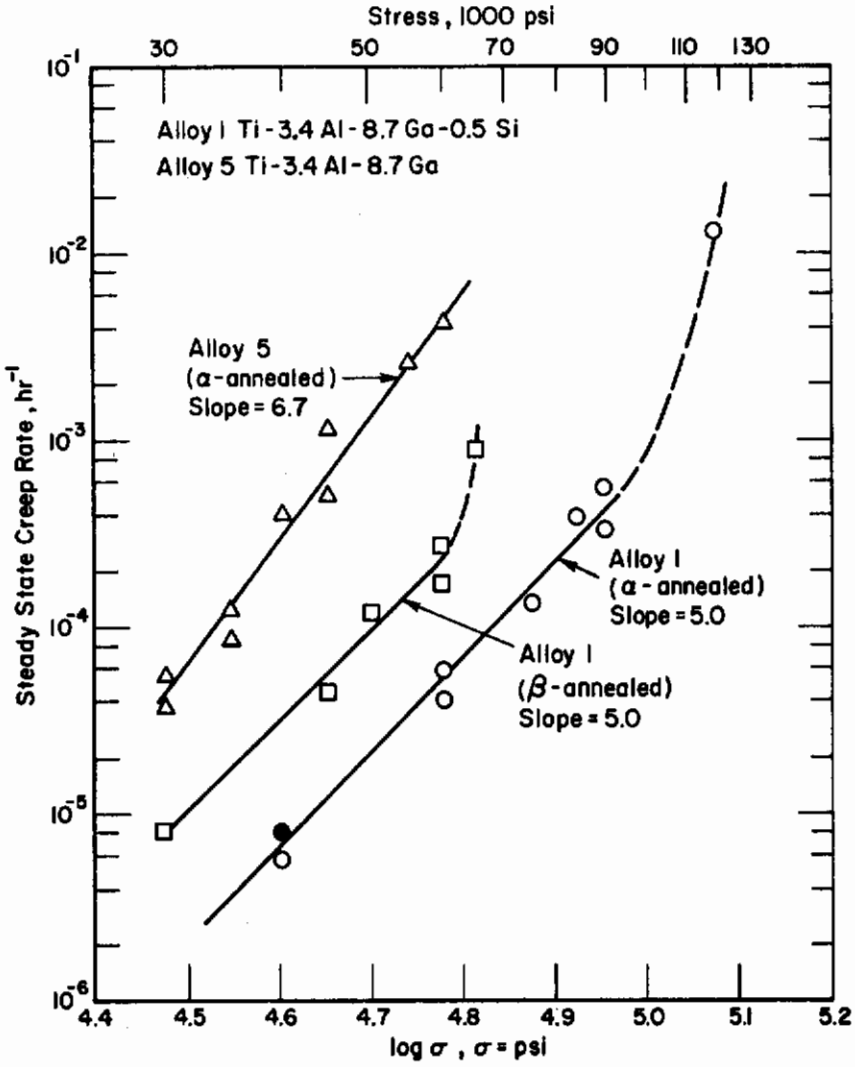

FIGURE I-8. Stress dependence of the steady state creep rate of Alloys 1 and 5 at 550°C. Solid point is for single specimen--not stress cycled.

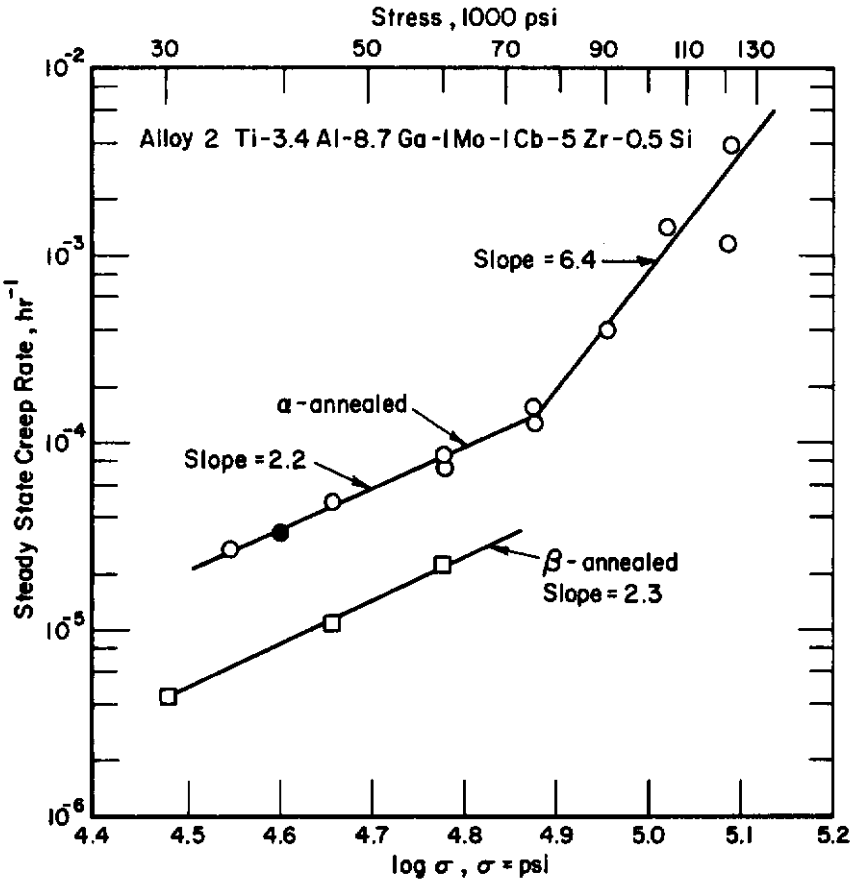

FIGURE I-9. Stress dependence of the steady state creep rate of α-annealed and β-annealed Alloy 2 at 550°C. Solid point is for single specimen--not stress cycled.

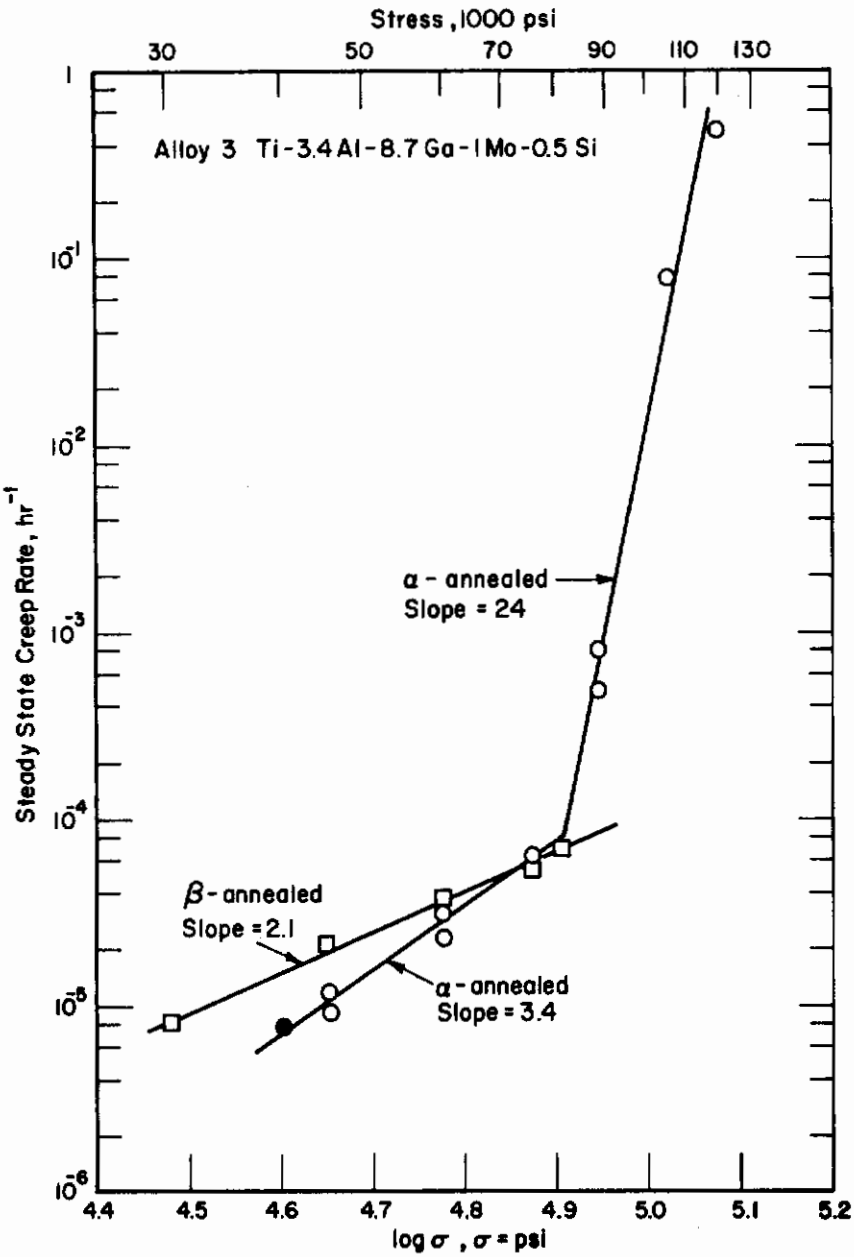

FIGURE I-10. Stress dependence of the steady state creep rate of α-annealed and β-annealed Alloy 3 at 550°C. Solid point is for single specimen--not stress cycled.

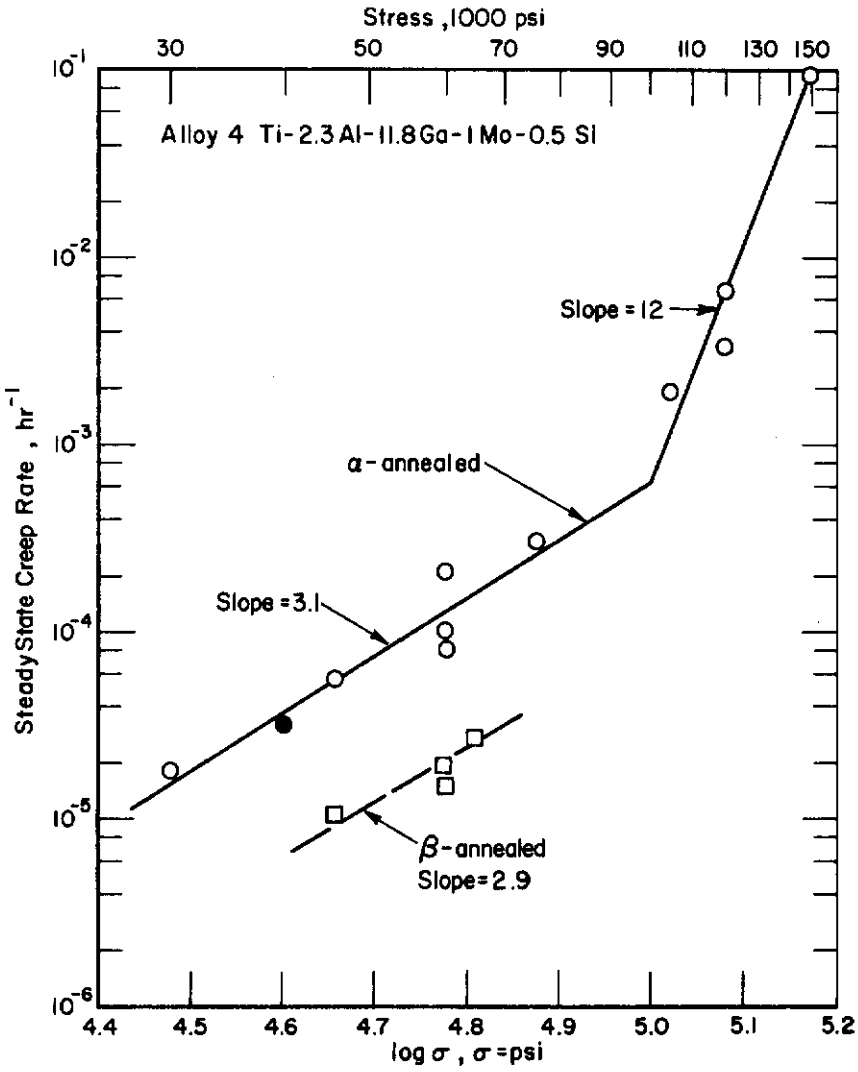

FIGURE I-11. Stress dependence of the steady state creep rate of α-annealed and β-annealed Alloy 4 at 550°C. Solid point is for single specimen--not stress cycled.

for both α-annealed and β-annealed alloys, and Figures I-12 and I-13 are summary plots for α-annealed and β-annealed alloys, respectively.

Figure I-8 illustrates the potent creep strengthening effect of silicon (presumably due to silicides) by comparing Alloy 1 (Ti-3.4Al-8.7Ga-0.5Si) with Alloy 5 (Ti-3.4Al-8.7Ga) in the α-annealed condition. Over the stress range 30,000 to 60,000 psi the steady state creep rates of Alloy 1 are approximately two orders of magnitude lower than those of the silicide-free Alloy 5.

All of the alloys in the α-annealed condition show an increasing stress dependence of creep rate at high stresses. If the results are treated as two separate regimes then the usual relation $\dot{\epsilon} \propto \sigma^n$, is obeyed with n = 2.2 to 5 at low stresses and n = 6.4 to 24 at high stresses. In general the β-annealed alloys could not be tested at high stresses since they were so brittle. However, Figure I-8 shows that the creep rate of β-annealed Alloy 1 starts to increase rapidly at the highest stress. At low stresses the stress exponents of β-annealed alloys were n = 2.1 to 5, similar to alloys in the α-annealed condition. The increasing stress exponent with increasing stress is common for many commercial alloys with complex microstructures, and has been observed previously[13] for creep at 500°C of the following β-annealed titanium alloys: Ti-0.29 Si, Ti-5.4Al-4.5 Sn, and Ti-5.9Al-5.0Zr-0.29 Si. Kehoe and Broomfield[13] suggested that in the low stress region creep of these alloys was controlled by drag of solute atmospheres around mobile dislocations. A similar argument was offered by Clauer and Wilcox[14] to explain creep of β-titanium alloys at low stresses over the temperature range 660-1100°C. Kehoe and Broomfield suggested that at higher stresses, where n = 5 to 10, dislocations can break away from solute atmospheres leading to sudden large elongations.

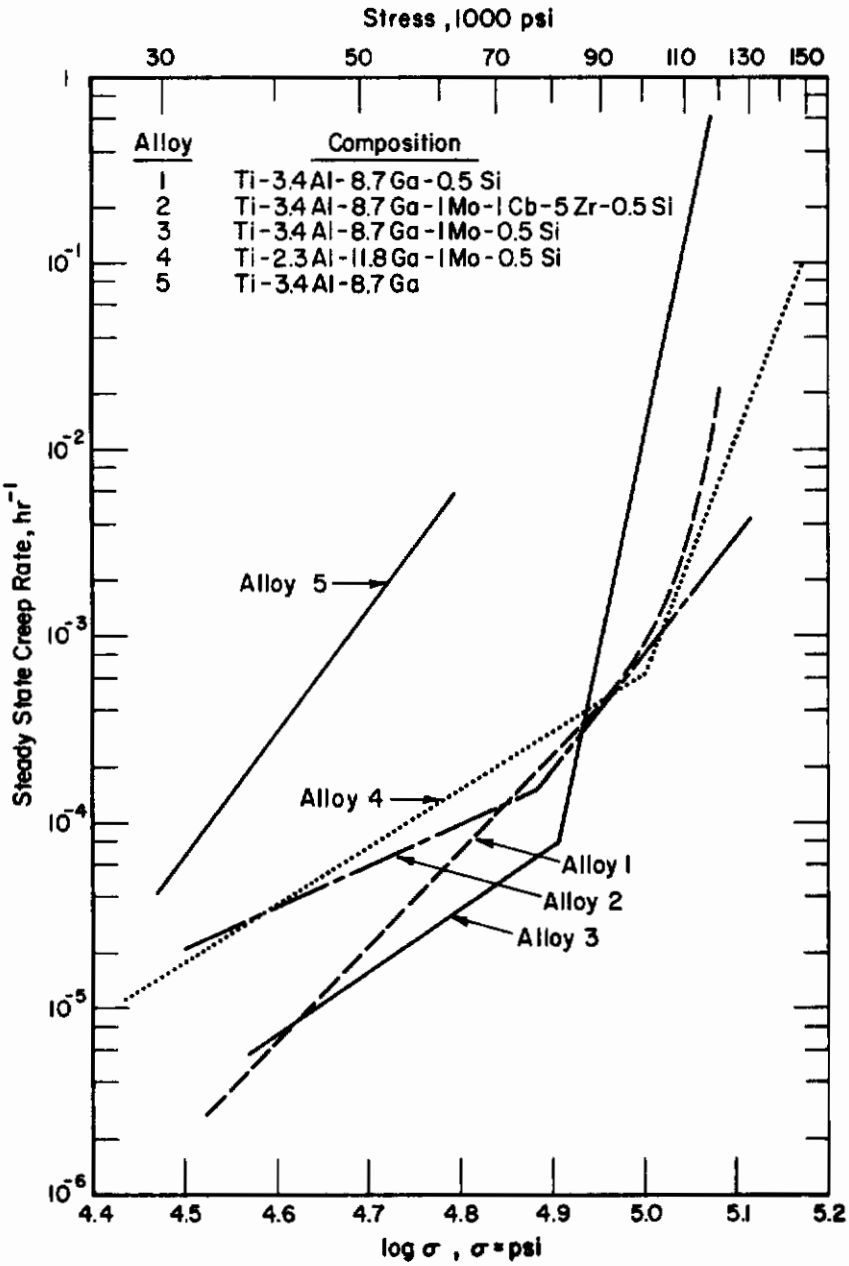

FIGURE I-12. Comparison of the stress dependence of the steady-state creep rate of α-annealed alloys at 550°C.

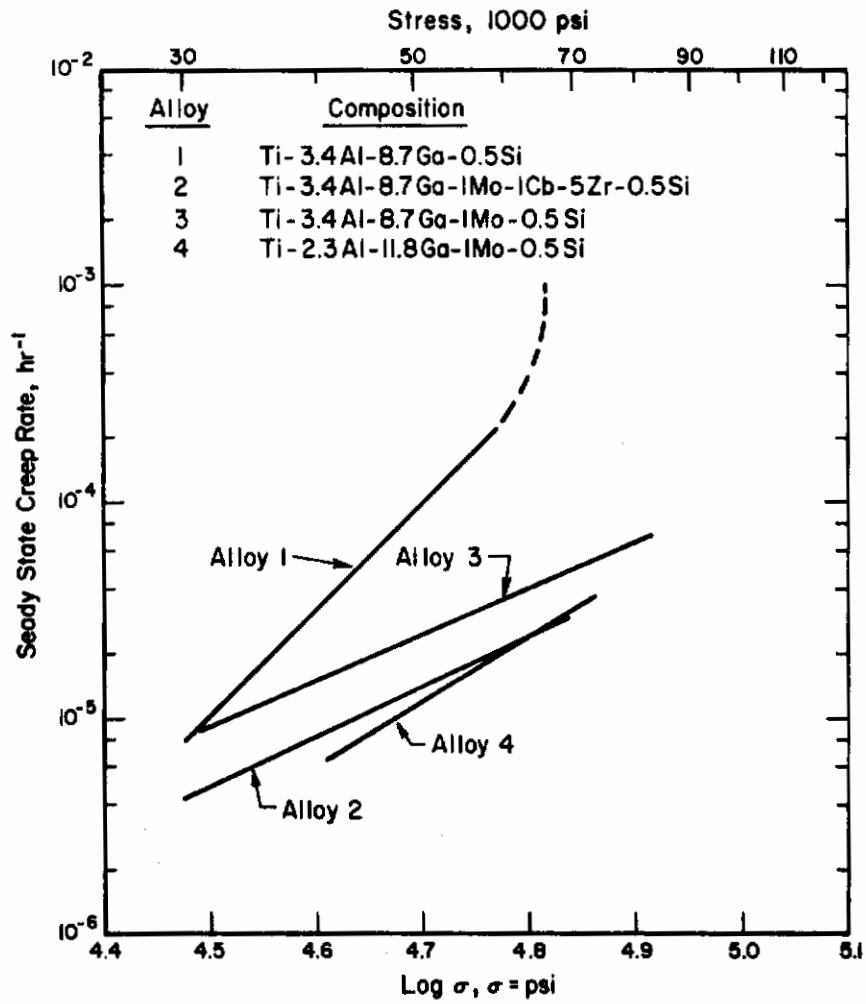

FIGURE I-13. Comparison of the stress dependence of the steady-state creep rate of β-annealed alloys at 550°C.

Comparing Figures I-12 (α-annealed) and I-13 (β-annealed), it is seen that over the stress range 30,000 psi to 70,000 psi the creep strengths of the alloys in the two conditions are roughly comparable, suggesting that these vastly different microstructures produced similar steady state creep rates. However the β-annealed alloys must be considered much inferior because of their poor ductility. It can also be seen in Figures I-12 and I-13 that there is no large effect of composition on creep rate in the low stress region, although alloy 4 (Ti-2.3Al-11.8Ga-1Mo-0.5Si) has the lowest creep rate for both heat treated conditions.

It is of interest to compare the creep properties of the present alloys with commercial alloys, and this is done by the Larsen-Miller plot in Figure I-14, derived from the data in Table I-5. It is seen that the stress for 0.2% creep for all of the present alloys agrees well with results for Ti-6Al-2Sn-4Zr-2Mo (STA), and that the Ti-Al-Ga-base alloys are less creep resistant (based on this parameter) than Ti-6Al-6Sn-2Zr-1Mo-0.25Si and Ti-6Al-2Sn-1.5Zr-1Mo-0.35Bi-0.1Si (T-11 alloy).

TABLE I-5. TIME TO REACH 0.2% CREEP STRAIN AND STRAIN IN 100 HR AS A FUNCTION OF STRESS AT 550°C FOR α-ANNEALED ALLOYS

Alloy	Stress, psi	Time to 0.2% Strain, hrs	Strain in 100 hr, %
1	40,000	42.5	0.3
2	40,000	8.2	0.7
2	45,000	4.5	-
3	40,000	7.4	1.1
3	45,000	3.7	-
4	40,000	7.8	0.8
4	45,000	5.0	-
6	30,000	29.5	-

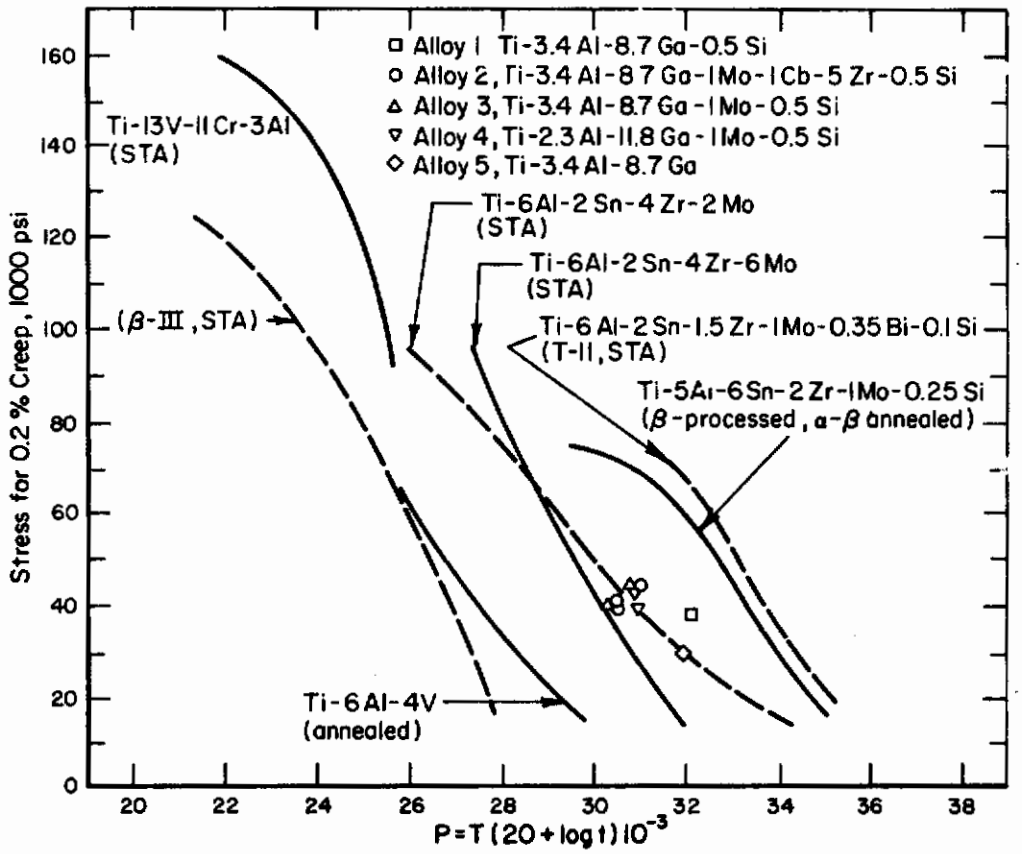

FIGURE I-14. Larsen-Miller plots for 0.2% creep strain of α-annealed alloys compared with commercial alloys.

The stability, measured in terms of post creep ductility, was examined for α-annealed Alloys 1, 2, 3, and 4 after creep in vacuum and for Alloy 3 after creep in air, and the results are listed in Table I-6. For specimens stress-cycled to 10-15% strain the ductility after creep was somewhat less than that before creep (5 to 7% total elongation compared with 10-12% before creep). However for specimens tested for 100 hours at 550°C and 40,000 psi in both vacuum and air the stability is excellent. The uniform and total elongations after creep are essentially the same as before creep, although the reductions in area are slightly lower for post-creep specimens. It would be useful to further examine this excellent stability by conducting 1000 hour tests in air.

The lack of stability of Ti-679 (Ti-2.25Al-11Sn-5Zr-1Mo-0.25Si) has been attributed to a combination of transformation of metastable beta to alpha + stable beta during creep, agglomeration of silicide particles and oxygen contamination.[15] Erdeman and Ross[15] found that the reduction in area of Ti-679 was only about 5% after creep in air for 100 hours at 538°C (0.1-0.3% creep strain) compared with 30 to 45% RA prior to creep. The stability results on the present alloys (e.g., see Alloy 3, Table I-6) are considerably more encouraging than those reported for Ti-679. This improvement may be associated with better oxidation resistance.

CONCLUSIONS

Ti-Al-Ga-base alloys have been synthesized with different microstructures produced by α-annealing and β-annealing. The α-annealed alloys were superior to β-annealed alloys because of poor ductility in the latter. The room temperature yield strengths of α-annealed alloys containing silicon

TABLE I-6. PRE- AND POST-CREEP TENSILE RESULTS OF α-ANNEALED ALLOYS AT ROOM TEMPERATURE. STRAIN RATE = 0.01 MIN^{-1}.

Alloy	0.2% Y.S., 10^3 psi		U.T.S., 10^3 psi		% Uniform Elong.		% Total Elong.		% Red. in Area	
	Pre-Creep	Post-Creep	Pre-Creep	Post-Creep	Pre-Creep	Post-Creep	Pre-Creep	Post-Creep	Pre-Creep	Post-Creep
1	142.6	146.7[a]	156.2	154.9	9.5	6.1	10.4	7.4	29.4	17.5
1	142.6	131.2[b]	156.2	150.1	9.5	12.0	10.4	12.8	29.4	24.9
2	172.0	180.0[a]	180.5	186.8	8.0	3.6	11.6	4.6	41.0	16.5
2	172.0	162.5[b]	180.5	181.3	8.0	9.6	11.6	10.3	41.0	21.0
3	150.0	166.2[a]	161.0	173.2	10.3	5.1	12.3	5.9	36.0	23.5
3	150.0	151.1[b]	161.0	171.9	10.3	9.9	12.3	11.4	36.0	28.8
3	150.0	148.2[c]	161.0	169.0	10.3	10.9	12.3	13.7	36.0	27.5
3	150.0	144.6[c,d]	161.0	166.9	10.3	7.6	12.3	8.9	36.0	21.6
4	167.5	174.0[a]	179.5	188.7	6.1	5.0	9.2	5.9	34.7	20.0
4	167.5	160.8[b]	179.5	180.0	6.1	12.3	9.2	15.1	34.7	23.7

(a) Stress cycled at 550°C to approximately 10% to 15% total strain in vacuum.

(b) 100 hours at 550°C and 40,000 psi (0.3-1.1% creep strain, see Table I-5) in vacuum.

(c) 100 hours at 550°C and 40,000 psi (2.5% creep strain) in air.

(d) 0.020 inch removed from gage diameter after creep and before tensile test.

were 143,000 to 172,000 psi with 10 to 12% total elongation. The tensile properties of the highest strength alloy (Alloy 2) are similar to Ti-6Al-2Sn-4Zr-6Mo over the temperature range 25 to 500°C.

The strengthening effects of silicon (presumably as dispersed silicide particles and/or as silicon in solid solution) were examined by comparing α-annealed Ti-3.4Al-8.7Ga and Ti-3.4Al-8.7Ga-0.5Si. A 20,000 psi increase in room temperature yield strength was caused by the silicon addition with an attendant decrease in total elongation from 23% to 10%. Silicon also decreased the steady state creep rate by about two orders of magnitude at 550°C over the stress range 30,000 to 60,000 psi.

At 550°C there was no large effect of composition or heat treatment on the steady state creep rate, all of the materials examined having rates within about an order of magnitude of each other at a given stress. Again the β-annealed alloys were inferior because of poor creep ductility. Two stress regimes were found for creep of α-annealed alloys with the stress exponent n = 2.2 to 5 at low stresses (~30,000 psi to 70,000 psi) and n = 6.4 to 24 at high stresses (~90,000 psi to 130,000 psi). The stress exponents for β-annealed alloys were n = 2.1 to 5 over the stress range 30,000 psi to 70,000 psi. Rate controlling creep processes cannot be definitely identified, but it is possible in the low stress regime that creep is controlled by dislocations dragging solute atmospheres.

Based on stress to produce 0.2% creep strain at 550°C the α-annealed alloys containing silicon have modest creep strength, similar to that of Ti-6Al-2Sn-4Zr-2Mo but less than that of Ti-5Al-6Sn-2Zr-1Mo-0.25Si and Ti-6Al-2Sn-1.5Zr-1Mo-0.35Bi-0.1Si (T-11, STA). However the α-annealed alloys have excellent stability, much superior to Ti-679 (Ti-2.25Al-11Sn-5Zr-1Mo-0.25Si). After 100 hour creep tests in vacuum and air at 550°C and 40,000 psi the post-creep elongation was identical to that before creep (10 to 14% total elongation).

Creep exposure caused a slight decrease in % RA (30% to 40% before creep compared with 20% to 30% after creep).

RECOMMENDATIONS

Based on reasonable tensile and creep strengths coupled with excellent post creep ductility, it appears that Ti-Al-Ga-Si-base alloys offer promise as a new class of high temperature titanium alloys. Additional research is needed, however, to fully assess their potential, e.g., (1) optimization of heat treatment to give the best combination of tensile and creep strength[16], (2) modification of β-stabilizing alloy additions, (3) additional alloy modifications such as the inclusion of 0.35 Bi, as in T-11, and (4) long time (1,000-10,000 hour) creep tests in air to assess stability under more severe creep exposures.

It would be desirable to understand why the present alloys exhibit such good stability. If, for example, it is because the alloys have good resistance to oxygen contamination[9] then the cause of this should be determined. The incorporation of gallium may have an effect here, and if so it should be regarded as an important alloying element in spite of its present high cost. Clearly more research is needed here.

REFERENCES

(1) K. S. Jepson, L. Larke and C. A. Stubbington, "The Effect of the Group III Elements Al, Ga, and In on the Creep and Stress Rupture of Titanium at 500°C," The Science, Technology and Application of Titanium, R. I. Jaffee and N. E. Promisel, Eds., Pergamon Press, London, 1970, p 861.

(2) T. K. Redden and C. E. Shamblen, "900 F Titanium Alloy Development", AFML-TR-70-168, September, 1970.

(3) J. C. Williams and M. J. Blackburn, "The Structure, Mechanical Properties and Deformation Behavior of Ti-Al and Ti-Al-X Alloys", Ordered Alloys, B. H. Kear, et al., Eds., Claitor's Publishing Co., p 425.

(4) H. L. Gegel and S. Fujishiro, "Synthesis of a New High Temperature Near Alpha Titanium Alloy", Second International Conference on Titanium, Cambridge, Massachusetts, May 2-5, 1972.

(5) M. J. Godden and W. N. Roberts, "Ductility of Ti-Al-Ga Alloys", ibid.

(6) M. Hoch, T. Sakai, J. J. Krupowicz and M. Delahanty, "The Ti-Al-Ga System", ibid.

(7) H. L. Gegel and M. Hoch, "Thermodynamics of α-Stabilized Ti-X-Y Systems", ibid.

(8) E. W. Collings, H. L. Gegel, and J. C. Ho, "Fundamental Design of Titanium Alloys", Met. Trans., submitted.

(9) H. L. Gegel and S. R. Lyon, Air Force Materials Laboratory, WPAFB, private communication.

(10) H. M. Flower, D. R. Swann and D.R.F. West, Met. Trans., 2, 3289 (1971).

(11) C. R. Mayo, et al., "Some Factors Affecting the Metallurgical Microstructures and Creep Properties of Ti-3Al-6Sn-4Zr-0.5Si Type of Alloy", U. K. Ministry of Aviation, S&T Memo 8/65, July 1966.

(12) K. C. Antony and J. W. Clark, "Dispersion Strengthened Alpha Titanium Alloys", AFML-TR-66-105, May, 1966.

(13) M. Kehoe and R. W. Broomfield, "The Mechanisms by Which Certain Solute Elements Improve the Creep Strength of Alpha Titanium", Second International Conference on Titanium, Cambridge, Massachusetts, May 2-5, 1972.

(14) A. H. Clauer and B. A. Wilcox, "Creep of β-Titanium Alloys", ibid.

(15) E. J. Erdman and E. W. Ross, "Long Time Stability of Ti-679 after Creep Exposure Times to 15,000 Hours", The Science, Technology and Application of Titanium, R. I. Jaffee and N. E. Promisel, Eds., Pergamon Press, London, 1970, p 829.

(16) G. S. Hall, S. R. Seagle and H. B. Bomberger, "Improvement in High-Temperature Tensile and Creep Properties of Titanium Alloys", Second International Conference on Titanium, Cambridge, Massachusetts, May 2-5, 1972.

TASK II

VAPOR DEPOSITION OF METALS ON ALUMINUM AND BORON

by

W. R. Stowell and D. Hausner

INTRODUCTION

The overall objective of this task is to evaluate the potential of thin-film diffusion brazing for joining boron-aluminum fiber-reinforced composites. Prior to its initiation a substantial amount of work was conducted at the AFML to develop diffusion brazing procedures for 7075-T6 and 6061-T6 aluminum alloys. Relatively thick foils (25-125 μm) were used in these early experiments. In the present effort, specimens of 7075 or 6061 aluminum are cleaned first by conventional mechanical and chemical methods. Specimens are then argon-ion bombarded to remove aluminum oxide and thin filler-metal layers (1-10 μm) are immediately vapor deposited on the clean joint surfaces. Boron specimens and boron-aluminum composite specimens will be coated in the same manner later in the program. Phase I of this Task consists of determining the process parameters for producing the most suitable vapor deposited filler metals and thicknesses. After diffusion brazing at the AFML, Phase II will include metallographic analyses and tensile tests on the brazed specimens.

RESEARCH PROGRESS

In one effort in Phase I of this Task, diffusion brazes made previously at the AFML have been evaluated metallographically and typical photomicrographs have been prepared (see Figure II-1). This work is summarized in

1G708 NaOH etch. 100X

(a) Brazed with 25 μm of Ag foil at 575°C and 3.5 psi for 1 hour. Post-braze heat treated for 1000 hours at 400°C.

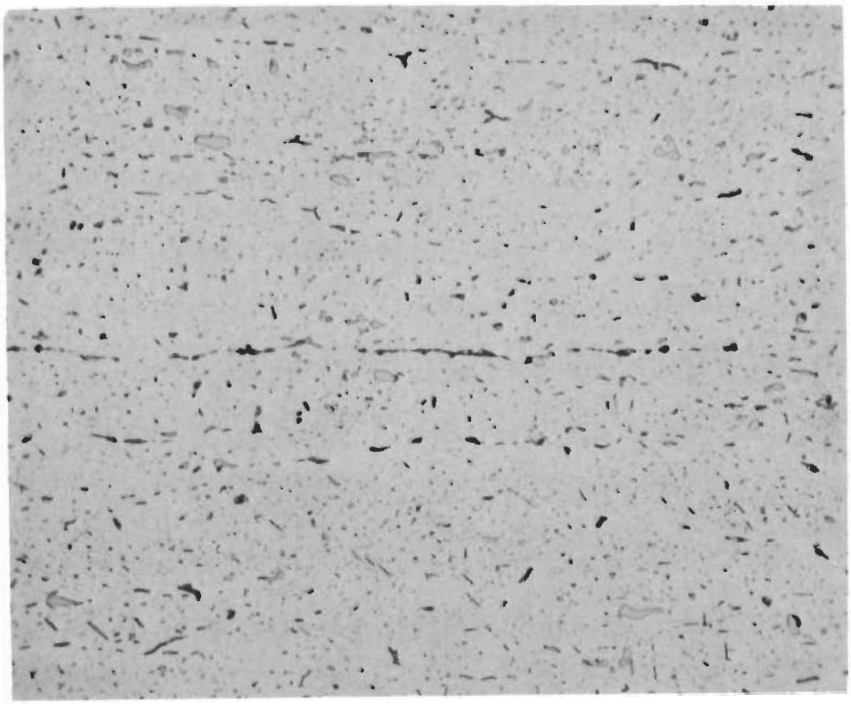

1G772 NaOH etch. 500X

(b) Brazed with 1 μm of electroplated Ag at 525°C and 200 psi for 1 hour.

FIGURE II-1. Aluminum Alloy 6061 Brazed with Silver.

Table II-1. Figure II-1a shows a wide diffusion zone and large pores in the braze. These resulted primarily from the relatively thick (25 μm) filler metal. A thinner filler metal (1 μm) eliminates the diffusion zone and the porosity in this system (Figure II-1b). The diffusion heat treatments at 300-500°C for up to 1000 hours were used to determine their ability to disperse the brazing filler metals from the joint. Grain size measurements of 6061 aluminum following the diffusion heat treatments indicated negligible grain growth except at 500°C for 1000 hours. This heat treatment produced a grain size of ASTM 6.9 compared to 7.5 for the as-brazed specimen. The grain size of 7075 aluminum brazed with zinc and diffusion heat treated could not be quantitatively measured because even after 1000 hours at 500°C the grains were still significantly elongated. However, practically no grain growth was apparent after heat treating at 300°C whereas some was evident at 400 and 500°C.

In addition to the brazed specimens, a few 7075 aluminum alloy forge welds made at the AFML were examined at Battelle. All of these were made between 1-inch-diameter cylinders in vacuum at 490°C for 1 hour with either 20 or 30 percent deformation, based on the increase in area of the interface region. Samples were examined in the as-welded condition, after heat treating to the T6 condition, and after 100 hours at 400°C plus the T6 heat treatment. All of the welded specimens displayed a flat interface. In the as-welded condition, small interfacial precipitates were seen at 800X, which were more discrete and separated further with 30 percent deformation than with 20 percent. All of the welds finally heat treated to the T6 condition looked similar at magnifications up to 800 times. A few small grains which probably nucleated during welding, were visible at the interface in each of these welds.

TABLE II-1. SUMMARY OF ALUMINUM BRAZING EXPERIMENTS[a]

Parent Alloy	Filler Alloy	Filler Alloy thickness, μm	Brazing Temperature, °C	Pressure, psi	Post-braze[b] Heat Treatment	General Braze Characteristics Determined Metallographically
6061	Ag	25	575	3.5	D	Numerous large voids
6061	Au	50	575	3.5	D	Separated voids and extensive cracking
6061	Al-12 Si	75	595	3.5	D	Occasional small voids
6061	Mg	25	450	200	A,T	Few voids and no cracks
6061	Mg	125	450	200	A,T	Large voids, cracked in the T6 condition
6061	Ag	1-58[c]	575	200	A,T	Separated small voids
6061	Cu	2-20[d]	560	200	D4	Narrow, discontinuous braze
6061	Ag	2-20[d]	575	200	D4	Narrow, discontinuous braze, some porosity
7075	Ag-28 Cu	0-3.2[c]	490	200	A,T	Separated small voids, cracked in the T6 condition
7075	Zn	100	400-420	3.5	D	Numerous large voids
7075	Mg	25	450	200	A,T	Separated voids and cracks
7075	Mg	125	450	200	A,T	Large voids, cracked in the T6 condition
7075	Mg	25	450,490	200	A,T,D2	Frequent voids and cracks
7075	Ag-28 Cu	2-20[d]	490	200	A,D4,T,D4 + T	Cracked except in the as-brazed condition

(a) All brazes were made in vacuum (10^{-5} torr) for 1 hour using preplaced foil except where otherwise noted.

(b) A - as brazed, D - diffusion treated at 300, 400, or 500°C for 0, 10, 100, or 1000 hours, T - heat treated to the T6 condition, D2 - diffusion treated at 400°C for 10, 100, or 1000 hours, D3 - diffusion treated at 420-480°C for 100 hours, D4 - diffusion treated at 400 or 500°C for 100 hours.

(c) Electroplated filler metal.

(d) Vapor deposited filler metal.

Vapor coated specimens have been prepared and sent to AFML for evaluation of their brazing characteristics. Table II-2 is a list of coated specimens which have been returned for brazing and evaluation. In preliminary evaluations, the brazes produced from the silver coated material were of higher quality than any produced using a sheet of silver filler metal. This was also true for the copper coated materials. However, because copper produced a brittle zone at the braze interface, it has been discontinued from the current program.

TABLE II-2. VAPOR DEPOSITED COATINGS FOR BRAZING

Group Number	Base Metal	Coating Materials	Thickness, μm
1	6061 Al	Ag	1,5,10
2	6061 Al	Cu	1,5,10
3	7075 Al	Ag 28 Cu	1,5,10
4	7075 Al	Zn plus Ag-28 Cu	1 5

Based on preliminary evaluations of brazed specimens at the AFML and at Battelle, the following observations and conclusions have been made to date:

(1) Silver appears to be the best braze material for 6061. The brazes are more ductile in the as-brazed condition than after a T6 treatment.

(2) Copper flows well on 6061 but produces brittle brazes. It has been deleted from further study.

(3) Magnesium or silver-28 weight percent copper were most suitable for 7075 aluminum brazing.

(4) Thin films (approximately 1 μm) generally produce better brazes than thick filler-metal layers.

(5) The silver-aluminum eutectic wets boron.

FUTURE WORK

After the most suitable filler metals and thicknesses have been selected during Phase I, metallographic analyses and tensile tests of diffusion brazed specimens will be conducted in Phase II.

TASK III

EVALUATE REFRACTORY OXIDE CRUCIBLE MATERIAL FOR INDUCTION MELTING OF TITANIUM

by

C. A. Alexander, N. M. Griesenauer, D. P. Moak, L. G. McCoy, and D. E. Niesz

INTRODUCTION

Current melting practices have been developed to avoid the problems caused by the extreme reactivity of titanium, its sensitivity to interstitial elements, and the lack of an inert crucible and mold. Consumable electrode arc melting in water-cooled molds is utilized for all large ingots. This process requires precise electrode fabrication to avoid ingot inhomogeneity (because only a fraction of the metal is molten at one time), and solidification patterns are sensitive to electrode characteristics. Thus, remelting is necessary to assure homogeneous and flaw-free ingots, adding significantly to the cost. Skull melting of titanium has been used for the production of castings of limited size. This technique provides a completely molten charge but is severely restricted because of lack of superheat control and the size limitation.

The development of a process for inductively melting titanium in an inert crucible could be a significant step in the reduction of cost of the metal and provide a higher quality product, particularly for precision castings. Induction melting would provide the advantages of superior alloy homogeneity arising from a controlled superheat, the inherent stirring action of an induction field, single batch melting, and the elimination of electrode fabrication and handling. Such an inert material could also be utilized as a mold or mold facing to allow the use of higher mold temperatures in precision casting. In addition, the identification of stable compositions might allow for their incorporation into titanium alloys as second-phase dispersoids, providing the basis for dispersion-strengthening.

In an effort to find a suitable crucible material, the results of past work in this area were reviewed and used along with thermodynamic and other considerations to generate a list of materials for experimental evaluations. Initial screening consisted of evaluating the interaction between titanium and the candidate materials in reaction couples and arc-melting experiments. Based on the results of these experiments, yttria was chosen for more detailed thermodynamic and crucible-melt studies.

BACKGROUND

The high melting point (~1668°C) and great chemical reactivity of titanium at high temperatures is well known. Titanium absorbs large amounts of oxygen, nitrogen and carbon, while only a small fraction of these interstitials may be detrimental to mechanical properties. Consequently, refractory materials such as oxides, carbides and nitrides, when dissolved, contaminate the metal, causing loss of desired properties such as ductility. An adequate container material, then, should have the following properties:

(1) Be inert or nearly inert to molten titanium. If reaction (e.g., reduction) occurs, the elements involved should not deleteriously affect the engineering properties of the metal.

(2) Have sufficient thermal shock resistance to survive repeated usage and thermal gradients during heating.

(3) Be essentially unaffected by air and moisture at room temperature.

(4) Be non-toxic.

(5) Have a potential of reasonable availability, durability, and cost.

(6) Show adequate electrical properties at high temperatures for induction melting.

Weber, et al.[1], have summarized previous work up to 1957 on molten titanium reactivity with container materials. They note carbides, oxides, nitrides, sulfides, borides, silicides, fluorides, complex oxyfluorides and intermetallics. Eastwood and Craighead[2] examined a large number of oxides, carbides, nitrides, silicides, borides, and refractory metals and concluded that, with the possible exception of zirconia, all were reactive. Weber, et al.[1] examined oxygen-deficient zirconia as a crucible material and developed a number of compositions modified by titanium. The 15 atomic percent Ti-ZrO_2 composition was shown to be inert to molten titanium for short times (< 1 minute) with little superheat.

Since Weber's work on titanium-modified zirconia, little experimentation on refractory ceramic materials for melting has been reported. Garfinkle and Davis[3] investigated the type of reaction between liquid titanium and TiC, ZrC, Cr_3C_2, TiB_2, MoB_2, CrB_2, TaB_2, $MoSi_2$, and CeS and found CeS to be the most resistant material to attack, although dissolution of the sulfide was observed.

A number of experiments were carried out by Lyons and Innouye[4] at the Air Force Materials Laboratory; and these experiments indicated that Y_2O_3 appeared to be the most promising candidate as a crucible for melting and casting of titanium. In an effort to further establish the usefulness of yttria for this application, a program to develop a technique for fabrication of crucibles of laboratory size, and a thermodynamic analysis of the interactions of titanium and yttria was performed.

RESULTS AND DISCUSSION

Thermodynamic Evaluations

In real thermodynamic systems one must consider the second law of thermodynamics in its most general form; namely, at equilibrium the chemical potential of each component must have the same value in all phases. In its broadest sense, then, when applied to the melting of titanium in yttria one must consider that a number of transport phenomena will occur until equilibrium is reached and that this final equilibrium condition will involve considerations of concentration of titanium, oxygen, and yttrium both in the metal as well as in the crucible.

Since it is known that there is considerable solubility of oxygen in titanium and that yttria can exist as an oxygen-deficient compound[5] the most immediate reaction of concern would be of the form:

$$Ti + Y_2O_3 = Ti\ (O\ in\ soln) + Y_2O_{3-x} \quad . \qquad (1)$$

Although it is not immediately obvious from Equation (1) there is also the consideration that Y may also go into solution as the oxygen potential is lowered. In an effort to evaluate experimentally the quantities necessary for evaluation of Equation (1) a series of mass spectrometric determinations was performed on molten titanium in contact with yttria crucible liners. Experiments were performed in the Nuclide 12-90-HT mass spectrometer, which has been described elsewhere[6,7]. The purpose of the experiments was primarily to determine the oxygen potential in molten titanium of known oxygen content and the oxygen and yttrium potential of yttria of a known stoichiometry. In both cases the oxygen partial pressure was computed from determination of ion intensities from reactions of the form:

$$Ti_{(g)} + 1/2\ O_{2(g)} = TiO_{(g)} \qquad (2)$$

and

$$Y_{(g)} + 1/2\ O_{2(g)} = YO_{(g)} \quad . \qquad (3)$$

From known thermodynamics for the above reactions, the equilibrium constants were determined, and from experimental values for ion intensities of Ti^+, TiO^+, Y^+ and YO^+ together with relative cross sections for the species, oxygen pressures were computed. In all cases, these oxygen pressures were less than 10^{-18} atm, even at 1760°C. The sensitivity limit of the mass spectrometer is about 10^{-10} atm; hence, one could not determine these oxygen partial pressures directly. Therefore, all oxygen partial pressures were calculated from the mass spectrometric data using Equations (2) and (3). From a series of measurements of pressures and compositions a value for a Sievert's law constant (X_o) for oxygen in titanium at 1687°C was determined. The data could be expressed by

$$X_o = 10^7\ (P_{O_2})^{1/2} \quad . \qquad (4)$$

No such simple equation was found for oxygen-deficient yttria; however, it was found that with an O/M of 1.47 ($Y_2O_{2.94}$) at 1687°C, the oxygen partial pressure was 10^{-19} atm. Based on the above values, a relationship between stoichiometry of the crucible and oxygen uptake into titanium can be established. This relation is shown in Figure III-1 along with equilibrium yttrium contents at selected points. It can be seen that for a crucible of the composition $Y_2O_{2.94}$ the titanium would be in equilibrium with it if the titanium contained 600 ppmw of oxygen and 40 ppmw of yttrium. Titanium containing more oxygen than this initially would be expected to transfer its excess oxygen to the crucible until an equilibrium value was reached. These

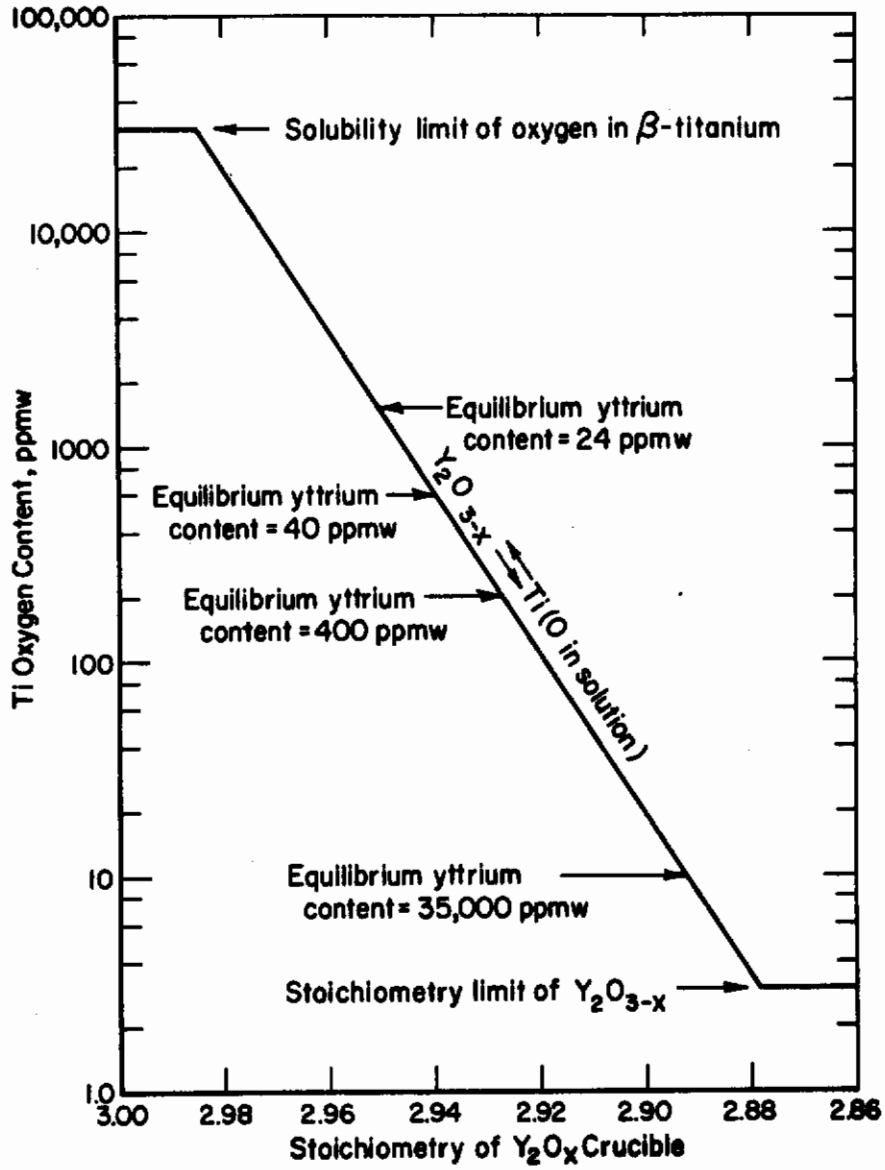

FIGURE III-1. Equilibrium Oxygen Distribution at 1687°C.

relations are predicated on the premise that there are no additional unknown complexes formed between titanium and the yttria crucible. In addition it is presumed that titanium is not soluble in yttria and that yttrium and oxygen are soluble in molten titanium. The limited experiments performed gave no indication of the existence of complexes, but solubility of titanium in yttria (probably as an ionic substitution for yttrium ions) was confirmed late in the investigation. The extent to which titanium substitution for yttrium would affect the above analysis cannot be determined until further data are obtained.

Neglecting the titanium solubility in yttria, there is sufficient information to determine the feasibility of producing an acceptable quality titanium in an yttria crucible. As a criterion for acceptance we have considered that 1500 ppm oxygen by weight is allowable. Conversion indicates that this corresponds to 4.5×10^{-3} atom fraction oxygen. Utilizing this value for X_o in Equation (4) indicates that the oxygen potential in molten titanium corresponds to 2×10^{-19} atm O_2. Stoichiometric Y_2O_3 at this temperature has a potential near 10^{-16} atm O_2; hence, one would expect a marked reaction between stoichiometric Y_2O_3 and titanium. If, however, the crucible were reduced to a composition of about $Y_2O_{2.94}$ prior to charging, then at temperature the oxygen potential would be matched between the oxide phase and the titanium phase and no driving force for transport would exist. Should titanium containing 1500 ppm be melted in a crucible whose stoichiometry is lower than $Y_2O_{2.94}$, then one would expect the titanium to give up some of its oxygen to the crucible. From an oxygen content standpoint, then, one would like to use as reduced a crucible as possible; however, there is a change of several orders of magnitude in the activity of yttrium. On a weight basis one finds the relationship:

$$a = 1.5 \times 10^{-2} w \quad , \tag{5}$$

where a is the thermodynamic activity of yttrium and w is the weight percent of yttrium expected to be dissolved. This is a rather crude Henry's law approach but should give order-of-magnitude values for the yttrium content in titanium. If one decides that 400 ppm by weight is the maximum allowed pickup of yttrium, then the activity of yttrium must be 6×10^{-4} or less. One now can calculate the oxygen pressure to which this yttrium activity corresponds. The data indicate at 1687°C that

$$(aY)\ (p_{O_2})^{0.75} = 3 \times 10^{-19} \quad , \tag{6}$$

where aY is the desired activity of yttrium and p_{O_2} is the oxygen pressure in atmospheres. Solving the above for oxygen gives $p_{O_2} = 3 \times 10^{-21}$ atm. From Equation (4) one then concludes that the oxygen content would be 5×10^{-4} atom fraction in the titanium. This value corresponds to less than 200 ppm by weight oxygen and thus it is certainly thermochemically feasible to expect good quality titanium products melted in yttria crucibles, providing the yttria has been pretreated to ensure it is of the proper stoichiometry. Further work is needed before the effect of titanium solubility in yttria can be assessed.

Crucible Production

The yttria crucible liners for the Nuclide mass spectrometer evaluations and the crucibles for the melting studies were prepared by hydrostatic pressing either with or without mandrels, green machining, and firing in a vacuum furnace or in a gas-fired kiln. Michigan Chemicals yttria powder* was

* Lot Y-1865-0, 165 ppm total impurities, surface area 16.5 m^2/g.

used for all crucibles. The powder was green pressed at 100,000 psi to 66 percent of theoretical density. The crucibles were sintered to greater than 97 percent of theoretical density at 1760°C in a gas-fired kiln or at 1760°C or 2000°C in a tungsten-element vacuum furnace. The crucibles were reduced by placing a small charge of titanium in the crucible and heating in vacuum at 1700°C until the weight loss corresponding to the desired stoichiometry was achieved. The stoichiometry was determined by measurement of weight change by thermogravimetric analysis during oxidation or reduction.

The crucible liners for the Nuclide mass spectrometric evaluations were 0.45 in. OD by 0.45 in. deep with a 1/16-in. wall. The lids were 1/16 in. thick with a 1/4-in. radial depression on the inside surface to give a 5-mil thickness at the center. A 20-mil-diameter hole was placed in the center of the lid. The details of the crucible liner and experimental facility, setup, and procedure for the mass spectrometry have been described elsewhere[6,7]. Melts were made in crucibles that were 1/2 in. ID by 1-1/8 in. high with a 1/8 in. wall thickness.

Melting experiments were performed in a cold-wall, resistance-heated vacuum furnace. A vacuum of 5×10^{-6} torr was maintained during the experiments. Temperatures were stepwise increased until a temperature of 1660°C was reached, then an increment of power was applied to the furnace to rapidly raise the temperature to about 1710 or 1760°C, depending upon the amount of superheat desired. The furnace was held at this temperature for the prescribed time, then the power was decreased to cause cooling to about 1600°C. Observations indicated that solidification began 20 seconds after the power reduction. After reaching 1600°C the furnace temperature was reduced in a stepwise manner until ambient conditions were reached.

Melting Experiments

The results of the evaluation of several melts in the small yttria crucibles are given in Table III-1. The comparative data for the crystal bar titanium melted in the substoichiometric crucibles (Melts B and C) show a marked effect on hardness and contamination levels (both yttrium and oxygen) when the melt temperature and hold time is increased. It should be noted, however, that the low oxygen content of the crystal bar metal served to provide a net driving force for melt/crucible reaction, in spite of the lower oxygen potential in the substoichiometric yttria. The degree of hardening of the titanium as a result of crucible attack is shown best in the comparative melts of the arc-cast titanium (Melt D) with yttrium metal intentionally added and the titanium melted in the substoichiometric yttria for only 2 minutes at an approximate 50°C superheat (Melt C). Metal hardness increased from R_B 52 to R_B 59, at approximately equivalent yttrium contents. This comparison shows that the effect of yttrium metal alone on the titanium is small, while if sufficient oxygen is available for scavenging, the yttrium combines with that oxygen and precipitates as Y_2O_3 on cooling, greatly increasing the bulk metal hardness. The melt of sponge (Melt A) described in Table III-1 in the fully oxidized Y_2O_3 crucible resulted in gross contamination of the metal compared with a similar melt in the substoichiometric yttria crucible (Melt B). Microstructures of the as-solidified titanium metal from the melts described in Table III-1 are shown in Figures III-2 through III-5. Comparison of the amount, distribution, and size of the precipitated Y_2O_3 particles in the titanium matrix in the microstructures show the relative degree of melt/crucible reaction. Clearly, the substoichiometric crucible resulted in less reaction.

TABLE III-1. INITIAL CRUCIBLE MELT RESULTS

	Starting Metal	After Melting
(A) EL-75 Ti Sponge. Induction melted 8 min at 1770°C under 1 atm argon in fully oxidized Y_2O_3 (air fired) crucible		
Oxygen[a], ppm	360	10,500 (1.05 w/o)
Yttrium[b]	ND[c]	3.60 w/o
Hardness	R_B 45	R_B 95[h]
(B) Crystal Bar Ti. Resistance heated 10 min at 1770°C in vacuum in substoichiometric Y_2O_3 crucible		
Oxygen, ppm	230	6,000 (0.60 w/o)
Yttrium	ND	2.20 w/o
Hardness	R_B 52	R_B 92[h]
(C) Crystal Bar Ti. Two min at 1730°C in vacuum in substoichiometric Y_2O_3 crucible		
Oxygen, ppm	230	3,200 (0.32 w/o)
Yttrium	ND	1.18 w/o
Hardness	R_B 52	R_B 85[h]
Yield Strength, ksi	~33[e]	70.2[f]
% Elongation	~ 40[e]	14.5[f]
(D) Crystal Bar Ti + 1.2% Y. Arc-cast under 1/3 atm He on water-cooled copper		
Oxygen, ppm	230	380 (0.038 w/o)
Yttrium, ppm	ND	12,000 (1.2 w/o)[d]
Hardness	R_B 52	R_B 59[h]
Yield Strength, ksi	~33[e]	58[g]
% Elongation	~ 40[e]	22[g]

(a) Vacuum fusion analysis.
(b) Calculated from quantimet analysis of v/o Y_2O_3 present.
(c) Not detected.
(d) Based on yttrium in charge composition.
(e) Typical values taken from literature.
(f) Sheet specimen, annealed 1 hr at 700°C.
(g) Bar specimen, cold worked approximately 25 percent.
(h) As-cast specimen.

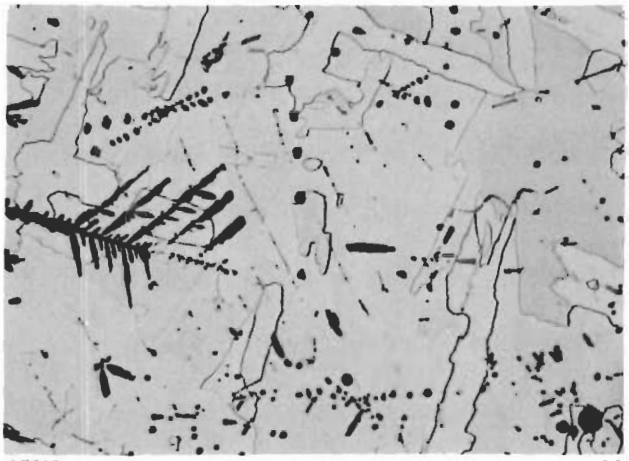

150X 0G766

FIGURE III-2. ETCHED MICROSTRUCTURE OF AS-SOLIDIFIED SPONGE TITANIUM MELTED 8 MIN AT 1770°C IN FULLY OXIDIZED YTTRIA. GROSS DISTRIBUTION OF PARTICLES AND DENDRITES OF PRECIPITATED Y_2O_3 (MELT A).

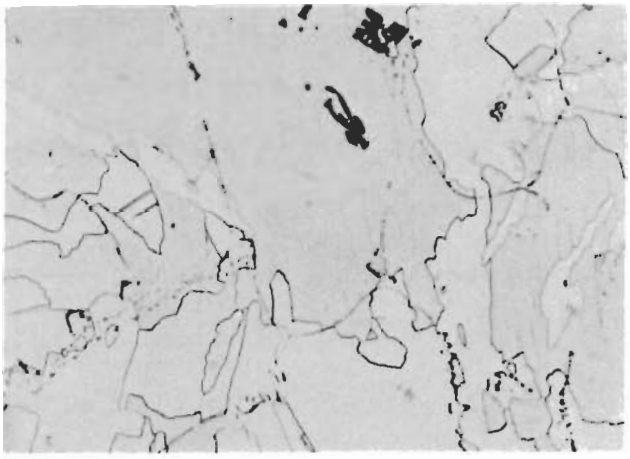

150X 0G764

FIGURE III-3. ETCHED MICROSTRUCTURE OF AS-SOLIDIFIED CRYSTAL BAR TITANIUM MELTED 10 MIN AT 1770°C IN SUBSTOICHIOMETRIC YTTRIA. NOTE DISTRIBUTION OF FINE Y_2O_3 PARTICLES ALONG PRIOR BETA-PHASE GRAIN BOUNDARIES AND FORMATION OF LARGE FLOWER-LIKE DENDRITIC PARTICLES (MELT B).

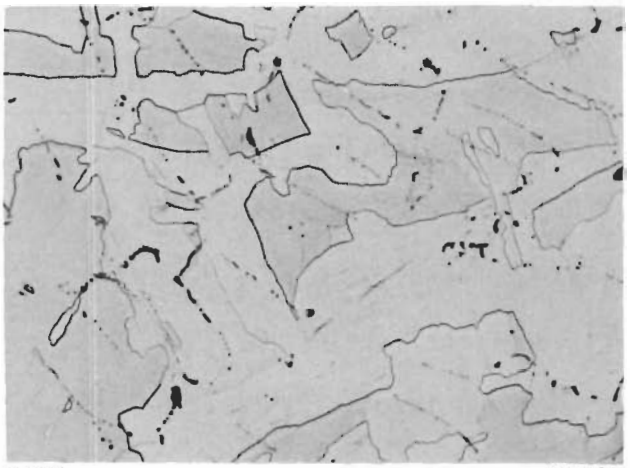

150X 0G763

FIGURE III-4. ETCHED MICROSTRUCTURE OF AS-SOLIDIFIED CRYSTAL BAR TITANIUM MELTED 2 MIN AT 1730°C IN SUBSTOICHIOMETRIC YTTRIA. FINE YTTRIA PARTICLES PRECIPITATED ON THE PRIOR BETA-PHASE GRAIN BOUNDARIES AND SOME LARGER PARTICLES ARE WITHIN GRAINS (MELT C).

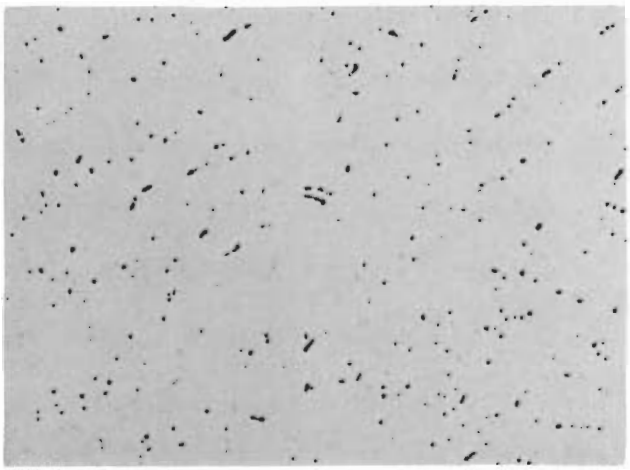

250X 0G907

FIGURE III-5. AS-POLISHED MICROSTRUCTURE OF AS-SOLIDIFIED CRYSTAL BAR TITANIUM ARC MELTED WITH 1.2 w/o YTTRIUM METAL ON WATER-COOLED COPPER HEARTH. VERY FINE PARTICLES OF YTTRIUM METAL ARE PRECIPITATED ALONG PRIOR BETA-PHASE GRAIN BOUNDARIES (MELT D).

It should be pointed out that the oxygen contents reported for the melted samples were obtained by vacuum fusion techniques and are considered to be below actual levels. The fusion bath temperature of 1950°C is probably too low to take all the Y_2O_3 particles into solution for reduction by carbon. This theory was substantiated by analyses of high-purity metal having known levels of oxygen by intentional additions of Y_2O_3 particles, analyzed to contain far less oxygen than was intentionally added.

The results of induction melts of commercial grade A-55 titanium rod in fully oxidized and "partially" reduced larger yttria crucibles are presented in Table III-2 and compared with arc-cast metal intentionally alloyed with 1.2 weight percent yttrium metal. The as-polished microstructures of resulting ingots are shown in Figures III-6, III-8, and III-7. Melts (E) and (F) in the yttria crucibles were made through the use of a molybdenum susceptor in the induction coil because of thermal shock failure of the 97 percent dense crucibles when the charge was coupled directly. This resulted in a "hot" wall crucible condition, enhancing melt/crucible reaction. Comparing the results of these two melts indicates little difference in contamination levels, also evidenced in the respective microstructures. Examination of the crucible from Melt (F) revealed that it was only partially reduced, with no effective decrease in oxygen potential. Tensile properties of the metal (fabricated and fully annealed rod) from Melt (E) were encouraging in that 22 percent elongation and a 0.2 percent yield strength of 77.2 ksi were obtained, even from metal produced in a fully oxidized yttria crucible. Melt (G) in comparison reveals the effect of the yttrium metal addition alone in reducing the bulk hardness of the titanium. To make sure that this effect was real, an identical ingot was prepared from the A-55 rod stock with no yttrium addition. Its average hardness was measured to be R_B 92, compared with the

TABLE III-2. INDUCTION MELT RESULTS

	Starting Charge	After Melting
(E) A-55 Rod. Induction-susceptor melted in fully oxidized Y_2O_3 for 1 min at 1730°C under 1/3 atm helium		
Oxygen	1,200 ppm	0.29 w/o
Yttrium	ND	~ 0.90 w/o
Hardness, R_B (a)	R_B 90	R_B 98 (c)
Yield Strength, ksi	55	77.2
% Elongation	35	22.7
(F) A-55 Rod. Induction-susceptor melted in partially reduced Y_2O_3 for 1 min at 1730°C under 1/3 atm helium		
Oxygen	1,200 ppm	0.28 w/o
Yttrium	ND	0.90 w/o
Hardness, R_B	R_B 90	R_B 100 (c)
Yield Strength, ksi	55	--
% Elongation	35	--
(G) A-55 Rod + 1.2% Y. Arc-cast in water-cooled copper 2.5 min under 1/3 atm helium		
Oxygen, ppm	1,200	1,550
Yttrium, w/o	1.20	1.20
Hardness, R_B	R_B 90	R_B 79 (c)
Yield Strength, ksi	55	--
% Elongation	35	--
(D) Crystal Bar Ti + 1.2% Y. Arc-cast in water-cooled copper 2.5 min under 1/3 atm helium		
Oxygen, ppm	230	380
Yttrium, w/o	1.20	1.20
Hardness, R_B	R_B 52	R_B 59 (c)
Yield Strength, ksi	~ 33 (b)	58.1 (d)
% Elongation	~ 40 (b)	22.1 (d)

(a) Hardness values were taken on as-cast ingots.
(b) Typical values taken from literature.
(c) As-cast specimen.
(d) Bar specimen, cold worked approximately 25%.

250X 0G910

FIGURE III-6. AS-POLISHED MICROSTRUCTURE OF INDUCTION-MELTED GRADE A-55 TITANIUM FOR 1 MIN AT 1730°C IN FULLY OXIDIZED YTTRIA (MELT E).

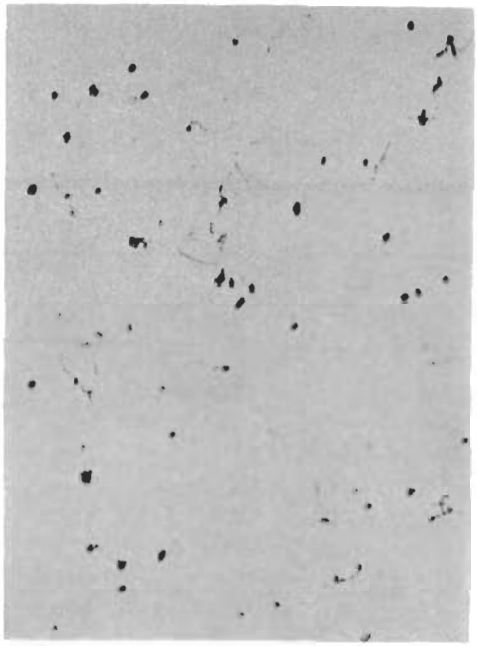

250X 0G909

FIGURE III-7. AS-POLISHED MICROSTRUCTURE OF INDUCTION-MELTED GRADE A-55 TITANIUM FOR 1 MIN AT 1730°C IN PARTIALLY REDUCED YTTRIA (MELT F).

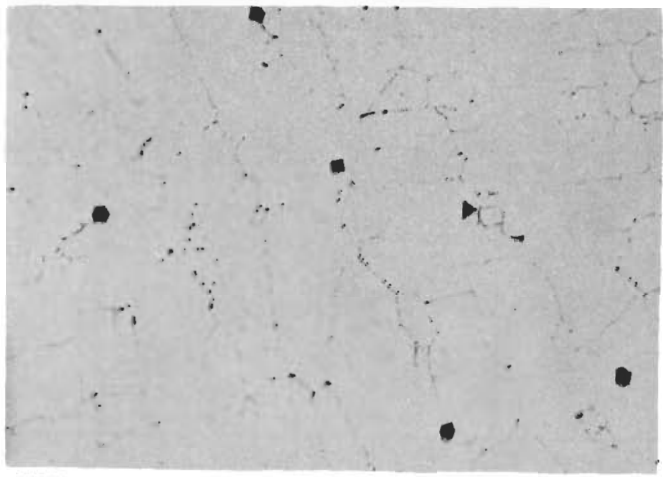

250X 0G908

FIGURE III-8. AS-POLISHED MICROSTRUCTURE OF ARC-CAST A-55 TITANIUM WITH 1.2 w/o YTTRIUM METAL. THE PRIOR BETA-PHASE GRAIN BOUNDARIES ARE OUTLINED BY PRECIPITATES (PROBABLY YTTRIUM METAL), WHILE RELATIVELY LARGE PARTICLES OF Y_2O_3 ARE RANDOMLY DISTRIBUTED.

R_B 79 for the titanium containing 1.2 weight percent yttrium. This clearly shows that the yttrium metal not soluble in the titanium will scavenge the large portion of oxygen from solution and precipitate a few yttria particles, effectively softening the titanium matrix. The oxygen analyses results reported in Tables III-1 and III-2 are total oxygen contents, i.e., the oxygen in solution and in the form of Y_2O_{3-x} particles. Even though the total oxygen levels of the crucible-melted titanium are relatively high (2900 ppm) compared to our acceptable criteria of 1500 ppm, the properties of the titanium matrix which are reflected in the tensile property values indicate the oxygen content in solution is acceptable. The tensile properties of the metal from Melt (E) are acceptable and compare well with commercially pure titanium containing approximately 1500 ppm oxygen.

CONCLUSIONS

Thermodynamic results and melting experiments indicate a potential for the use of substoichiometric yttria as a container for liquid titanium. The interaction appears more severe than the thermodynamics would predict, apparently because titanium can substitute for Y^{+3} in the yttria lattice. The yttria-titania system has not yet been investigated, but titanium was present in the yttria crucible wall after melting titanium in the crucible. Analysis shows that the probable effect of titanium solution in the yttria crucible during a melting trial would be to drive the yttria to its stability limit. Thus, a high yttrium content would be expected in the titanium (see Figure III-1). An yttria crucible saturated with titanium and having the appropriate oxygen content should provide the inert crucible desired.

The thermochemical data would tend to indicate that in addition to the promise of yttria as a crucible material there is a great potential for use of yttria as a mold material or mold facing for high-quality-shaped castings at mold temperatures as high as 1200°C. Computations based on thermodynamic values obtained during the melting experiments indicate that at 1200°C the equilibrium partial pressure of oxygen over $Y_2O_{2.94}$ would be about 10^{-30} atm and that any melt-mold interaction, although not appreciable, would be confined to within 10 to 20 μm of the interface. By judicious choice of stoichiometry this interaction may be even further minimized.

RECOMMENDATIONS

It is recommended that additional effort should be directed toward

(1) Obtaining additional mechanical property data on titanium melted in yttria crucibles with selected stoichiometries

(2) Fabricating porous yttria crucibles with improved thermal shock fracture resistance, and

(3) Obtaining some additional thermodynamic data to resolve some of the questions regarding the thermodynamic compatibility of Y_2O_{3-x} and titanium containing less than 1000 ppm of oxygen.

In addition to the above recommendations regarding use of Y_2O_{3-x} as a crucible for melting titanium, it is strongly recommended that yttria be considered as a mold facing for titanium casting. This may allow titanium to be cast using essentially the same technology as is now used for casting superalloys.

REFERENCES

(1) B. C. Weber, W. B. Thompson, H. O. Bielstein, and M. A. Schwartz, J. Amer. Ceram. Soc., 40, No. 11, 363-373 (1957).

(2) L. W. Eastwood and C. M. Craighead, AFML-TR-6218, Part I (1950).

(3) M. Garfinkle and H. M. Davis, ASM Trans., 48, No. 4, 520-530 (1965).

(4) S. R. Lyon and S. Innouye, Air Force Materials Laboratory, WPAFB, private communications.

(5) R. J. Ackermann, E. G. Rauh, and R. R. Walters, J. Chem. Thermo., 2, 139-149 (1970).

(6) Karl A. Gingerich, J. Chem. Phys., 49 14-18 (1968).

(7) R. S. Carbonara and G. D. Blue, High Temp. Sci., 3, 225-230 (1971).

TASK VI

LOW TEMPERATURE MECHANICAL TREATMENTS TO ENHANCE FORMABILITY OF TITANIUM ALLOYS

by

J. D. Boyd

INTRODUCTION

Experiments performed at the AFML[1] indicated that Ti-6Al-4V (solution-treated at 980°C and furnace cooled), has an enhanced deep-drawability at cryogenic temperatures (Table VI-1). The present research program was initiated to study this phenomenon further. The objective was to delineate the metallurgical conditions which give the best cryogenic formability of selected commercial titanium alloys, and to investigate the deformation mechanisms which promote the enhanced formability.

The effects of specific metallurgical parameters on the "formability" of a metal or alloy are complex, and generally cannot be treated analytically. Rather, empirical formability parameters are determined from tests such as Olsen Cup tests or bend tests which simulate specific forming operations. However, certain generalizations can be made. For example, in a drawing operation it is necessary to avoid triaxial tensile plastic instability (i.e., a "neck"), and important metallurgical parameters are (1) a significant rate of work hardening at high strains, and (2) an inclusion-free microstructure. Thus, deep drawability should vary directly with the number of operative shear systems. At least five independent shear systems are required for general plasticity in a polycrystalline material, but additional systems would contribute to the strain hardening and minimize void nucleation at microstructural inhomogeneities such as grain boundaries or inclusions. In titanium and certain titanium alloys the number of operative shear systems increases as the temperature decreases from room temperature to -196°C due

TABLE VI-1. THE EFFECT OF TEMPERATURE ON OLSEN CUP TEST PARAMETERS[1]

Specimen	Room Temperature		-196°C	
	Load at Rupture (lb)	Depth of Penetration (in.)	Load at Rupture (lb)	Depth of Penetration (in.)
Ti (comm. pure)	600	0.315	700	0.370
Ti-8Al-1Mo-1V	800	0.170	900	0.170
Ti-6Al-4V, #1	700	0.127	400	0.200
Ti-6Al-4V, #2	600	0.126	450	0.185

to (1) twinning, and (2) strain-induced martensitic transformations. Thus, it is to be expected that these materials would have enhanced drawability at cryogenic temperatures.

EXPERIMENTAL

In the present program the effects of cryogenic temperatures on the formability of commercial-purity titanium, Ti-6Al-4V, and Ti-4.5Sn-6Zr-11.5Mo (β-III) were investigated. The experimental materials in the form of 0.045 in.-thick sheet were obtained from commercial vendors, and the chemical analyses are given in Table VI-2. Tensile blanks measuring 6" x 3/4" were cut from this material and sealed in Vycor tubes (evacuated and back-filled to 1/3 atmosphere with argon) for heat treatment. Following heat treatment the blanks were surface ground and tensile specimens with 1.25 in. x 0.375 in. gauge sections were prepared. Conventional tensile tests at a strain rate of 1.3×10^{-4} sec^{-1} were performed at room temperature and -196°C. The latter were accomplished by

TABLE VI-2. CHEMICAL ANALYSES OF EXPERIMENTAL MATERIALS

Alloy	Analysis, Weight Percent									
	Al	Sn	Zr	V	Mo	C	N	O	H	Fe
Ti-50 A	-	-	-	-	-	0.023	0.012	0.11	0.003	0.10
Ti-6Al-4V	6.3	-	-	3.9	-	0.033	0.014	0.136	0.008	0.17
β-III	-	4.6	6.5	-	11.5	0.01	0.012	0.112	0.008	0.05

surrounding the gauge sections of the specimen with a container filled with liquid nitrogen, and directing a continuous stream of liquid nitrogen onto the gauge section during the test.

Bend tests were performed using a standard bend fixture. Sheet specimens were progressively bent around mandrels having the following decreasing radii (inches): 3/4, 1/2, 3/8, 1/4, 3/16, 1/8, 3/32, 1/16, 3/64, 1/32, 1/64, and "sharp". For the tests in liquid nitrogen, the bend fixture was immersed in a dewar. After each bend the specimens were examined at 40X in a stereomicroscope and "failure" was determined by the first visible detection of a crack on the tension side of the specimen. The bend "T-value" was the final mandrel radius divided by the sheet thickness. All specimens had essentially the same thickness of about 0.045 inches.

RESULTS AND DISCUSSION

Tensile Deformation

The possible effects of strain-induced martensite transformations on low-temperature formability were investigated by deforming in tension specimens of Ti-6Al-4V and β-III in the solution treated and quenched condition, and enhanced

ductility by twinning was examined in Ti-50A by similar tension tests. For a certain range of solution treatment temperatures the two alloys contain some mechanically unstable beta phase, which transforms martensitically under stress to a face-centered cubic phase. The amount of unstable beta is determined by the solution-treatment temperature, and the amount which transforms to martensite depends on the deformation conditions. From thermodynamic considerations, it is expected that the volume fraction of strain-induced transformation product will increase with decreasing deformation temperature. In order to determine the solution treatment temperature which produces the maximum amount of mechanically unstable beta phase, a series of specimens of Ti-6Al-4V and β-III were solution treated at various temperatures, water quenched, and tested at room temperature at a strain rate of $1.3 \times 10^{-4} sec^{-1}$. The yield stress and uniform elongation for the Ti-6Al-4V and β-III specimens are shown in Figures VI-1 and VI-2, respectively. A solution treatment temperature of 816°C was selected as that which produced the minimum yield stress and maximum uniform elongation in the room temperature tests. Sherman and Kessler[2] had previously shown that this solution treatment temperature resulted in a maximum elongation and minimum yield strength in Ti-6Al-4V as a result of equilibration of the beta to a mechanically unstable condition.

Accordingly, specimens of Ti-6Al-4V and β-III, as well as Ti-50 A, were solution treated at 816°C and water quenched. In addition, some specimens of Ti-6Al-4V and β-III were solution treated at 816°C, furnace cooled to 650°C and air cooled to room temperature. The latter treatment was employed to evaluate metallurgical conditions similar to those investigated by Fujishiro[1] (Table VI-1). Representative microstructures for the various alloy conditions

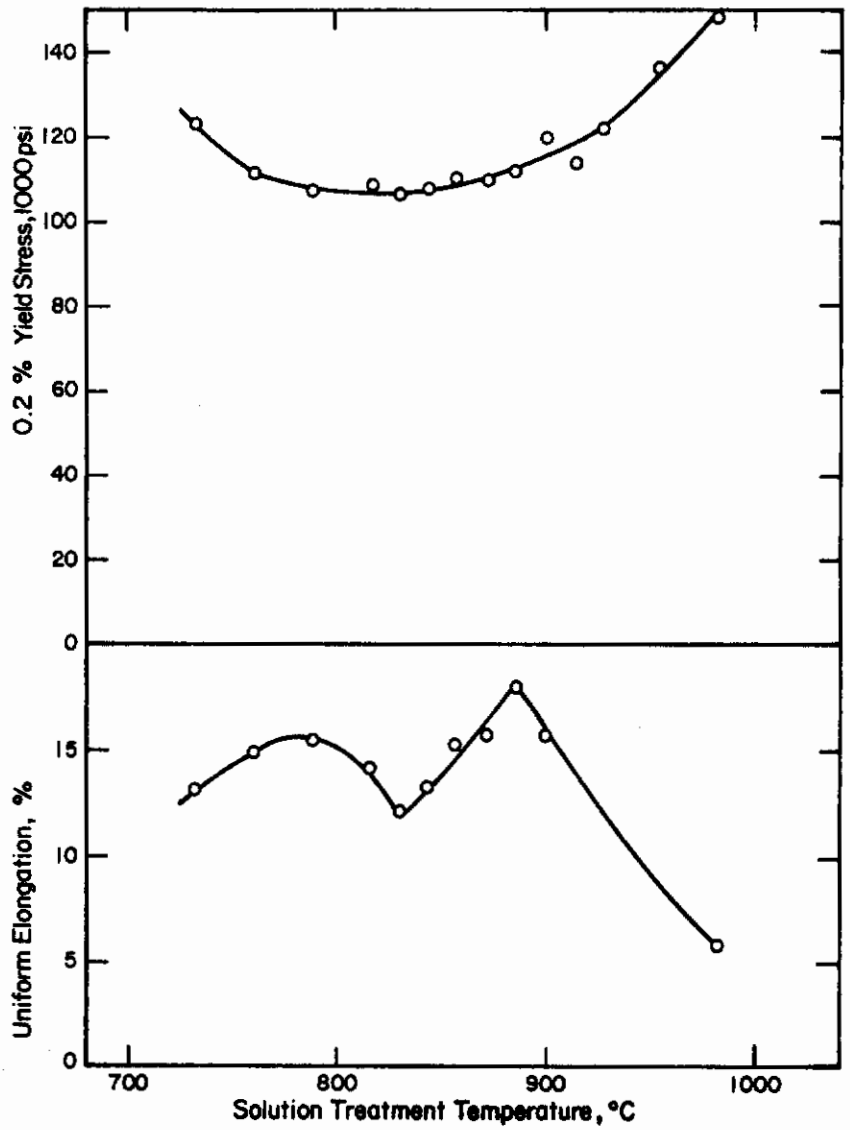

FIGURE VI-1. Yield strength and uniform elongation of Ti-6Al-4V as a function of solution treatment temperature. All specimens were quenched and tested at room temperature.

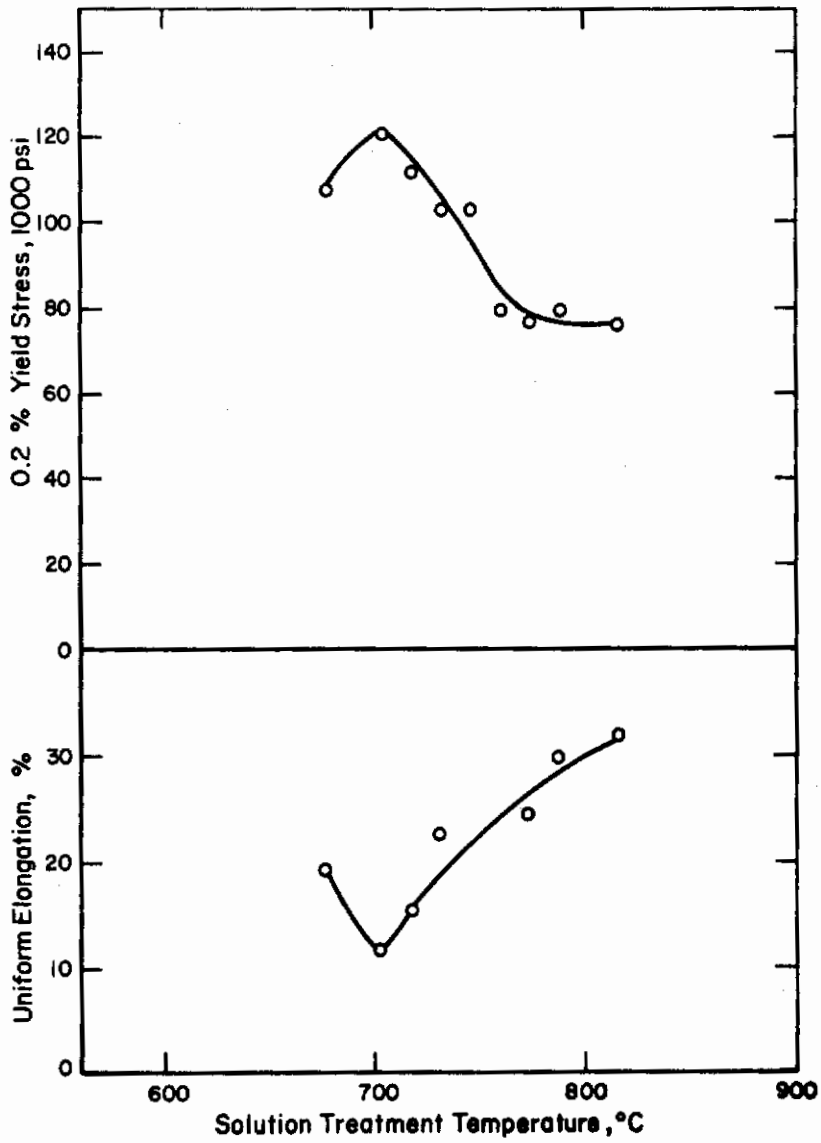

FIGURE VI-2. Yield strength and uniform elongation of Ti-4.5Sn-6Zr-11.5Mo (β-III) as a function of solution treatment temperature. All specimens were quenched and tested at room temperature.

are shown in Figure VI-3. Tensile specimens were deformed in tension at room temperature and -196°C, and the results are summarized in Table VI-3. The commercial purity titanium exhibits a pronounced increase in uniform elongation with decreasing temperature in accord with previous studies.[3] However, there is little variation in uniform elongation with test temperature for either of the Ti-6Al-4V heat-treated conditions. The β-III alloy also shows no improvement in ductility at the liquid nitrogen test temperature. The enhanced ductility in Ti-50A at -196°C is attributed to a much greater abundance of twinning than in comparable tests at room temperature, as illustrated in Figure VI-4.

Bend Studies

Bend tests at 25°C and -196°C were made on the three alloys having the same heat treated conditions as specimens deformed in tension. In addition, coupons were annealed seven hours at 980°C and furnace cooled (a duplication of Fujishiro's[1] treatment) and seven hours at 980°C, 925°C, and 870°C followed by air cooling. The results, listed in Table VI-4, again show that Ti-50 A has greater formability at -196°C that at room temperature. However, for all heat treatments the bendability of Ti-6Al-4V and β-III at -196°C is inferior to that at room temperature. The only exception was Ti-6Al-4V annealed seven hours at 816°C, furnace cooled to 650°C and air cooled, where a T-value of 4.1 was found for tests at both 25°C and -196°C (see Figure VI-5). The very brittle behavior at -196°C (Figure VI-6) of β-III annealed four hours at 816°C, furnace cooled to 650°C, air cooled (T-value = 11.1) probably was due to the presence of precipitated omega-phase.

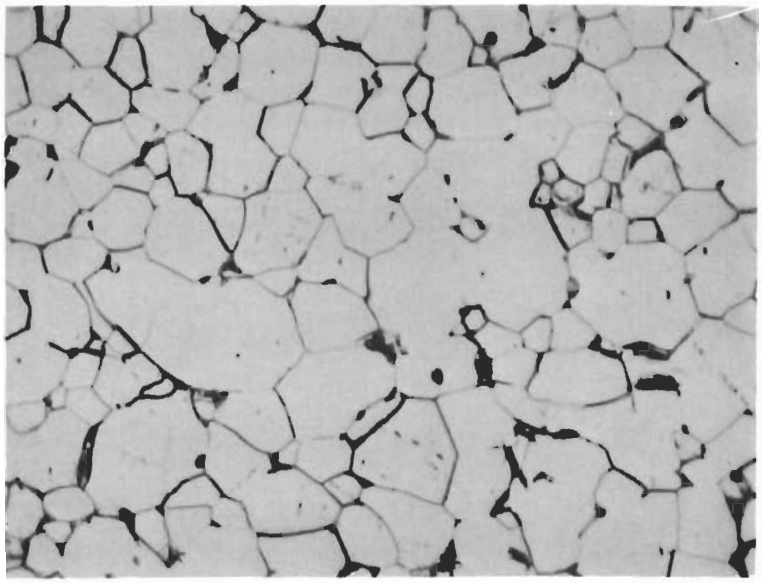

(a) Ti-50A, annealed 7 hours at 816°C, W.Q., 250X.

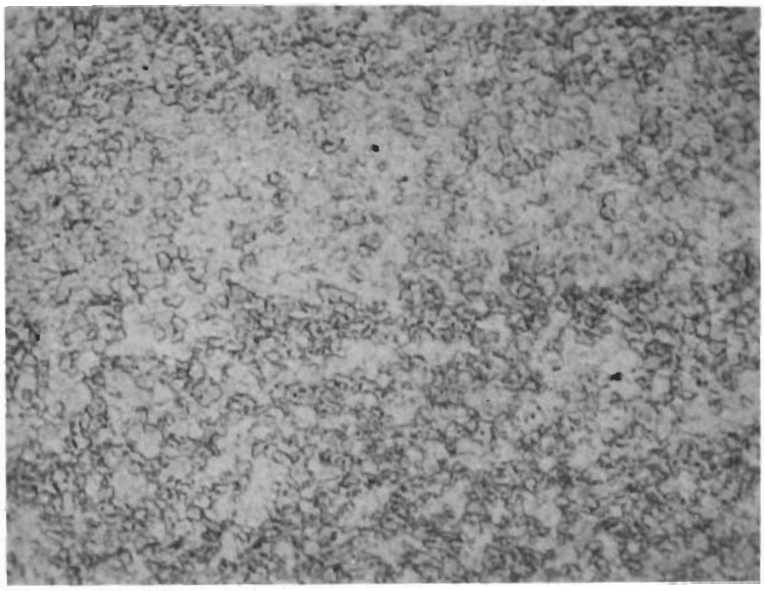

(b) Ti-6Al-4V, annealed 7 hours at 816°C, W.Q., 250X.

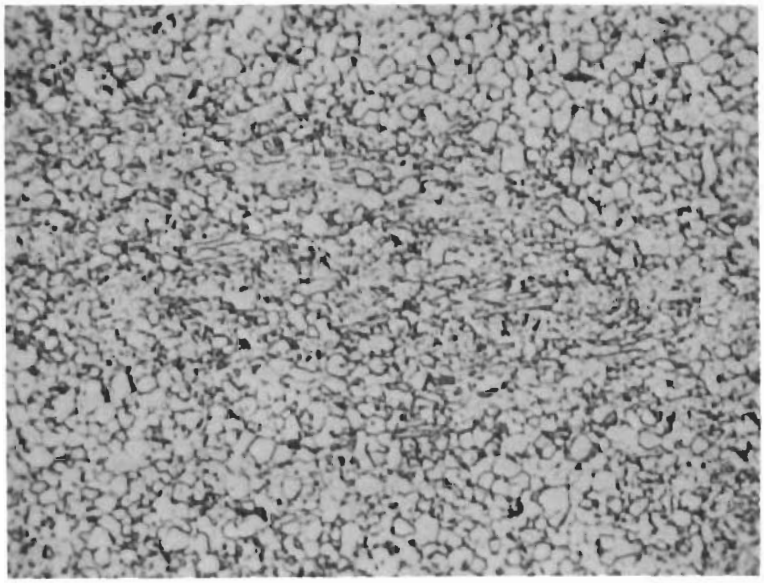

(c) Ti-6Al-4V annealed 7 hours at 816°C, F.C. to 650°C, A.C., 250X.

FIGURE VI-3. Microstructures of titanium alloys.

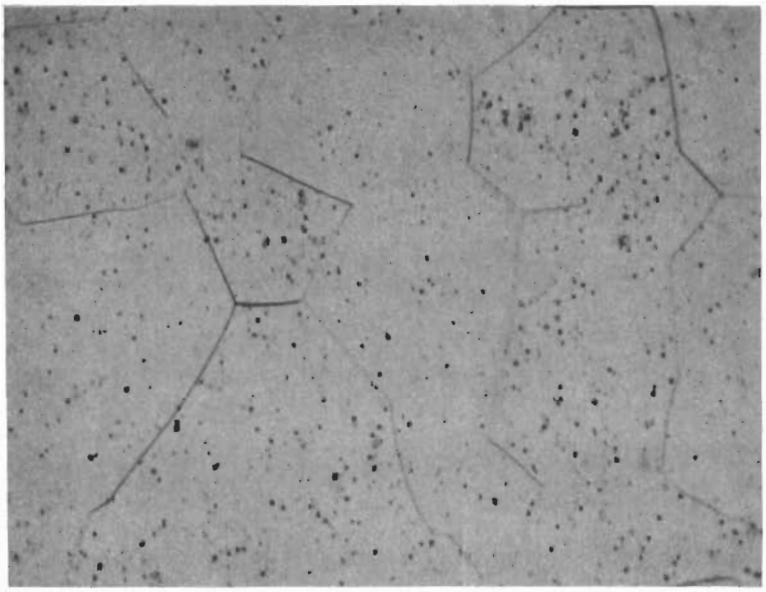

(d) Ti-4.5Sn-6Zr-11.5Mo, annealed 4 hours at 816°C, W.Q., 250X.

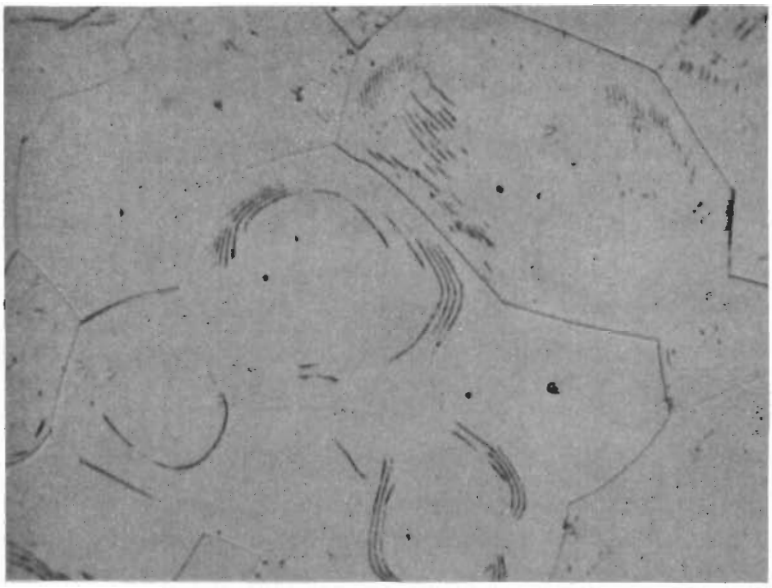

(e) Ti-4.5Sn-6Zr-11.5Mo, annealed 4 hours at 816°C, F.C. to 650°C, A.C., 250X.

FIGURE VI-3. Microstructures of Titanium Alloys (Continued).

TABLE VI-3. TENSILE DATA FOR ALL ALLOY CONDITIONS TESTED AT ROOM TEMPERATURE AND -196°C. Strain rate was $1.3 \times 10^{-4} sec^{-1}$.

Material and Condition(a)	Test Temperature, °C	0.2% Yield Stress, ksi	Uniform Elongation, %
Ti-50 A	25	47.7	19
7 hrs at 816°C, W.Q.	-196	98.7	48
Ti-6Al-4V	25	114	15
7 hrs at 816°C, W.Q.	-196	186	16
Ti-6Al-4V	25	135	12
7 hrs at 816°C, F.C. to 650°C, A.C.	-196	217	13
Ti-4.5Sn-6Zr-11.5Mo	25	94.9	27
4 hrs at 816°C, W.Q.	-196	118	broke in shoulder
Ti-4.5Sn-6Zr-11.5Mo	25	132	7
4 hrs at 816°C, F.C. to 650°C, A.C.	-196	215	4

(a) F.C. = furnace cool, A.C. = air cool, W.Q. = water quench.

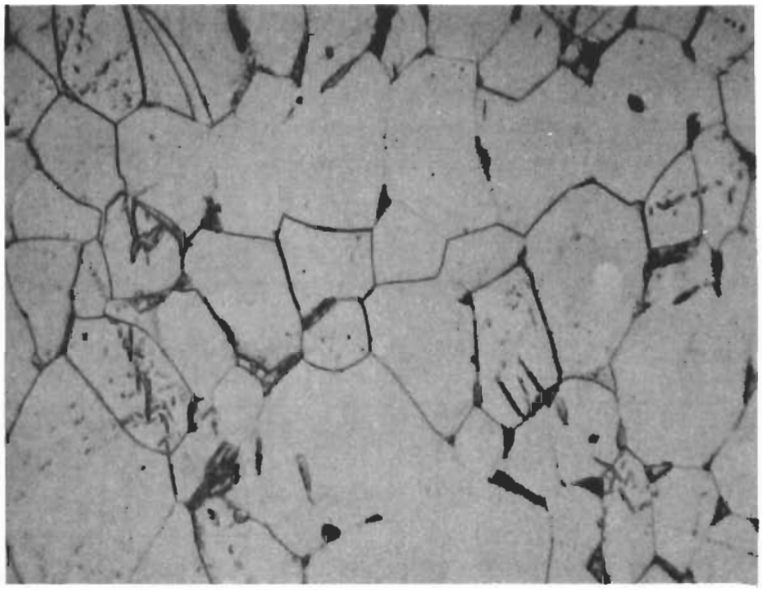

(a) T = 25°C. 500X

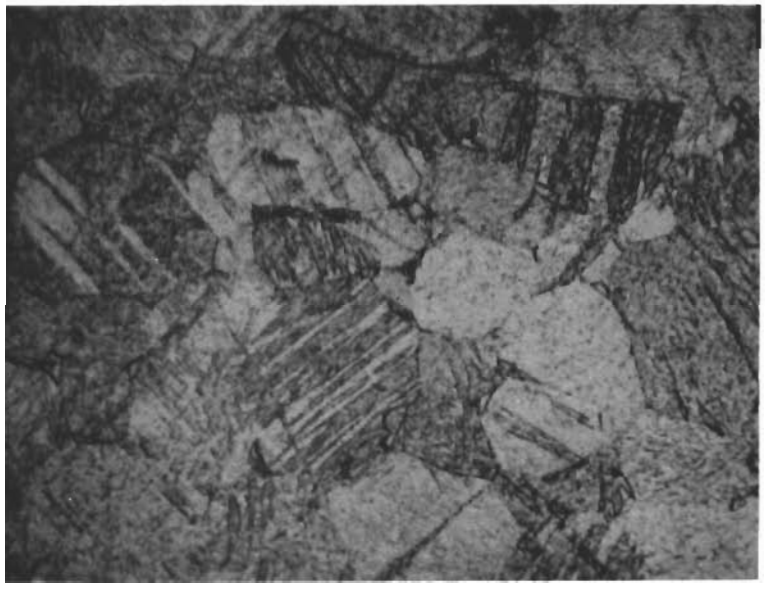

(b) T = -196°C. 500X

FIGURE VI-4. Micrographs of Ti-50 A deformed in tension showing greater abundance of twinning at -196°C than at room temperature.

TABLE VI-4. BEND RESULTS FOR Ti ALLOYS TESTED AT ROOM TEMPERATURE AND -196°C

Alloy	Condition[a]	Test Temp, °C	Bend T-Value
Ti-50A	7 hrs at 816°C, W.Q.	25	1.4
Ti-50A	7 hrs at 816°C, W.Q.	-196	~ 0
Ti-4.5Sn-6Zr-11.5Mo	4 hrs at 816°C, W.Q.	25	~ 0
Ti-4.5Sn-6Zr-11.5Mo	4 hrs at 816°C, W.Q.	-196	2.1
Ti-4.5Sn-6Zr-11.5Mo	4 hrs at 816°C, F.C. to 650°C, A.C.	25	1.0
Ti-4.5Sn-6Zr-11.5Mo	4 hrs at 816°C, F.C. to 650°C, A.C.	-196	11.1
Ti-6Al-4V	7 hrs at 816°C, W.Q.	25	3.0
Ti-6Al-4V	7 hrs at 816°C, W.Q.	-196	4.6
Ti-6Al-4V	7 hrs at 816°C, F.C. to 650°C, A.C.	25	4.1
Ti-6Al-4V	7 hrs at 816°C, F.C. to 650°C, A.C.	-196	4.1
Ti-6Al-4V	7 hrs at 980°C, F.C.[b]	25	2.1
Ti-6Al-4V	7 hrs at 980°C, F.C.[b]	-196	4.6
Ti-6Al-4V	7 hrs at 980°C, A.C.	25	2.3
Ti-6Al-4V	7 hrs at 980°c, A.C.	-196	4.4
Ti-6Al-4V	7 hrs at 925°C, A.C.	25	2.9
Ti-6Al-4V	7 hrs at 925°C, A.C.	-196	4.6
Ti-6Al-4V	7 hrs at 870°C, A.C.	25	2.5
Ti-6Al-4V	7 hrs at 870°C, A.C.	-196	4.8

(a) W.Q. = water quench, F.C. = furnace cool, A.C. = air cool.

(b) This treatment is a duplication of Fujishiro's[1] which gave enhanced formability in Ti-6Al-4V (see Table VI-1).

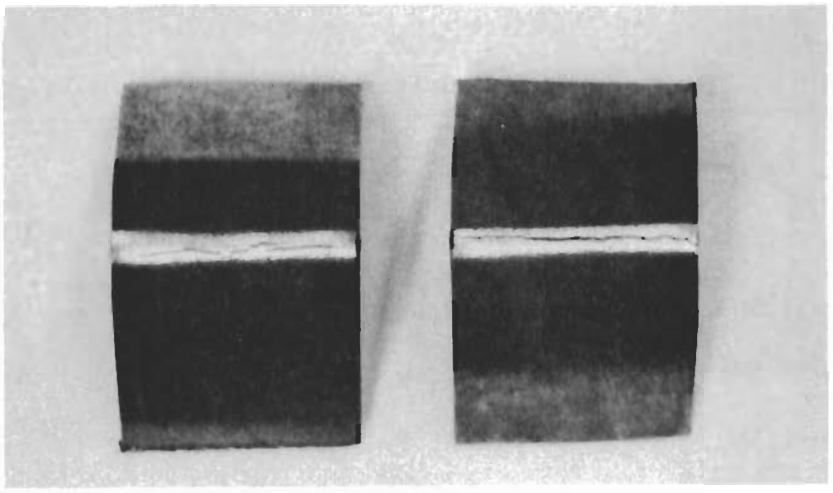

(a) (b)

FIGURE VI-5. Bend tests on Ti-6Al-4V annealed 7 hrs at 816°C, F.C. to 650°C, and A.C. (a) T = 25°C, 2.5X, (b) T = -196°C, 2.5X.

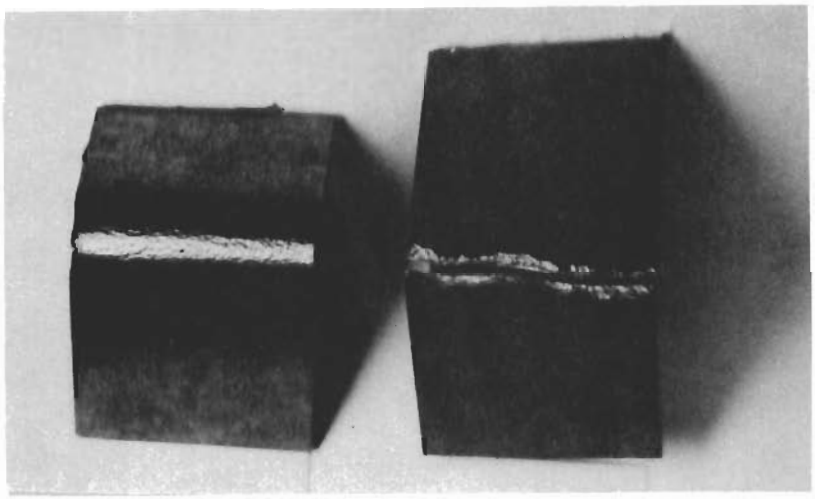

(a) (b)

FIGURE VI-6. Bend tests on β-III alloy annealed 4 hrs at 816°C, F.C. to 650°C, and A.C. (a) T = 25°C, 2.5X, (b) T = -196°C, 2.5X.

CONCLUSIONS

Tension and bend deformation studies have shown that commercially pure titanium (Ti-50 A) is more ductile and has better formability at -196°C than at room temperature. This is associated with the fact that twinning is much more abundant at the lower temperature, the greater number of operative shear systems providing enhanced ductility.

Ti-6Al-4V and β-III (Ti-4.5Sn-6Zr-11.5Mo) were heat treated to a variety of conditions and tested at 25°C and -196°C in tension and bending. In no case was low temperature tensile ductility significantly greater than that at room temperature, and in general the bendability at -196°C was inferior to that at room temperature. The absence of improved low temperature formability in these two alloys suggests that the anticipated benefits of the strain-induced martensitic transformation of unstable beta were not realized.

RECOMMENDATIONS

Under the conditions examined in this study, Ti-6Al-4V and β-III alloys showed no enhanced tensile ductility or bendability at liquid nitrogen temperature, compared to equivalent tests at room temperature. This is in contrast to earlier work[1] on deep-drawing of Ti-6Al-4V, and the lack of agreement is not understood. It may still be possible to take advantage of the strain-induced martensitic transformation of unstable beta to enhance titanium alloy formability at low temperatures; e.g., by different heat-treatment practices. However, based on the results of this research, it is recommended that no further work along these lines be undertaken at present.

REFERENCES

(1) S. Fujishiro, Air Force Materials Laboratory, WPAFB, private communication.

(2) R. G. Sherman and H. D. Kessler, Trans. ASM, 48, 657 (1956).

(3) F. C. Holden, H. R. Ogden, and R. I. Jaffee, Symposium on Titanium, A.S.T.M. Spec. Tech. Pub. No. 204, 1957, p. 14.

Unclassified
Security Classification

DOCUMENT CONTROL DATA - R & D

(Security classification of title, body of abstract and indexing annotation must be entered when the overall report is classified)

1. ORIGINATING ACTIVITY (Corporate author) Battelle Columbus Laboratories 505 King Avenue, Columbus, Ohio 43201	2a. REPORT SECURITY CLASSIFICATION Unclassified 2b. GROUP

3. REPORT TITLE

Research on Metallurgical Synthesis

4. DESCRIPTIVE NOTES (Type of report and inclusive dates)

Technical Report (15 June 1971 through 30 June 1972)

5. AUTHOR(S) (First name, middle initial, last name)

B. A. Wilcox, G. T. Hahn, and R. I. Jaffee

6. REPORT DATE	7a. TOTAL NO. OF PAGES	7b. NO. OF REFS
December, 1972	108	44

8a. CONTRACT OR GRANT NO	9a. ORIGINATOR'S REPORT NUMBER(S)
F33615-71-C-1679 b. PROJECT NO. c. d.	9b. OTHER REPORT NO(S) (Any other numbers that may be assigned this report)

10. DISTRIBUTION STATEMENT

Approved for public release; distribution unlimited.

11. SUPPLEMENTARY NOTES	12. SPONSORING MILITARY ACTIVITY
	Air Force Materials Laboratory Air Force Systems Command Wright-Patterson Air Force Base, Ohio

13. ABSTRACT

This research program consists of various tasks on metallurgical synthesis, which are aimed at developing improved microstructures in metals and ceramics of interest to the Air Force. The tasks are considered "next step" research, in that prior critical experiments have demonstrated the feasibility of a concept. The research is aimed at developing the potential usefulness of the basic concept, and to determine the circumstances under which it might be expected to operate. The tasks discussed in this report deal chiefly with research on aluminum and titanium alloys.

DD FORM 1 NOV 68 1473

Unclassified
Security Classification

14. KEY WORDS	LINK A		LINK B		LINK C	
	ROLE	WT	ROLE	WT	ROLE	WT
Microstructural synthesis in metals and ceramics						
Task A						
melt spun aluminum						
fine grained aluminum alloys						
superplastic aluminum alloys						
aluminum alloy SAP						
Task B						
attritor milling						
dispersion hardened titanium						
Task I						
creep of alpha-titanium alloys						
silicon effects						
creep mechanisms						
Task II						
vapor deposition						
aluminum/boron						
Task III						
titanium melting						
yttria crucibles						
thermodynamics						
Task VI						
titanium alloys						
low temperature formability						